



# **Laser Welding of Dissimilar Materials**

**Influence of Laser Welding Parameters  
in the Joint Quality of Dissimilar Metals**

by

Juan Simón Muzás, Mat. 01623297

**Bachelor Thesis**

for obtaining the academic degree  
Bachelor Student

performed at the  
**Technischen Universität Wien**

Supervisor  
Dr. Gerhard Liedl

Institute of Production Engineering and Laser Technology

Faculty of Mechanical and Industrial Engineering

Wien, June 2017

## **Abstract**

The aim of this thesis is to investigate parameters influence in the laser welding of dissimilar metals experimenting with steel and copper by implementing reasoned parameters in the weld of samples using an Ytterbium Fiber Laser and afterwards examining the seams through different methods and draw conclusions in order to suggest an optimize procedure for welding these pair of dissimilar metals.

Seven pairs of plates of the chosen specific materials clamped in a designed fixation system were welded with the laser according to the selected parameters that were thought the most interesting ones for the research and proceed afterwards to a macro and micro analysis of the seams observing their features using optical microscope and submitting them to a chemical analysis with SEM-EDX measurements. These analysis were used for drawing solid conclusions of which parameters are preferred to obtain a high quality weldement of these pair of metals attending to general requirements and mechanical properties.

The results revealed which range of parameter values, implemented laser variants and techniques are beneficial to acquire a good weldement leaving for further researches test experimentally the mechanical properties of the examined samples in order to confirm the deductions exposed in this investigation.

# Contents

<b>1</b>	<b>Introduction</b>	<b>5</b>
1.1	Motivation . . . . .	6
1.2	Objectives . . . . .	6
1.3	Background . . . . .	6
<b>2</b>	<b>Literature review</b>	<b>8</b>
2.1	Laser . . . . .	8
2.2	Fiber Laser . . . . .	9
2.2.1	Laser beam material interaction in fiber laser of austenitic steels .	10
2.2.2	Threshold for conducting welding . . . . .	11
2.2.3	Keyhole welding with fiber laser . . . . .	12
2.2.4	Weld pool and weld properties . . . . .	14
2.3	Broad metallurgical aspects . . . . .	15
2.3.1	The HAZ . . . . .	15
2.3.2	The Fusion Zone . . . . .	16
<b>3</b>	<b>Experimental Procedure</b>	<b>19</b>
3.1	Materials . . . . .	19
3.2	Experimental equipment . . . . .	21
3.2.1	The laser robot . . . . .	21
3.2.2	The sample fixation system . . . . .	22
3.2.3	Cutting and polishing laboratory equipment . . . . .	23
3.2.4	Optical Microscopes . . . . .	24
3.2.5	SEM microscope for EDX test . . . . .	25
3.3	Process variants and welding parameters . . . . .	25
3.3.1	Spatial configuration and first considerations . . . . .	25
3.3.2	Welding parameters . . . . .	26
3.4	Implementation and visual examination . . . . .	29
<b>4</b>	<b>Experimental results</b>	<b>32</b>
4.1	Nature and characteristics of the samples . . . . .	32
4.2	Macrostructure of laser beam welds . . . . .	34
4.2.1	Geometrical or appearance defects. . . . .	34
4.2.2	Internal or invisible defects. . . . .	36
4.2.3	Quality or property of defects. . . . .	39
4.3	Microstructure and diffusion of laser beam welds . . . . .	39
<b>5</b>	<b>Conclusions and Outlook</b>	<b>46</b>

*Contents*

<b>Appendix. Equipment, Drawing Plans and EDX Measurements</b>	<b>49</b>
<b>References</b>	<b>85</b>

# 1 Introduction

Nowadays laser welding of metals is now an important industrial technology, in contrast this technique is still in its infancy. Apparently laser welding is a straightforward operation that can be easily implemented, however the reality is completely different and basically consists of joining two metals together using laser radiation achieving a balance between a number of competing physical and metallurgical effects to obtain a weld with the desired quality and mechanical properties. In addition, factors such as reproducibility and competitive cost are crucial to make laser welding attractive in many industrial applications. Improvements in this field can only be implemented by a deep understanding of the laser welding process itself, the influential factors and the way in which this process can be controlled.

Nevertheless, the industry is progressing fast and finding new challenges as it achieves others, this phenomenon is especially intense in electric and electronic fields. For instance, increasingly there is the need for finding an optimal weld of dissimilar materials such as copper-aluminium in lithium car batteries. Aluminium is much cheaper than copper and some components can be replaced by aluminium without affecting notoriously conductivity properties, however getting a good junction is crucial in order to not debilitate mechanical and electrical properties and therefore not affect the life of products. Further examples are the welding of steels and copper, widely used in fields such as power generation, chemical, petrochemical, nuclear, oil, automotive and aircraft industries for the purpose of tailoring component properties, normally these kinds of applications require high strength and also weight reduction is desired. Obtaining the desired properties is crucial due to it is strongly related with the functionality, life time of complex and expensive structures and obviously the security. Furthermore, the welding of two different materials is always much more complex than homogeneous welds owing to differences in properties like thermal conductivity, thermal expansion among others that affect the weldability of materials, also during the process undesired phenomena may happen as intermetallic phases, excessive and dangerous hardness zones that overall affect directly the performance of the weld and that it is convenient to avoid. What makes interesting the use of laser welding instead of using conventional methods such as shielded metal arc, gas tungsten arc, gas metal arc, submerged arc and so on is the fact that the obvious material mismatches in terms of chemical and thermomechanical properties between steel and copper make it difficult to achieve a defect-free dissimilar joint. However the accurate nature of the laser welding process makes attractive their use [4].

The present scientific report deals with the dissimilar welding of steel and copper by using a Ytterbium Fiber Laser available in the laboratory where the tests were performed structured following a scientific method and ensuring the reproducibility of the experiments for further researches.

### 1.1 Motivation

The motivation beyond this project is mainly gain deep knowledge about one of the most recent fields in materials science and metallurgy. Since my first years of my Bachelor when I was attending to my first lectures about this engineering field I realised my interest towards this subject. Furthermore, last summer I took an internship in the Innovation Center of Faculty of Technology and Metallurgy of the University of Belgrade being part of a research team and working in a project about seeking optimal sterling silver alloys for a wide range of applications. There I gained theoretical and practical knowledge that I hope it has been useful to perform this research.

### 1.2 Objectives

The purposes of this Bachelor Thesis is to research and optimise the laser welding of dissimilar metals, more specifically steel and copper welds, by performing tests with samples using a Ytterbium Fiber Laser Robot and analyse the microstructure and important parameters according the specific applications following the scientific methodology. However, few systematic experimental researches concerning laser weld of steel and copper using lap configuration have been done. The obtained results are interpreted and considered to propose an improvement in the welding process in order to reach a better weld in terms of mechanical properties and overall quality of the weld.

### 1.3 Background

Laser welding is a relatively new technique. During 1960 decade many developments related to laser were carried out leading huge progresses in this field and creating many new opportunities for materials processing, one of them was laser welding. By 1962, there had been several reports on metallurgical applications of lasers, including welding, and this was followed by a number of fundamental studies of laser welding. In 1965, Pflunger and Maas realised the advantages of laser welding in comparison to soldering of fine wires in electronic components and summarize these as follows: elimination of unnecessary metal interfaces in the current path, elimination of flux, higher mechanical strength, greater resistance to vibration and shock, higher operating temperature potential, minimum possibility of degradation of heat sensitive components during assembly and increase reliability. Soon, it was found that these advantages for specific electronic applications could be effective in other joining applications, these were discussed in a series of early reviews in laser applications in industry at the end of 1960 decade and beginning of the following decade.

In the beginning of 1970 decade, emphasis was placed on pulsed laser welding as continuous wave (CW) devices of high power, however the average power of these lasers was low due to their low efficiency and most of them were pulsed ruby laser radiation. Luckily, Nd:YAG lasers with a higher average power capability soon offered a better alternative for spot welding and seam welding via overlapping spot welds despite it was not until CW power levels in excess of 1 kW were available that full seam welding

## 1 Introduction

capability could be demonstrated. In that time also the first trials using CW  $CO_2$  laser radiation took place in multikilowatt range showed the strong points, capabilities but also the limitations. The following years development and optimization of high power  $CO_2$  laser welding techniques was reported by research groups in Japan, Germany, United Kingdom and Soviet Union and most of these researches were focused on obtaining more compact, reliable laser resources of high-beam quality and understanding the complex interaction with matter, joint design and further parameters such as speed, high-beam quality, beam focussing and plasma effects in relation to weldability. Nevertheless, those studies were carried out at limited available output powers about 20 kW fact that made necessary to progress in the study of these parameters as laser technology were becoming more mature [29].

## 2 Literature review

In this chapter the principles of lasers and keyhole welding are explained along with other typical phenomena in laser welding in order to set the bases for further research and analysis

### 2.1 Laser

The word laser is an acronym for Light Amplification by Stimulated Emission of Radiation, as a physical object is an optical oscillator in which the oscillating radiation is amplified by a process of stimulated radiation, the *stimulation* process, which is the core of lasing action, was predicted by Einstein in 1916. He showed that electromagnetic radiation i.e. light, consists of photons emitted by the light source either spontaneously or through stimulation [11]. In addition, he calculated that if an atom ready to emit a photon at some random time to a random direction, it means spontaneous emission, was passed by a stray photon, the atom would be stimulated by the stray photons presence and this would cause the atom to emit its photons. Considering lasers, the main feature regarding to the stimulated emission of radiation is that photons emitted to go exactly to the same direction as the original photon and have exactly the same frequency. This laid the foundation for amplifying light to generate a high intensity beam of light which is coherent, collimated and monochromatic and therefore has great focusability.

It is a natural process that if a molecule or atom is in an excited state, in essence a higher vibration state or electronic orbit, then it will give up that energy if acted by on a quantum of the same energy. It is similar to a form of resonance shaking the energy free from the excited species provided the shaking is done at precisely the correct frequency. If this principle is translated to the laser machine, it is carried out by using two parallel reflectors that form an optical cavity, any radiation within the cavity travelling along the optic axis will oscillate back and forth for ever unless lost by absorption or diffraction out of the cavity decaying spontaneously. This seed radiation will be amplified by the stimulated emission process along the optic axis of the cavity at the speed of light. The oscillating radiation rapidly builds up and if one of the reflectors is partially transparent then the laser beam will emerge. It will parallel due to the nature of the oscillating cavity and of a near single frequency due to the nature of the stimulated emission process. Mention that laser radiation is one of the purest frequency forms of radiation that we have available [10]. To obtain the excited species in the first place requires an energy input in the form of an electric discharge ( $CO_2$  and excimer lasers), electric current (diode lasers), radiation of a frequency that can be absorbed by the species to be excited (Nd:YAG and fiber lasers). Furthermore, requires additional equipments such as external cooling devices and maintenance requirements among other elements and they are becoming more complex as the engineering of these machines are

becoming more mature. Regarding to the interaction of optical energy with matter it is important to consider what happens when electromagnetic radiation interacts with matter. Electromagnetic energy is a waveform travelling at the speed of light (300000 km/s) in which the magnetic field oscillates  $90^\circ$  out of phase with the electric field and each field as it decays stimulates the other to rise. The electric field is the one important in interactions with matter, since the atoms and molecules tend to have electric charge. As matter is composed by atoms and molecules and an atom is composed by a nucleus that occupies an small volume in comparison with the total atomic size and is surrounded by high speed electrons which form an *electric cloud* around the charged nucleus. This cloud can interact and link adjacent nuclei forming a molecular structure. When a laser beam flows into this structure, the electric field of the radiation can interact with the electric field of the structure putting forces on the various parts concerned. Focusing on welding applications, if the laser beam is strong enough, the heating may become extreme and the material will melt, boil or even become plasma.

## 2.2 Fiber Laser

Fiber lasers represents the new generation of solid state lasers in materials processing, the first laser suited for materials processing was introduced in 2000 and it had an output power of 100 W [28], nowadays fiber lasers with multi-kilowatt output powers are available for materials processing, commercial systems having up to 100kW powers. In a fiber laser beam is generated in a silicon fiber that contains a core doped with rare earth as Ytterbium, Erbium, Thulium, which is the lasing media. The principle of generating laser beam in a fiber laser, for instance an Ytterbium doped fiber, that emits photons at a wavelength of 1070 nm is transported to the processing head through a optical fiber in order to increase the operability and flexibility of the workstation. The raw beam coming from the transport fiber is collimated and then focused by the optics inside of the welding head to achieve a small enough focal point diameter that can be used for keyhole welding [6].

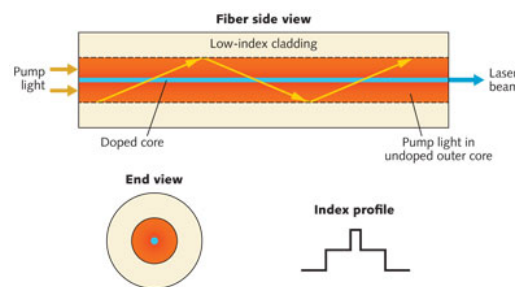


Figure 2.1: The structure of a fiber laser includes a doped inner core, which is the laser itself; an undoped outer core, called inner cladding through which the pump light is channelled and an outer cladding [9]

### 2.2.1 Laser beam material interaction in fiber laser of austenitic steels

When the laser beam impacts the surface of the material, part of the energy is reflected away from the material and the rest is either absorbed or transmitted. The case at hand, the laser beam hits steel and the part that is transmitted is close to zero, being the energy either reflected or adsorbed. For processing of laser materials, absorptivity is highly desirable since it increases the effectiveness of the process due to the direct relation to the deposition rate of energy from the laser beam o the material. This is one additional main benefit of the fiber laser over other lasers such as  $CO_2$  laser which generates ten times higher wavelength. In Fig. 2.2 can be appreciated that fiber laser is situated at the same vertical line as Nd:YAG laser in a wavelength value of 1070 nm approximately [11].

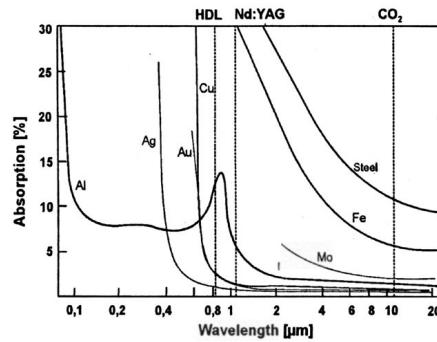


Figure 2.2: Absorption of light in % at a different wavelengths on metallic materials at room temperature [17]

Absorption is depicted through the absorptivity ( $A$ ) according to equation 2.1 valid for an opaque surface such as that of a metal.

$$A = \frac{4 n}{(n + 1)^2 + k^2} \quad (2.1)$$

It is important to consider that absorption may be enhanced by a variety of factors, including temperature, surface roughness, oxidation and changes in morphology and it also changes at the melting point. Furthermore, it takes place in a depth from the surface ( $\delta$ ) that for steels can be determined according to equation 2.2. This fact is due to laser radiation that impacts the surface of the metal is absorbed by electrons, an electron that absorbs a laser photon makes a transition from one continuum state  $E_i$  to another state  $E_f$  with  $E_f - E_i = h \cdot \nu$ , the energy of the laser photon. With this excess of energy, the electron is out of equilibrium and rapidly gives up the energy through collisions with other electrons and with lattice phonons. The short period of time ( $10^{-15} - 10^{-14}s$ ), over which occurs after absorption of a laser photon ensures that the electron gas within the metal never becomes superheated under the radiation, condition that prevail in laser welding [29].

$$\delta = \frac{\lambda}{4 \pi k} \quad (2.2)$$

### 2.2.2 Threshold for conducting welding

A good model for evaluating conduction welding are the Rosenthal equations that use a series of simplifying assumptions: steady-state heat flow, point heat source, negligible heat of fusion, constant thermal properties, no heat losses from the workpiece surface and no convection in the weld pool. The Rosenthal's Two-Dimensional Equation can be applied in welding of thin sheets. Because of the small thickness of the workpiece, temperature variations in the thickness direction are assumed negligible and heat flow is assumed two dimensional. This equation can be used to calculate the temperature  $T(x, y)$  at any location in the workpiece  $(x, y)$  with respect to the moving heat source [15].

$$\frac{2 \pi (T - T_o) \kappa g}{Q'} = \exp\left(\frac{v x}{2 \alpha}\right) \cdot K_o \cdot \frac{v r}{2 \alpha} \quad (2.3)$$

Material	Thermal Diffusivity, $\alpha$ ( $m^2/s^2$ )	Volume Thermal Capacity, $\rho C_s$ ( $J/m^3K$ )	Thermal Conductivity, $\kappa$ ( $J/m s K$ )	Melting Point (K)
<b>SS 304</b>	$5.3 \cdot 10^{-6}$	$4.7 \cdot 10^6$	24.9	1773
<b>Cu</b>	$9.6 \cdot 10^{-5}$	$4.0 \cdot 10^6$	384.0	1336

Table 2.1: Thermal Properties of stainless steel and copper

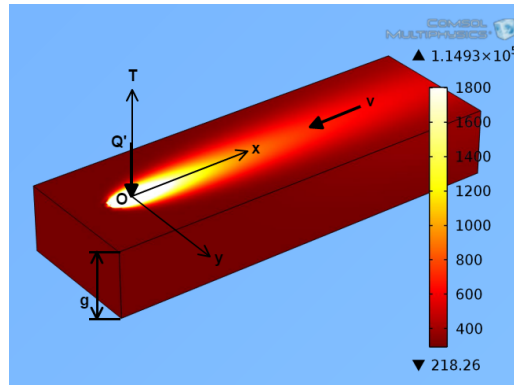


Figure 2.3: Simulation taken as an example of application of Rosenthal's 2D equation that shows the gradients of temperature in a random welding of a sheet [1]-modified

In Fig. 2.3 is represented the coordinate system  $(x, y)$  with origin (O) in the heat source, that is the point of impact of the laser beam in the surface of the sheet of

thickness ( $g$ ) providing an energy ( $Q'$ ). The coordinate system is moving with the heat source at a speed,  $v$ , that matches with the welding speed. Despite this point could be analyse much deeper, the purpose is set the basis for understanding the temperature distribution and the relation with keyhole and heat affected zones that lead to define the quality of a welding.

### 2.2.3 Keyhole welding with fiber laser

Laser beam welding can be performed through two different categories depending on the laser density. These two ways are named conduction-limited welding that occurs in steels for power densities lower than  $1 \text{ MW/cm}^2$  and keyhole welding that takes place for upper values. These modes created by different power densities lead to distinct results.

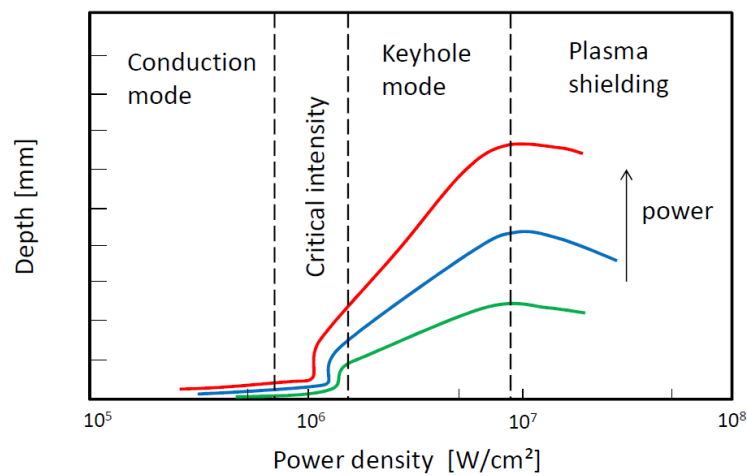


Figure 2.4: Relation between Depth, Power Density and Power with the range of each welding category [20]

**Conduction-limited welding.** The material is only melted and the heat conducts further to the material from the melt pool, which is similar to the arc welding processes. Weld penetration is achieved by the heat transfer of the laser conducting down into the metal from the surface. Weld beads created through this mode look wide and does not have huge penetration [12].

**Keyhole welding.** It occurs when the material starts to vaporize. The recoil pressure caused by the evaporating metal opens a vapour cavity to the molten material. This is called the keyhole and it is kept open by the vapour pressure as the forces caused by the surface tension and hydrostatic pressure of the surrounding molten metal at to collapse the keyhole [11]. A keyhole with a simplified geometry, the equilibrium is maintained if the following equality is fulfilled in all points on the surface of the keyhole ( $r, z$ ):

## 2 Literature review

$$p_v + p_l = p_\sigma + p_g + p_h \quad (2.4)$$

The pressure terms  $p_v$ ,  $p_h$  and  $p_l$  tend to keep the keyhole open, whereas  $p_g$  and  $p_\sigma$  are restoring pressures. All terms have a dependence on depth  $z$  and keyhole radius  $r(z)$ . However, the influence of  $p_l$  and  $p_g$  is small compared with such terms  $p_\sigma$  and  $p_v$ , in addition  $p_h$  is small at low welding speed and can be neglected, therefore it is reasonable to raise the following approximation.

$$p_\sigma \sim p_v \quad (2.5)$$

The fact that in a welding procedure appears the keyhole phenomenon is beneficial because the laser beam is reflected multiple times from the walls of the keyhole and part of the provided energy of the beam is absorbed to the material every time according to the so called Fresnel phenomenon. In full penetration laser welding this means that heat is brought to the joint along all thickness of the material and a narrow weld is produced with high melting efficiency. In keyhole welding the absorption of the beam can be over 90% and the absorption increases as the depth of the keyhole increases since there would be more reflections inside of the keyhole. At the same time Fresnel phenomenon is higher at the bottom of the keyhole than close to the surface so that at the bottom more metal is vaporized and the recoil pressure is higher which counters the increase of the hydrostatic pressure at the bottom keeping the keyhole open all the way. Stability of the keyhole is highly important in order to produce successful free of defects and full penetration welds and maintain a good penetration depth, therefore dynamic of the keyhole is narrowed related to the formation and geometry of eventual defects on the weld seam. Furthermore, closings and reopenings of the keyhole when showed equalities are not fulfilled by many reasons, during the process leads to gas traps inside the molten material which is seen as porosity once the molten material solidifies. It can be avoided by increasing the output power of the laser so increasing the evaporation rate of the material. Inclination angle of the laser beam influences also the configuration and geometry of the keyhole, perpendicular laser beam to the surface leads to a non-tilted keyhole so that the vapour plume is directed perpendicular as well and the force of the vapour jet is much less effective [29].

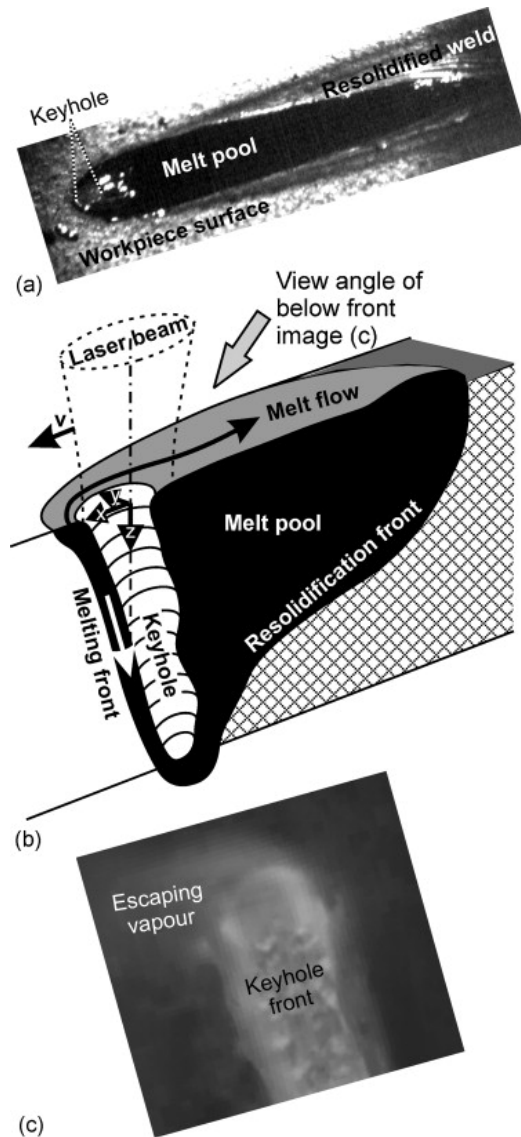


Figure 2.5: Process of keyhole laser welding (a) high speed image of the top surface, slightly tilted from the side as points the arrow in the draw, (b) sketch of a vertical x-z-section of the melt pool and the keyhole and (c) high speed image of the upper part of the keyhole front surface waves also slightly tilted from the rear side [14]

#### 2.2.4 Weld pool and weld properties

As the heat input and the welding speed both increase, the weld pool becomes more elongated, shifting from elliptical to teardrop shaped. Also as increases the welding speed, increases the length-wide ratio, however the influence of this parameter on the weld pool is stronger for low thermal conductivity values, therefore it would be greater for

stainless steels than for copper [15]. The first result that produces the effect of melting is expansion of the surface under the laser beam because of density change associated with the formation of the liquid, there are some models that estimate that value in approximately 10% of the depth of the melt. The thermal gradient causes a surface tension-driven flow of liquid away from the center of the laser beam. This flow is toward the edge of the melt pool for a negative surface tension coefficient, and the flow occurs in a surface layer from the outer part of the melt pool towards the center. Then it is directed into the center of the melt pool and down towards its bottom. This phenomenon based in a mass transfer flow due to surface tension gradient is called Maragoni convection. A microdepression takes place under the laser beam and vortices are generated in the melt pool as well as microconvection cells near the solid-liquid interface ought to the negative pressure arising on solidification [29]. Furthermore, Heiple's Model about Maragoni convection proposed that when a surface agent is present in the liquid metal in a small but significant amount, the surface tension gradient can be changed from negative to positive reversing Maragoni convection and leading to the generation of a much deeper weld pool (Fig. 2.6). This occurs in steel and stainless steel with agents such as S or O. According to the nature of the described convection, the liquid metal carries heat from the heat source to the pool bottom more effectively than for negative surface tension gradients, thus increasing the weld penetration [15].

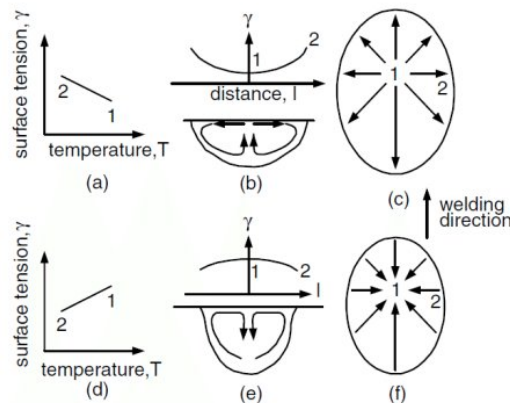


Figure 2.6: Heiple's model for Maragoni convection in a weld pool: (a, b, c) low sulphur-steel; (d, e, f) high-sulphur steel [3]

## 2.3 Broad metallurgical aspects

### 2.3.1 The HAZ

The temperature versus time at a particular point in a metal during and after welding is a critical parameter in determining such factors as microstructure, heat affected zone (HAZ) and tempering. Temperature profile at a particular point in laser welding or so called thermal cycle, corresponds to a rapid rise to a peak value of temperature followed

by a quasiexponential decay. Thermal cycle can be used to infer the effect of welding on the region of the HAZ adjacent to the weld. Heating rate in this region determines grain growth though the dissolution and coarsening precipitates, it determines the thermal history of the HAZ before onset cooling. The final microstructure is determined by this prior treatment and the cooling rate. In steels the HAZ is adjacent to the weld and displays the effect of temperature cycling to a peak temperature,  $T_{max}$ , which is less than the melting point but may be sufficient to initiate other transformations. The cooling rate in the HAZ may be approach 1000 °C/s but varies with the location as does  $T_{max}$ . Normally the width of the HAZ is comparable to that of the weld itself and is a region of altered hardness and variable microstructure. Hardness is dependent on the absorbed energy,  $q$ , and tends to decrease as  $q$  increases. Because the thermal cycle depends on the distance from the fusion zone interface, composition, microstructure and mechanical properties vary over the HAZ being greater the hardness near the fusion zone due to a relative high proportion of lath martensite as expected due to huge cooling rates to presence of acicular ferrite and polygonal ferrite of more than 0.5 mm from the fusion zone interface. A small amount of high-carbon austenite and retained austenite is inferred in all positions. Also there is a narrow correlation between hardness and welding speed, the maximum hardness within the fusion zone is found to increase almost linearly with the welding speed, however the HAZ is virtually independent of the speed [29].

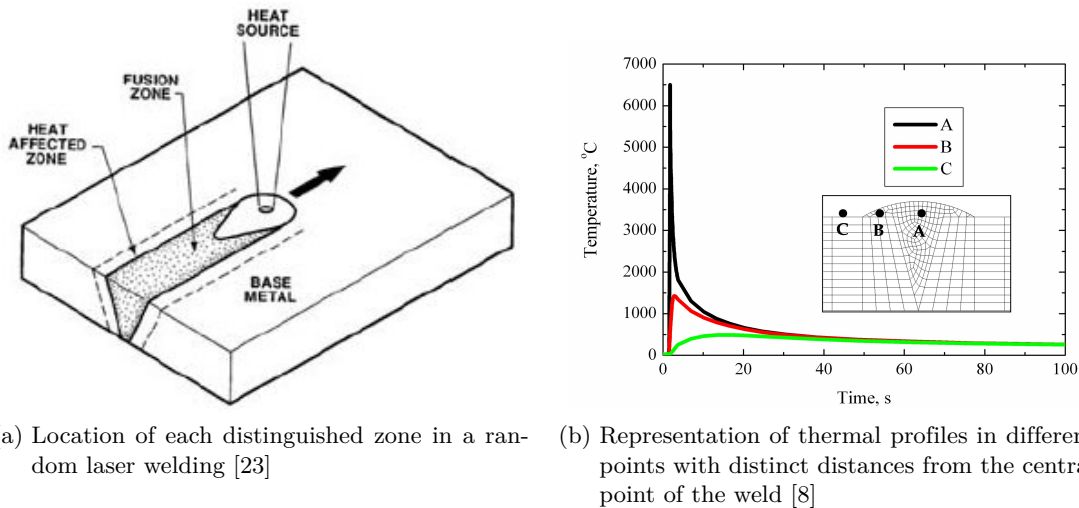


Figure 2.7: Zones in a laser weld and thermal cycle that represents the different cooling rates depending on the distance from the fusion zone

### 2.3.2 The Fusion Zone

The fusion zone contains the region at which the laser radiation is absorbed,  $T(t)$  profiles in general extend to higher temperatures than those existing in the HAZ. If key hole is formed or the surface temperature in a conduction weld reaches the vaporization temperature for an alloy constituent, then selective vaporization can result the loss of minor

elements and therefore can have profound influence on the hardness and mechanical properties of the weldment and additionally changes in phase and redistribution of precipitates. The liberation of volatile elements including hydrogen can result in porosity that may extend over the size range from  $\ll 1 \mu\text{m}$  to macroscopic bubbles. Rapid cooling rates, segregation in the melt and the presence of impurities can lead to solidification cracking in susceptible alloys. In addition, transverse and longitudinal stresses play a major role in cracking but may be minimized through control over the time dependence of laser power input to the workpiece. Liquation cracking or hot tearing also is problematical in many materials and its initiated by grain boundary segregation and enhanced at high cooling rates. The solidification rate,  $v_s$  is related to the welding speed,  $v$ , as follows:

$$v_s = v \cdot \cos \theta \tag{2.6}$$

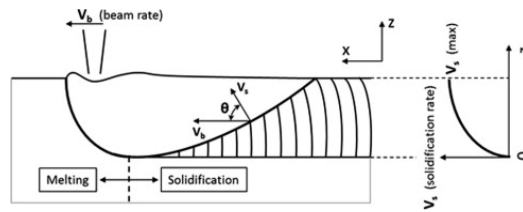


Figure 2.8: Melt pool formation where  $v_s(\text{max}) = v_b$  being  $v_b$  the welding speed [21]

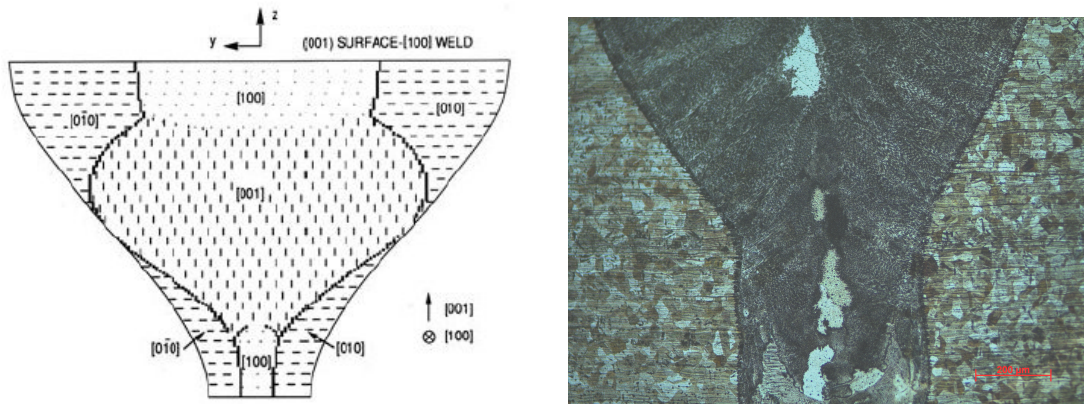


Figure 2.9: Dendrite regions growth of the fusion zone of Sample No. 1

## 2 Literature review

The local solidification varies from the top of the weld to the bottom whereas the solidification front propagates with time from the substrate toward the top of the weld pool. Solidification takes place from the solid-liquid interface into the weld pool and therefore epitaxial growth may take place with grain growth initiated by the grains in the region of the HAZ closest to the fusion zone boundary. In addition, individual grains will have a substructure resulting from microsegregation and are influenced by the solute content of melt. The characterization of the solidification can be performed through  $G/\sqrt{R}$  where  $G$  is the thermal gradient in the direction of solidification and  $R$  is the rate of advance of the solidification front. The microstructure becomes more dendritic as  $G/\sqrt{R}$  decreases while the spacing between dendrites increases with freezing time. The fact that the dendrites grow in the direction of the heat flow gives way to a disoriented grain structure in regions close to the center of the weld pool. The growth of specific grains will be enhanced when the heat flow direction corresponds to the appropriate crystallographic orientation (Fig. 2.9). In polycrystalline materials, grains with the optimum crystallographic orientation relative to the direction of the heat flow will be able to grow efficiently, thus grain growth direction varies drastically among an upper, medium-depth and depth point in the weld section existing a huge influence of the weld pool geometry in determining columnar grain growth. This suggests that weld speed and its relation to thermal properties of the base material are important factors in determining the grain structure in laser welds [29].

## 3 Experimental Procedure

### 3.1 Materials

Specific steel and copper materials were used in order to maximize the quality of the weld without paying too much attention to the final application of the ensemble. More specific applications of this couple are the cooling systems and heat exchangers in order to enhance the heat transfer through the copper, which in turn will reduce the weight of construction. In view to this first assumption, 304 Austenitic Stainless Steel has been selected, provided with dimensions ( $L \times W \times T$ )  $13.5 \times 7 \times 1.5$  mm by the laboratory with an arithmetical mean roughness ( $R_a$ ) of approximately  $0.20 \mu\text{m}$  and Commercially Pure Copper delivered in plates of  $7.8 \times 5 \times 1.5$  mm with a roughness  $R_a$  of approximately  $0.10 \mu\text{m}$ . Due to the available space to fix the samples for the welding procedure as well as the fixation system designed that will be exposed later, stainless steel plates were cut to get samples with dimensions of  $9.7 \times 7 \times 1.5$  mm by using  $CO_2$  laser. Meanwhile the copper ones were used as provided due to the difficulty to cut them by using laser as copper has a very high thermal conductivity and also because it was not strictly required for the proper fixation and later welding procedure.

For the selection has been taken into account the weldability of each material. This feature of both metals is very important because not only is related to the alloy type and composition, but also to the practicality of welding these particular materials together within acceptable conditions regarding to laboratory facilities and posterior production process that it means considering limitations in welding speed, requirements for joint, and so on [29]. In our particular case we have to focus specially on the fact that many desirable dissimilar material combinations create intermetallic regions and segregations of high or low melting point phases that cause brittleness, it means the apparition of weaker zones than either the two materials in the weld. However, according to [2] welding stainless steels within the 3XX series ('3' identifies the steel as an austenitic steel) are highly recommended owing to the excellent quality of the welds, low porosity and good corrosion resistance in comparison with other stainless steel series [29]. Moreover, it is the most common one use in main applications. Furthermore, we can evaluate the weldability of the steel by calculating the carbon equivalent value (CEV), this value is based on the chemical composition of the material and it can be used to evaluate the susceptibility to cold cracking and the formation of martensite that result in an increased hardness at the weld zone [11]. According to International Institute of Welding materials with a CEV below 0.41 are considered to have good weldability and the values can be evaluated as follows:

$$CEV = C + \frac{Mn}{6} + \frac{Cr + Mo + V}{5} + \frac{Cu + Ni}{15} \quad (3.1)$$

### 3 Experimental Procedure

According to Table 3.1, assuming that our steel has the amount of each element corresponding to the superior limit the CEV value would be 0.13, much lower than the one that sets the weldability limit.

	C	Si	Mn	S	P	Cr	Ni	N	Fe	Cu
<b>SS 304</b>	<0.08	<0.75	<2.00	< 0.030	<0.045	18.00-20.00	8.00-12.00	<0.10	Balance	-
<b>Cu</b>	-	-	-	<0.004	-	-	<0.002	-	-	99.9

Table 3.1: Chemical composition of each specimen, wt%

Regarding to copper [29] points out the acceptable quality of the welding in thin sheet with Nd:YAG radiation, claim that we can assume true by using our Ytterbium Fiber Laser, very similar to the Nd:YAG one.

After analysing the weldability of each material separately the next step is prevent possible drawbacks and risks in order to avoid them the maximum possible by choosing proper values of the weld parameters. Looking through literature all references point out the fair quality Duley (1999) [29] or just acceptable quality Amada Miyachi (2016) [2] of the laser weldability of this dissimilar metal combination. First of all we have to take into account that stainless steel and commercially pure copper have significant differences such as chemical composition and thermodynamic properties that it makes dissimilar welding of these materials difficult, the thermal conductivity and thermal expansion coefficient of copper are significantly higher than those of the stainless steel, in fact the main setback of the selected steel is the poor heat dissipation during high temperature service leading the formation of undesirable phases such as sigma phases and chromium carbide precipitation [5]. Luckily, unlike other dissimilar metal joints such as aluminium-copper, welding austenitic steel and commercially pure copper has a great metallurgical compatibility and lack of formation of intermetallic compounds.

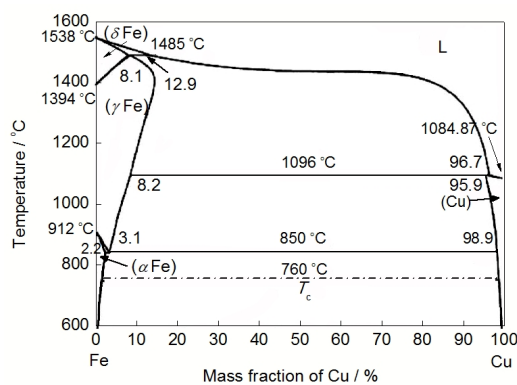


Figure 3.1: Binary diagram Fe-Cu [25]

### 3 Experimental Procedure

If we take a look to the diagram Fig. 3.1, it shows that the iron can be alloyed with copper in all ratios within the limits set in a maximum solubility in  $\delta$ -Fe 6.5%, in  $\gamma$ -Fe 8%, in  $\alpha$ -Fe 1.4% at 850°C. Copper dissolves 4% of iron at 1049°C and 0.2% at 650°C. The solubility is determined by the similarity of the crystal lattices of components, difference in atomic radius and electronegativity value. For instance, Cu, Ni, Co and Fe has a slight difference of atomic radiuses and electronegativity respectively, just point out the close situation of these elements within the periodic table, in fusion welding it means that these materials can be dissolved in each other forming a row of solid solutions [25].

Regarding to corrosion resistance, an important factor in most of the applications we can think about, the galvanic series shows us that austenitic stainless steel and pure copper have a rather similar electronegativity value, fact that is beneficial to reduce the speed of galvanic corrosion. Furthermore, the high content in chromium (18.00-20.00%) guarantee oxidation resistance of the stainless steel by using a passivation oxidation film. Therefore, corrosion should not be a problem that we must face during and after the welding process. Overall and despite the numerous setbacks it can be said that one of the main advantages of this composite structure of stainless steel and copper combines good mechanical properties and corrosion resistance of the stainless steel with the heat conductivity of the copper.

## 3.2 Experimental equipment

### 3.2.1 The laser robot

The welding process was performed by using the Laser Robot available in the laboratory, composed by a laser unit YLR-1500 CT made by the firm IPG Photonics assembled to the head of a six-axis M2004 serie robot produced by ABB Robotics. Both devices are located in a closed room that keep the operator away during the welding process due to the dangerousness of the radiation. The door and other important systems that have to work properly to ensure the safety of the operation have interlocking systems so that the laser cannot operate at least the complementary systems can ensure enough safety. The operator can control both laser and manipulator through a computer unit and look the activity performed inside the room through two monitors connected to two cameras.

The laser unit is a diode-pumped CW fiber laser of near infra-red spectral range (1070 nm) with a output power up to 1.5 kW and water cooled. The focal length is 200 mm due as these lens are installed in the laser. In order to have an idea about some limitations of the laser, mention that the minimum spot size was 120  $\mu\text{m}$ , the fiber diameter was 0.1 mm and according to the features only can provide continuous pulses up to the output power previously mentioned. The communication with the operator during the welding process is carried out through LaserNet software installed in the computer unit and informs about eventual incidences, laser values and parameters, temperature, state of the cooling system among other.

The six-axis robot that moves the laser head during the welding process and therefore is in charge of welding parameters such as speed or orientation, is controlled through a controller unit IRC5 by using a manual or automatic mode. To use the automatic mode,

### 3 Experimental Procedure

firstly is required to program the movements through RobotStudio software installed in the computer that controls and registers the activity of the manipulator. In addition, the manipulator can be operated through a manual operator unit called FlexPendant that in the experiments was used to make controlled simulacres at low speed after programming the movements and before change to automatic mode for the welding process, in order to check the correct movement and avoid eventual collisions of the laser head.



Figure 3.2: In first term the held device, in the background the robot actuator and laser head

#### 3.2.2 The sample fixation system

The design of the fixation system for performing various experiments is an important phase in the test procedure due to the quality of them depends on ensure the reproducibility in order to be able to compare them reasonably and perform them again in the future by other people. At the same time, it is important that the fixation system must be not only functional but also simple in order to ease the fixation and liberation of the assemblies without excessive effort and time. After evaluating the possibilities that the multiple laboratory resources offered, it was came up with the system showed in Figure 5.1 fixing the samples as the photo depicts. For further details are enclosed the drawing plans of the whole system and each of the parts that compose the assembly consisting in 10 elements in total most of them produced by RobotStudio company. In the assembly drawing plans No. 1/7 and No. 2/7 some measures were not included since the purpose is to know precisely the location and orientation of normalized parts and avoid unnecessary represented dimensions for our purpose. The union of the elements with the base is performed by using 7 bolts with hexagonal socket head (*Allen bolts*) reference AS 1420 Metric with a metric of 8 mm and 25 mm length and suitable plain washers reference DIN 125-A. Also for fixing part 7 in base 1 was required use 2 bolts of same type and suitable washers but with a metric of 6 mm. The orientation of the assembly respect the laser robot can be seen in Figure 3.2.

#### 3.2.3 Cutting and polishing laboratory equipment

In order to prepare the welding samples for the posterior analysis samples No. 2, 3, 5 & 6 were cut by using a circular vertical axis saw (Fig. 5.2) to obtain a section of them taking into account which points of the welding bead were apparently most interesting to analyse. That it means, edges were avoided and were selected points located approximately one third and two thirds of the total length of the weld line in most cases. The main drawback of the mentioned saw available in the Laboratory of Laser Technology is that was not enough precise and the disc had a thickness of 1.5 mm. Luckily the quality of the cut was acceptably good yielding to a non-tedious and polishing process afterwards. The polishing process was performed using a disc polishing machine with grained papers P150, P320, P800 and P1200 (designation according to ISO) maintaining them wet to avoid generation of deep scratches in the samples. After improving the quality of the surface in both sides of each sample, they were submerged in Adler reagent (9 g Copper ammonium chloride + 150 ml HCl + 45 g  $FeCl_3 \cdot 6H_2O$  + 75 ml  $H_2O$ ) [22] during 30 s each side and one per one (Fig. 5.8) and finally they were pulled out, cleaned with water, with ethanol afterwards to get rid of the moisture and being dried at the end.

Samples No. 1 & 7 were prepared more suitably with the equipment available in the laboratory of *Institut für Werkstoffwissenschaft und Werkstofftechnologie* (Institute of Material Science and Technology). Firstly, the weld plates were cut in order to obtain two samples of the weld for each one, one that shows longitudinally the weld bead and another one transversally. For this task were used two distinct disc cutting machines with horizontal axis, the first one to obtain the transversal samples and a rough sample of the longitudinal ones with a disc model 10S25 Struers (Fig. 5.4) and the second machine (Fig. 5.7) let us cut accurately the rough longitudinal sample obtained with the previous cutting machine maintaining and controlling a precise offset along the weld line performed with a disc model 10S15 Streuers. This offset measured respect the exact centre of the weld line was removed in the polishing process in order to analyse the exact centre with the microscope. The final result can be seen in Fig. 5.5. The next step was embed the four obtained samples in two mounted transparent thermoplastic cylinders using 20 g of ClaroFast powder per cylinder. Later, they were polished carefully due to two crucial aspects had to be taken into account (Fig. 5.3). In one hand, the offset previously measured must be removed and in the other hand, once it was reached this exact desired plane the quality of the surface had to be the wanted one after having polished the samples with series of proper grained paper. To control both features after using each paper the samples were measured carefully in order to not generate additional defects with a electronic caliper to control the amount of offset removed and the surface quality was checked through an random light microscope.

### 3 Experimental Procedure

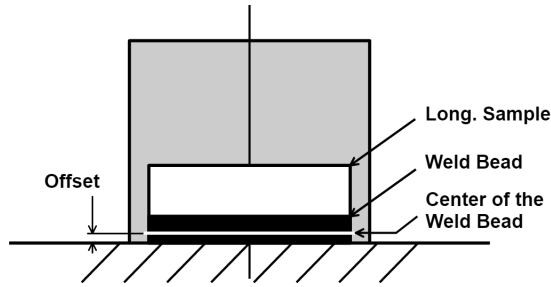


Figure 3.3: Schema of the offset

Offset [mm]	
Sample No.1	Sample No.7
1,4	1,2

Table 3.2: Initial offsets

Polishing	
No. grain	t [min]
P320	5,0
P500	4,0
P1200	2,0
P2400	1,0
Mol 3 $\mu\text{m}$	1,5
P4000	1,0
Mol 3 $\mu\text{m}$	2,0
Nap 1 $\mu\text{m}$	2,0
Chem	3,0

Table 3.3: Number of grain of the papers used and time in the disc polishing machine

#### 3.2.4 Optical Microscopes

The optical microscope used for analysing macrostructure details in Samples No. 2, 3, 5 & 6 corresponds to the one called Zetopan produced by the Austrian company Reichert (Fig. 5.9). The magnification used were objectives of x12.5, x40, x32 and x63 with different apertures. The photos were taken with a camera coupled to the microscope and the program Camera Control Pro 2 installed in a computer. Photos of Samples 1 & 7 were taken using a high quality light microscope produced by Zeiss Axio with remote control movement of the stage and automatic exchange lens system. The objectives used were x25, x50, x100, x200, x500 and x1000 with different aperture values. The photos were taken with a proper camera coupled in the device and the program MetaMorph with several options such as the multilayer one that let take several photos and join them later for obtaining one high resolution image with proper focus of all regions with different depths.

#### 3.2.5 SEM microscope for EDX test

The EDX measurements were performed with a Scanning Electron Microscope (SEM) Quanta FEG 250 (Fig. 5.10), available in *Einrichtung für Transmissions-Elektronomikroskopie* (Center of Transmission Electromicroscope) with the program Edax Team for obtaining the results. However, due to these two samples where mounted in non conductive material, it was required to generate a thin film of 4 nm thick made of Au and Pd in the upper surface in order to allow the movement of the electrons through the samples (Fig. 5.6). This film was generated adding Au-Pd paste connections from the top to the bottom of samples and introducing them after in a vacuum sample preparation device during 5 min.

### 3.3 Process variants and welding parameters

#### 3.3.1 Spatial configuration and first considerations

As mentioned previously, welding steel and copper may have some drawbacks we have to face to. In the process of choosing the most proper welding parameters we have to consider the high reflectivity of copper, specially in the samples that were used with a very low roughness superficial quality. Related to this problem and following the indications pointed out by Kurynstev (2017) [25] in the wake of performing four different experiments in very similar conditions as ours but using butt configuration instead, he reaches to the conclusion that as stainless steel absorbs approximately 35% of the radiation and pure copper only less than 5% while the rest is just missed, it is beneficial to use an off-set of the laser beam onto stainless steel side of 2 mm in order to profit better the energy, ensure a longer interaction of molten stainless steel with copper because steel needs to be in a liquid state for maximum time but at the same time limit the amount of copper dissolved in the molten steel because reducing the melted copper reduces a transition zone created in the welded joint with numerous filler particles near the interface between Cu plate and the intermixing zone, phenomenon that happens due to the penetration of copper into grain boundaries of solid steel and that it is not beneficial at all as indicates [26]. Furthermore, two more disadvantages are avoided. First one, by the fact that not focusing the laser beam directly on the copper plate, according to the very high expansion coefficient and thermal conductivity of copper in comparison with steel, we reduce the possibility to get large misfit strains and residual stresses that it would be appear in the joint leading to solidification cracking of it. The second one, it is the porosity defect very common originated from hydrogen which is highly soluble in liquid copper [4]. Melting points of each metal has to be considered as well, stainless steel 304 serie has a melting point located in between 1400-1450°C and commercially pure copper about 1084°C, it would be beneficial to have the metal with a lower melting point the one which receives the laser beam, however the first observations has apparently more weight. According to our requirements, the weld must be performed in a lap seam configuration, therefore in view of the previous observations and taking into account that both samples have the same thickness, copper plate must be located

below stainless steel plate in order the laser beam just focus on the steel plate and the melted mass penetrates into the copper.

### 3.3.2 Welding parameters

The welding process was performed by creating a straight weld line as can be seen in further sections. Therefore after solving spatial configuration issues, only is needed to define the following parameters: output power, welding speed, penetration depth, focusing, shielded gas and blowing direction of shield gas.

**Laser Power, welding speed and penetration.** The operational range of a laser welding system is the first parameter defined through the relation between laser power and welding speed for a given material and specified weld penetration depth. The Fiber Laser used has a maximum output power of 1,5 kW and maximum speed about 250 mm/s. The three first ones are strongly related according to the following regression equation 3.2.

$$\frac{P}{v \cdot d} = a + \frac{b}{v} \quad (3.2)$$

Metal	Laser	a (kJ/mm <sup>2</sup> )	b (kJ/mm <sup>2</sup> )	r
SS 304	CO <sub>2</sub>	0.0194	0.356	0.82
Mild Steel	CO <sub>2</sub>	0.016	0.219	0.81
	Nd:YAG	0.009	0.309	0.92
Aluminium alloys	CO <sub>2</sub>	0.0219	0.381	0.73
	Nd:YAG	0.0065	0.536	0.99

<sup>a</sup> Units are  $P$  (kW),  $v$  (mm/s),  $d$  (mm).

Table 3.4: Fit Parameters a and b (see eq. 3.2) and Regression Coefficient, r, for Laser Welding Data

Mention that for the welds performed it was used the parameters  $a$  and  $b$  for Mild Steel and Laser Nd:YAG due to their similarities with the Ytterbium Fiber Laser. If we express welding speed in function of depth penetration for an output power of 1 kW according to equation 3.2, that matches power output, welding speed and penetration depth, we obtain the following graph (Fig. 3.4). All these parameter values were selected according to the graphs showed in Figure 3.5. Overall we can appreciate that the conclusions can be reached both following Figure 3.5 or the graph in Fig. 3.4 obtained from the showed equation.

### 3 Experimental Procedure

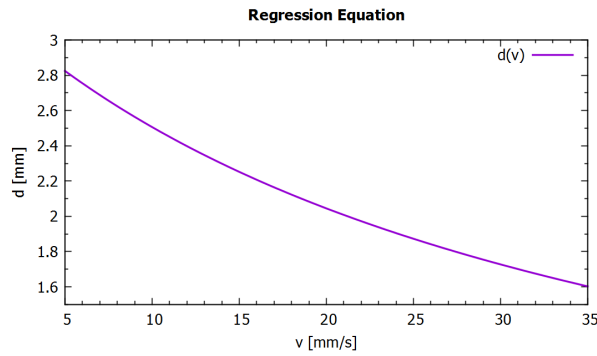
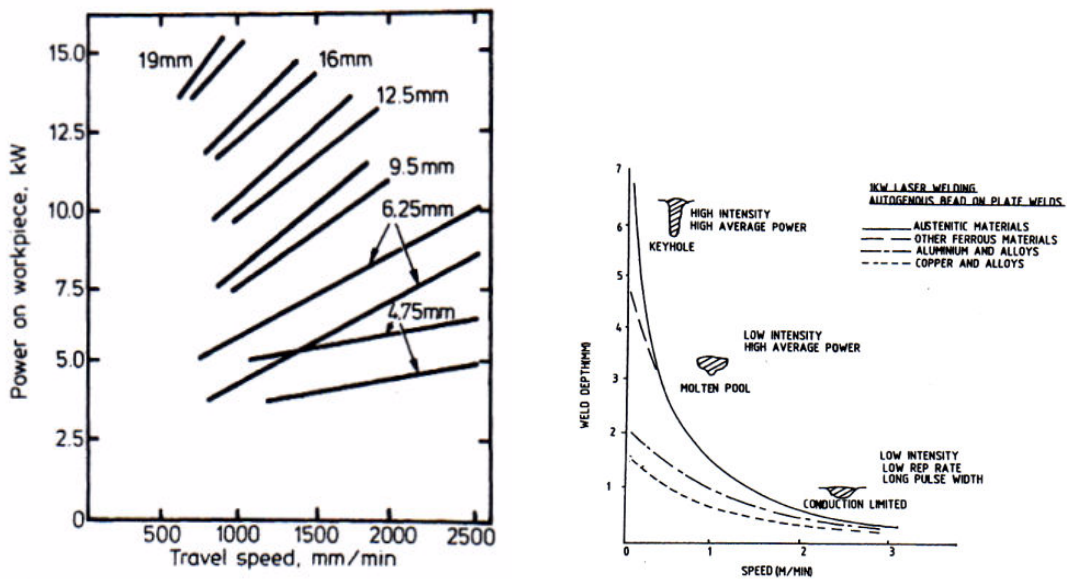


Figure 3.4: Regression equation 2.1, penetration as a function of welding speed



(a) Laser power as a function of welding speed for different thickness mild steel plates      (b) Welding performance of 1 kW Nd:YAG laser

Figure 3.5: Graphs that match power output, welding speed and thickness [29]

**Focussing.** The focal point is the area where the laser beam focused, regarding to this parameter, first we must know where the focus actually occurs, in the laser we use is located 6.6 mm from the head laser. When the diameter of the focal point is taken into consideration, power density and interaction time can be defined as follows:

$$q_p = \frac{4 \cdot P}{\pi \cdot D^2} \tag{3.3}$$

### 3 Experimental Procedure

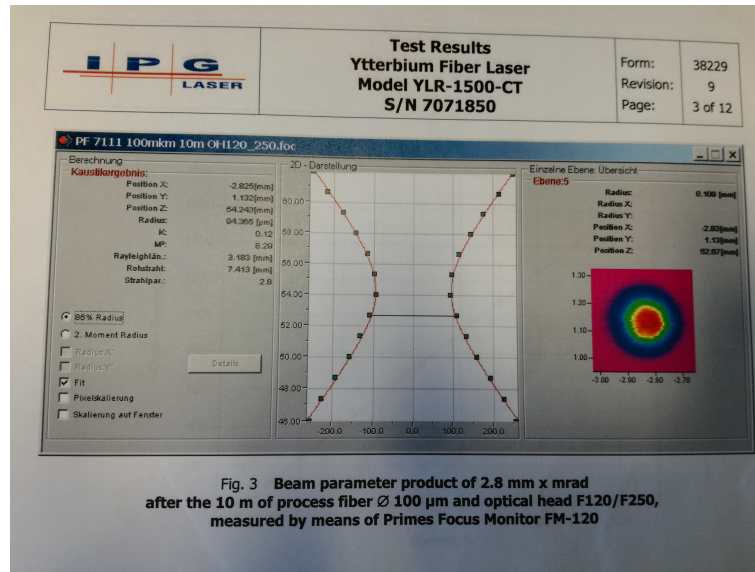


Figure 3.6: Graph obtained from the documentation of the Fiber Laser used

We have to consider that a very high power density and small focal point diameters imperfections such as humping and undercut are produced [11]. Although the laser intensity is highest in the focal plane, it decreases along the optic or laser beam axis in either direction away from the focal plane as the laser diverges. The focussing value is expressed with the f/number and it is positive when the focus plane is below the surface of the workpiece and negative above of it. This number is greater or smaller from zero when the farthest the focus plane is from the workpiece surface. Like other parameters, we have to consider the focussing limits of our laser system, therefore it is important to know that the small size that we can obtain with the Fiber Laser available is 120 µm. However, the expected effects related to the defocussing number are not trivial, according to some literature Duley (1999) [29] or Reijonen (2015) [11] that agree the maximum penetration is not produced when the focal plane matches with the surface, if not when it is located -5 mm in the surface, that it means the beam diameter is more than doubled, this phenomenon is in part ought to the enhancement in multiple reflections. We will return to consider this parameter analysing the samples.

**Shield gas.** The first role of this gas often is to prevent oxidation of the weldment and creation of slag in the vicinity of the fusion zone. The second, and critical one, is to suppress plasma formation in the vapour over the weld zone and to blow away any plasma that may be created in the welding process, the latter role ensures that the laser beam can reach the weld zone with minimal interruption, thus improving weld quality and enhancing the uniformity of such factors as penetration depth and weld bead profile. The most common gases used as shield gases are Argon (Ar) and Helium (He), Nitrogen also can be used as a replacement of He and has many of the same properties but is much cheaper. The main difference depicted in the weld by using one or other gas is that the

### 3 Experimental Procedure

penetration is considerably shallower in Ar gas than He gas [10], however since is being used a fiber laser and the thickness of the samples is not relatively big, the use of ar is enough for our propose. The critical parameters related to the shield gas is the type of gas, the gas flow rate and the nozzle angle and distance from the weld point.

The shielded gas used was Ar with a purity of 99.999% with a flow rate of 20 L/min by using a nozzle of 8 mm of diameter coupled to the fixing system that already was installed in the laser head with the configuration, distances and angular values depicted in the drawing plan No. 1/7 in the Appendix and keeping a distance from the lowest part of nozzle perpendicular to the upper workpiece surface of 1,2 mm.

#### 3.4 Implementation and visual examination

Sample No.	Parameters				
	P [kW]	v [mm/s]	d [mm]	Q [L/min]	f [mm]
<b>1</b>	1,0	25	1,87	20,0	66
<b>2</b>	1,0	20	2,05	20,0	66
<b>3</b>	1,5	25	4,21	20,0	66
<b>4</b>	1,0	25	-	20,0	71
<b>5</b>	1,0	10	2,51	20,0	66
<b>6</b>	1,5	25	-	20,0	71
<b>7</b>	1,0	15	2,25	20,0	66

Table 3.5: Selected welding parameters for each sample and predicted penetration depth in each case

In order to be able to draw consistent conclusions about the quality of the weld according to the welding parameters and conditions, it has been performed seven samples by changing one parameter in each one taking as a reference the first one as shows Table 3.4. For sample No. 6 have been modified output power and focussing at the same time in order to compensate one each other and obtain a reasonable good joint to be analysed afterwards in contrast with sample No.4. In order to ensure the reproducibility apart from the considerations regarding the fixation system, has been used the same pulse profile for all of them with an speed output power of 10 ms both in the on and off of the laser. The output power is delivered constantly with a specific value. The chosen values for the described parameters have been selected according to the reasons depicted but also taking as a reference experiments performed in very similar conditions. In the experiment described in the paper of Li (2017) [16] it is used an Ytterbium Fiber Laser for welding two plates of copper and maraging steel of 2 mm thick in butt configuration setting the parameters to output power of 2000W, welding speed 50 mm/s, without any defocussing, with a slight offset towards steel and using Ar as a shielded gas with a

### 3 Experimental Procedure

flowing rate of 20 L/min. Other articles used as a reference as well have been Weigl (2010) [18] and Chengwu (2009) [4].

On visual examination of the weld bead of the samples in Fig. 3.7 we can easily notice that samples No. 1 and 7 have the most uniform aspect without apparent porosity and defects. The worst objective quality can be appreciated at naked eye in sample No. 4 because was not physically joined due to an excess of welding speed or a lack of output power and sample No. 5 because a defect of welding speed overheated the steel and stainless steel penetrated partially the copper leaking down through it as we can observe by looking at the solidified drops of steel in the opposite surface of the laser beam. At the same time it can be seen in sample No. 3 an appreciable superficial and periodical porosity along the weld line. Regarding to the weld bead dimension samples No. 5 and No. 7 show a wider one due to the notable reduction of the welding speed from 25 mm/s to 15 mm/s and to 10 mm/s respectively. In this first evaluation we cannot draw further conclusions for the rest of the samples excepting for sample No. 6 that shows and inexplicable surface oxidation perhaps due to a slight misalignment of the shield gas nozzle. For reaching further and more convincing conclusions it was decided to analyse the macrostructure and microstructure of the best and the most interesting two samples mentioned No. 1 and No. 7 in the Institute of Material Science and Technology by using a high resolution optical microscope. Samples No. 2, 3, 5 and 6 were analysed in *Institut für Fertigungstechnik und Hochleistungslasertechnik* (Institute of Engineering Production and Laser Technology) by using a random optical microscope. Sample No. 4 was simply not analysed due to the lack of valuable results that can provide a non joint sample with even wide zones without weld bead. The exact preparation process of the samples can be read in the section Experimental Equipment.

### 3 Experimental Procedure

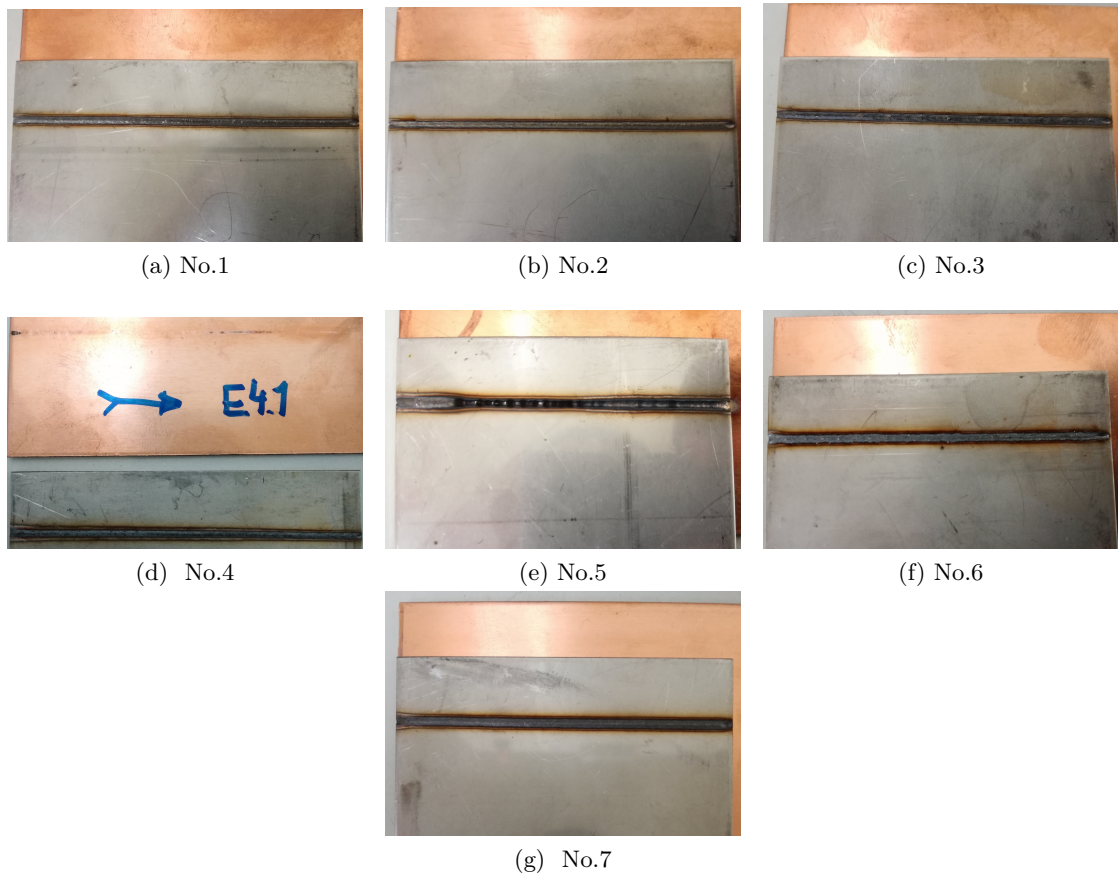


Figure 3.7: Weld bead of each of the 7 samples obtained. From now forwards, in all photos showing a welding bead, direction of welding goes from left to right side of the picture

## 4 Experimental results

### 4.1 Nature and characteristics of the samples

Considering the selected welding parameters depicted in Table 3.2, and from the photos taken (Fig. 4.2) it can be seen rapidly that all samples except sample No. 6 and presumably sample No. 4 due to the complete lack of penetration, correspond to the keyhole welding category. The other two samples due to its proximity to the limit value that set the difference between the two types of welding categories set around  $1 \text{ MW/cm}^2$  are in the transition between these two types. For instance using equation No. 3.3 and knowing that the laser beam with 5 mm of defocussing has a diameter of 0.35 mm, we obtain a delivered power density of  $1.55 \text{ W/cm}^2$ . In Fig. 4.2(d) it can be seen that sample No. 6 shows the typical features of a conduction-limited welding even though in one side could be observed the root of a incipient keyhole since, however a width and non-depth melt pool is the highlighted characteristic. Regarding to other features it is highly appreciable that sample No. 3 (Fig. 4.2(b)) and especially in sample No. 5 (Fig. 4.2(c)) has a wider and deeper fusion zone in comparison with sample No. 1 (Fig. 4.2(a)) with indices of turbulence since the interface shows swirls in many points may it cause because a higher output power was used (1.5 kW) and a much slow welding speed was implemented (10 mm/s), respectively, making the viscosity lower and therefore the liquid in the melting pool much more fluid and vulnerable to turbulences. Samples No. 1 & 7 were extensively analysed, in some regions of the longitudinal weld bead samples the flow lines of the melt according to Maragoni convection can be perceived since a non perfect alignment of the cut plane with the central line of the seam shows it (Fig. 4.1). Mention that focussing in fusion zone of samples No. 1 & 7 (Fig. 4.2(e, f)), sample No. 7 presents a wider fusion zone that No. 1. due to the higher influence of a lower welding speed.

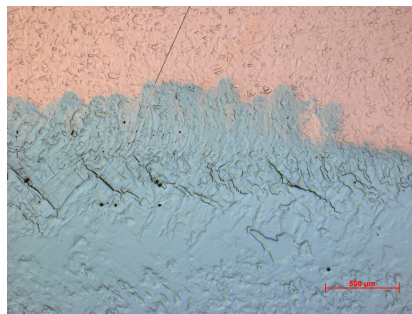


Figure 4.1: On the left of the photo melt flow currents of steel going up can be clearly seen as in the right not due to the misalignment of the surface cut plane and the central weld line

#### 4 Experimental results

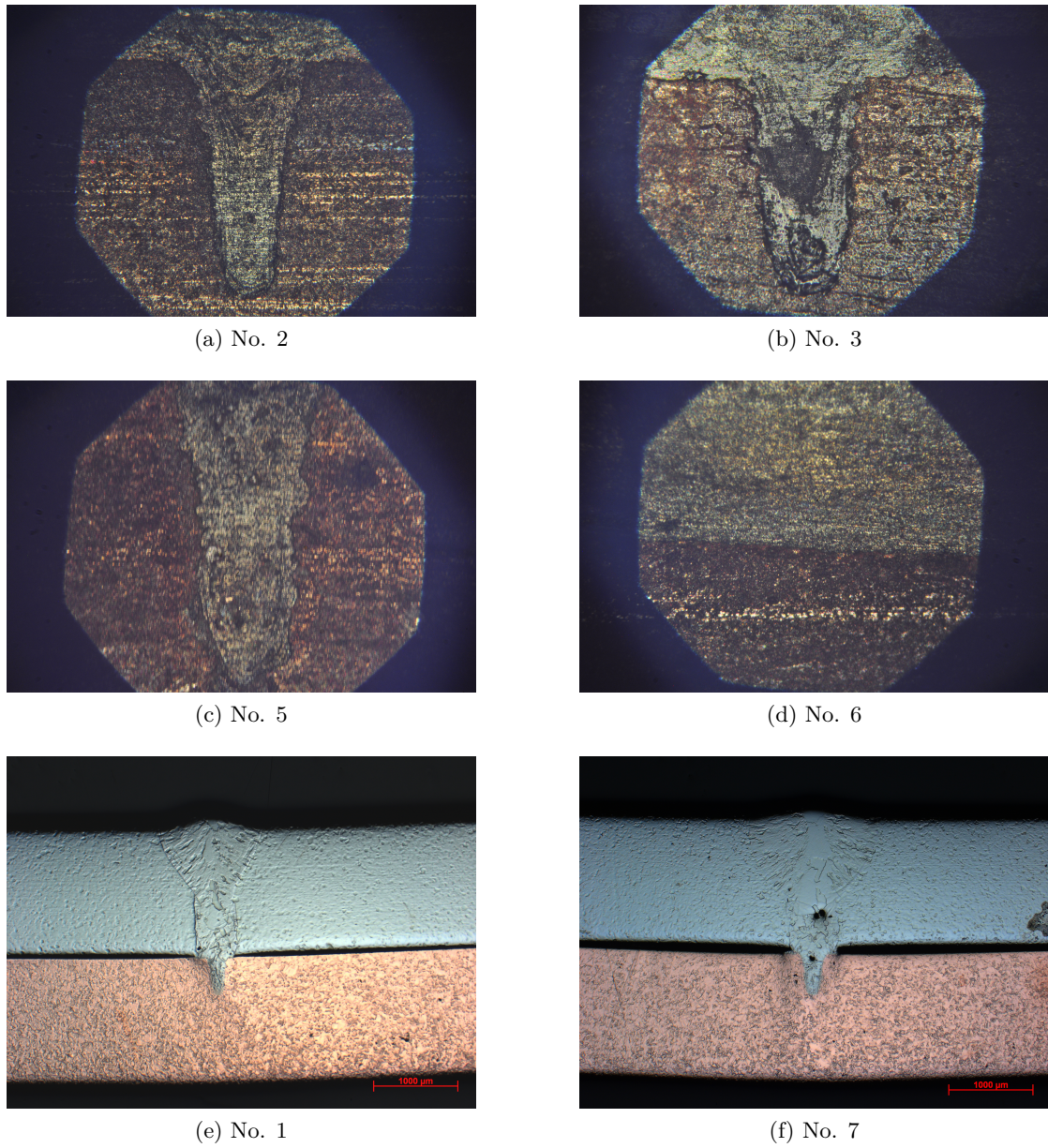


Figure 4.2: Transversal view of the weld seams of each sample obtained with a magnification of x12.5 using Bertrand lens for better contrast (a, b, c, d) and with a magnification of x50 (e, f)

## 4.2 Macrostructure of laser beam welds

In laser welding, a variety of defects or imperfections may occur depending on the kinds of material and their compositions, welding conditions and so on. In laser welding we can distinguish three main characteristic groups: geometrical or appearance defects, internal or invisible defects and property or quality defects.

### 4.2.1 Geometrical or appearance defects.

**Laser welding deformation or distortion.** This category includes distortion or deformation, residual stresses or even cracking of the weld joint due to volume changes of thermal expansion and contraction produced by the thermal cycles. In thin plates or sheets with great thermal expansion, welding deformation takes place easily like in sample No. 7 (Fig. 4.2(e)) showing a relative wide gap between copper and steel plates due to the physical constraints imposed by the designed fixation system that made especially the steel plate to buckle. It has a higher thermal expansion coefficient than copper. Mention as well that it is a defect difficult to avoid. If we compare with sample No. 1 (Fig. 4.2(f)) we can see rapidly that the gap is much narrower due to the input heat was much less larger as can be seen in Table 3.4. It is true that some complex and costly methods can reduce even eliminate this phenomenon such as rapid cooling or quenching of the welded part and its vicinity just after the molten pool, keeping welded products cooled to room temperature in the fixture, formation of a parallel full-penetration weld bead or improve the fixation system and make it more robust. However, luckily the deformation and distortion is much smaller in laser welding than in other fusion welding procedures since the heat input and bead width of laser are generally smaller and narrower, respectively, than those of any other welding process. This defect it is an indication that constrained dilatation and therefore stresses may favour hot cracking in the welding and it is analysed in Hot cracking section.

**Poor surface appearance of laser welds.** The surface of the laser weld and surroundings is exposed to high temperature during laser welding process and despite of the use of shielding gas to protect the molten pool and its vicinity from oxidation, some degree of oxidation occurs from the deposition of ultrafine particles produced by evaporation or spatters of melt particles. This effect was detected in Sample No. 6 (Fig. 4.3). Despite may it is not perceptible in photos of Fig. 4.2(d), sample No. 6 presents some spatters in both sides of the laser weld surface probably provoked by the high output power and defocussing of the laser beam. In continuous wave (CW) laser welding some reasonable measures can reduce this phenomenon like adopting an extremely small beam spot in comparison with the molten pool size, enlargement of the keyhole inlet by a proper flow of shielding gas or a forward inclination of the laser beam.

**Burn-through or melt down.** Burn-through is a phenomenon that consists of the melt in a molten pool is dropped down during welding to form an underfilled bead with concave top surface and convex bottom surface (Fig. 4.4b). It happens in full penetration

#### 4 Experimental results

welding of plates and thin sheets with wide bottom surface as in the analysed samples. It occurs more readily in materials with lower surface tension. In stainless steel plates it mainly takes place with high output powers, with a lack of oxygen in the keyhole so that produces a full penetration weld. Melt lower temperatures near the bottom rear end of the molten pool with a low content of oxygen has such high surface tension to pull the higher temperature liquid near the keyhole tip resulting in the formation of bottom humps as happened in sample No. 5 (Fig. 4.4a) due to the reasons given as can be seen in Table 3.4.

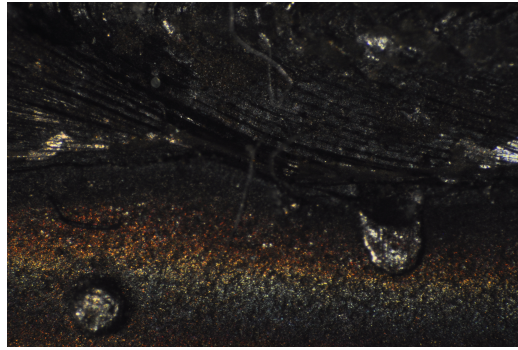


Figure 4.3: Spatters detected in both sides of the seam in sample No. 6

**Humping.** It is the periodical formation of humps of weld metal on bead surface as has clearly sample No. 3 and slightly sample No. 6. This phenomenon may occur in a narrow weld bead with a very small focused beam during high speed welding and it is owing to the backward flow of a melt ejected by plume ejection and the high surface tension of the accumulated melt due to molten pool width. Despite can be suppressed by defocussing the laser beam as was done largely with both samples, an excess of speed could be the reason why still humping occurred.



(a) Burn-through phenomenon detected



(b) Underfilled bead caused by the meltdown defect

Figure 4.4: Burn-through effects in sample No. 5

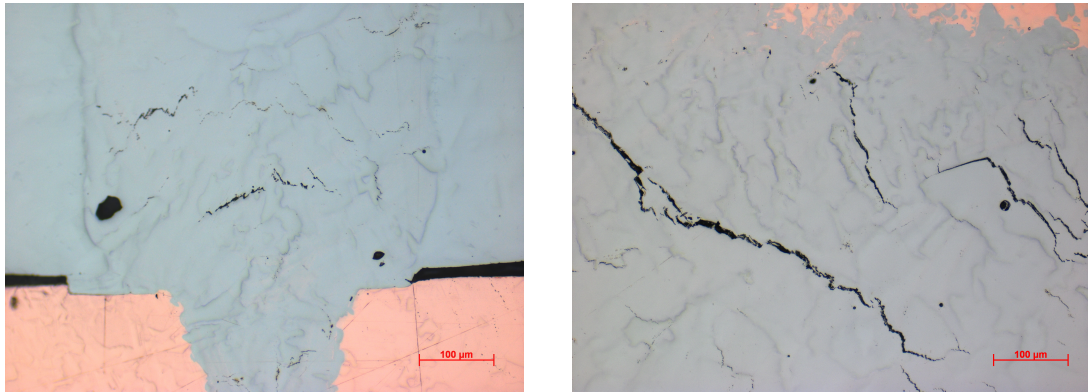


Figure 4.5: Image of one hump, it can be appreciated the drastic change of the seam appearance. These periodical humps were distanced approximately 5 mm one each other in sample No. 3

### 4.2.2 Internal or invisible defects.

**Hot cracking.** Also called high temperature cracking in the weld fusion zone and the HAZ is called *solidification cracking* and *liquation cracking* respectively. In austenitic stainless steel it occurs along the grain boundaries and it was detected in both two samples No. 1 & 7, analysed with a sufficient magnification lens. In particular, solidification cracking can occur easily during high speed welding with CW laser. The causes are attributed to microsegregation and resultant formation of low solidification temperature liquid films along the grain boundaries. In mild tensile strength steels as considered austenitic ones, hot cracking or pear-shaped cracking may take place near the middle or bottom part of a partially penetrated deep weld bead (Fig. 4.6b) made with relative high power. Some cracks, specially in sample No. 1 are filled with copper as can be seen in the crack of Fig. 4.7. The causes may be ascribed to the formation of retained liquid areas due to the melt flows near the bottom part of the laser and it is highly common in welding dissimilar materials due to the high cooling rates of copper and residual strengths [25], may generated by the fixation system and constrained dilatation of the assembly and also but presumably to a lesser extent, due to some intermetallic compounds formed. Despite the very low concentration of S and P, they are the main culprits of the existence of these compounds [19].

#### 4 Experimental results



(a) Solidification cracks in the weld fusion zone of Sample No. 7 (b) Hot-cracking detected along the weld bead of sample No. 1. It can be perceived how most of them surround the grains (intergranular cracks) and as exposed happens in the middle of the weld bead.

Figure 4.6: High temperature cracking and solidification cracking detected in both samples No. 1 & 7



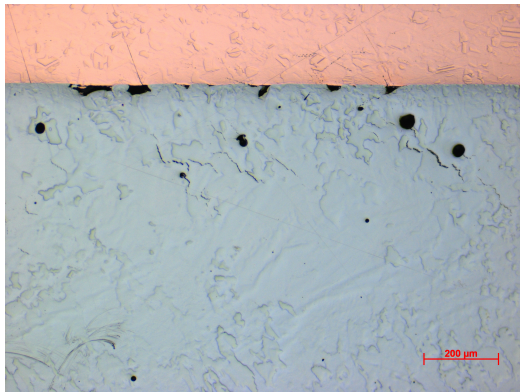
Figure 4.7: Some liquation cracks detected on the bottom of the photo and in the HAZ of sample No. 1.

Despite the high sensitivity to the hot cracking, the cold cracking is not a problem since austenitic steels are not susceptible to cold cracking [7]. To support this fact mention that no rests of hydrogen in any region has been found in the EDX measurements.

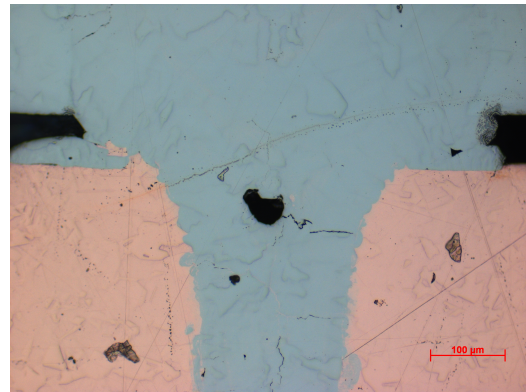
**Porosity.** It refers to blowhole, pore, wormhole, pit or bubble. This defect is very easy to be formed in laser welding, in the keyhole type of deep penetration welding, the majority of bubbles, which are generated from the tip of a keyhole during welding, lead to the formation of porosity in weld fusion zone. It has been observed extensively in samples No. 1 & 7 showing pores of 30-50 µm mainly and despite it is complex to avoid, using a proper selection of shielding gas flow rate for eliminate suitably hydrogen

#### 4 Experimental results

and oxygen sources, inclination of the laser beam or creation of a stable conical-keyhole or even the formation of a heat-conduction type welding are some measures to control porosity. However, clearly sample No. 1 has much lower porosity than sample No. 7 as can be perceived in Fig. 4.2(e, f) due to the welding speed in this last one was much lower (15 mm/s). In Fig. 4.9 a longitudinal weld bead area of approximately 5.5 x 3 mm is considered, in the photo of sample No. 1 can be counted until 3 pores of about 50  $\mu\text{m}$  whilst in the photo of sample No. 7 can be counted 9, that it means that overall sample No. 7 has slightly more porosity.

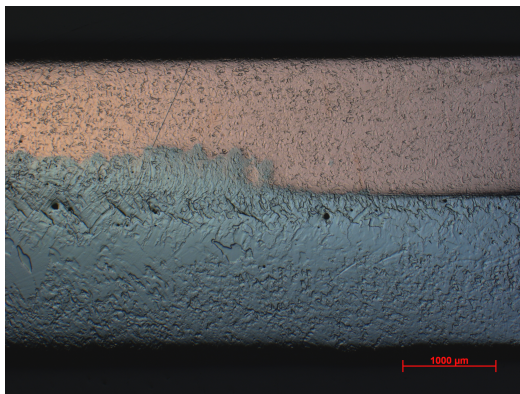


(a) Angular pores in the interface between stainless steel and copper plates probably generated due to rests of organic material (f.i. grease) that evaporated and left these non-round pores

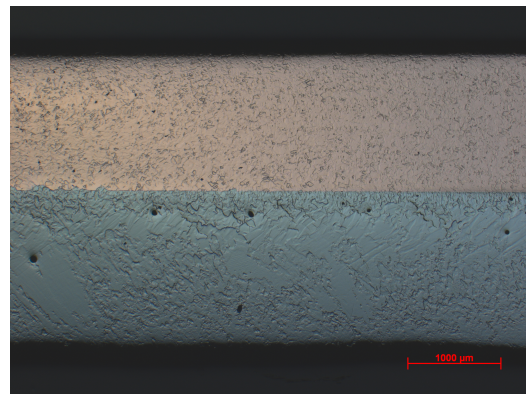


(b) Central pore with a scratch initiated in it and few inclusions. The brown line upper the pore was generated due to preparation of the samples, this defects are characterized by regular patterns such as fine lines and highly aligned and very small dark dots

Figure 4.8: Different kind of defects in laser weld beads



(a)



(b)

Figure 4.9: Number of pores detected for a same arbitrary area located far from the edges with two photos taken with 25x magnification. There are much more hot cracking in sample No. 1, though

**Inclusions.** A particular defect observed in samples No. 1 & 7 is the presence of angular pores of 60-70  $\mu\text{m}$  along the weld bead in the interface between stainless steel and copper plate but in the side of the steel (Fig. 4.8a). It can be provoked by rests of grease despite all samples were cleaned with ethanol before the laser welding process. In some other regions has been detected very small circular pores in the steel just in the interface as well, due to the very linear distribution, they could be created from the air trapped between the two plates owing to the existence of an obvious gap between the plates. Inclusions has been observed as well (Fig. 4.8b) characterized by no-regular colourful dots in steel and copper regions near the weld bead.

**Macrosegregation.** It is present in the weld fusion zone in the case of laser welding dissimilar materials and can be detected immediately with EDX measurements. It will be analyse deeply in the diffusion phenomena point.

**Microsegregation.** Necessarily occurs due to the solidification process in fusion welding of alloys. It can be detected with EDX measurements and consists of segregation at micro scale along cellular dendritic boundaries, it can be observed in Fig. 4.7 as small circular dots in the fusion zone. As a result the solidification temperature of the melt falls during solidification leading to the occurrence of solidification cracking and degradation of the strength of the weld joint. It is effective to prevent through solid solution heat treatment of the joint after welding.

### 4.2.3 Quality or property of defects.

The presence of defects reduce the mechanical properties in general. Nevertheless formation of harder phases such as lower bainite and martensite the hardness is higher than those of the base metal and it does not mean that is necessarily good (embrittlement). A rather common defect such as porosity that always leads to a reduction of strength and strain and can be avoided by increasing the welding speed. In terms of fatigue strengths and hybrid weld joints are generally higher than those of other fusion welding processes. In some steels, failures like stress-corrosion cracking and boundary corrosion may take place in the HAZ. Selection of proper materials depending on the specific application and an accurate process is crucial to increase the lifetime of the weld and avoid a chemical degradation such as the precipitation of carbides in the HAZ of austenitic steels that promotes corrosion starting in grain boundaries.

## 4.3 Microstructure and diffusion of laser beam welds

In laser welding of austenitic stainless steel, solidification structure strongly depends on welding speed from obtaining microstrucutres consistent with primary ferritic solidification structure in the weld zone at low welding speeds to obtain essentially austenitic microstructure with high tendency to hot cracking at high welding speeds. However this effect is appreciable for large differences between implemented welding speeds (f.i. 4

## 4 Experimental results

mm/s and 20 mm/s) and therefore it could not be seen in the analysed samples. Firstly it is important to consider the microstructure of base materials.

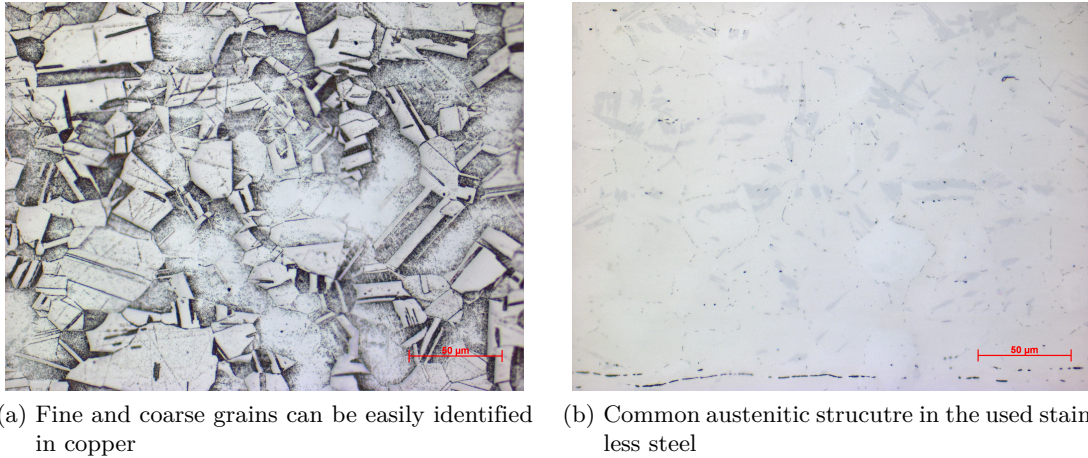


Figure 4.10: Base materials, commercially pure copper and austenitic stainless steel with a magnification of 500x

Fig. 4.11b corresponds to a view of the boundary of the fusion zone with the HAZ of the stainless steel of sample No. 1. The interface between the HAZ and the fusion zone can be identified rapidly because of presence of a vein of martensite along the border as black non-aligned lines (marked as 3). Formation of this microstructural element is common in locations where the highest thermal gradients occur such as the boundary of the fusion zone and in the centreline of the weld as well [29]. At the same time, it can be detected that, specially the fusion zone, is covered by equal-distributed circular black dots within the fusion zone owing to the oxidation of the surface despite of being cleaned with ethanol the surface after each procedure as described. Also, copper globules can be seen and specially near the cracks in the austenitic dendrites of the fusion zone due to the low solubility between iron and copper at solid state [5]. Dendrites (2) can be easily be observed growing from the upon-right corner towards the lower-left corner of the photo, despite there are also minor regions of cellular grains (1). In any case, dendrites show a bright aspect and are surrounded by a black contour. According to the chemical composition of the austenitic stainless steel used (Table 3.1) and the EDX measurements, despite they were performed in interface regions, but some of them like *Bereich 2* - Area 2 of sample No. 7 QS (Fig. 4.16) shows a very low content of copper and expected values of alloying elements it can be concluded that austenitic stainless steel is about 70 wt% Fe. For this Fe content, corresponds the pseudobinary of the Fe-Cr-Ni ternary system depicted in Fig. 4.11a. According to the content of Cr and Ni, they fall into  $\gamma$ -region, that it means that dendrites are composed by austenite ( $\gamma$ ) that is the primary solidification phase surrounded by  $\delta$ -ferrite that are black particles surrounding the bright austenitic dendrites that forms when the three-phase triangle is reached during the terminal stage of solidification. These are called *interdendritic ferrite* [15].

## 4 Experimental results

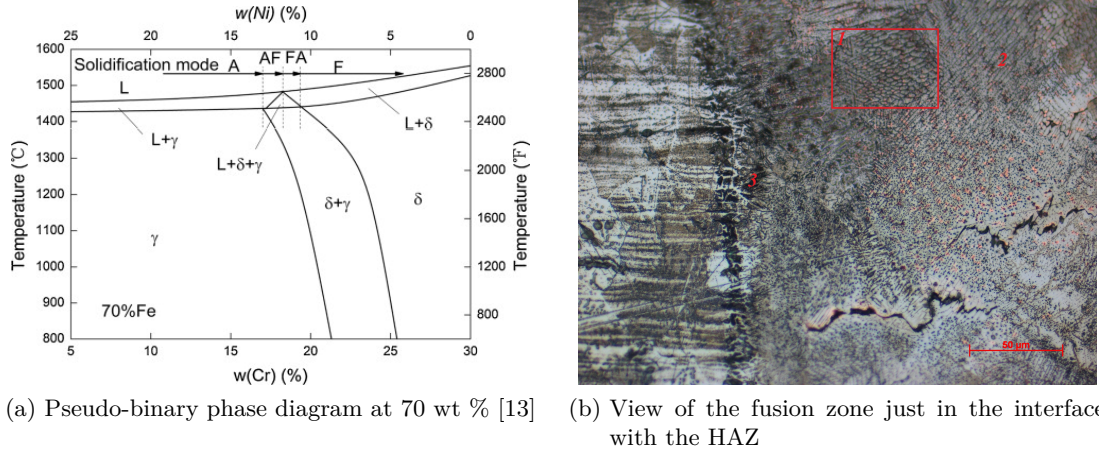


Figure 4.11: Primary austenite solidification and postsolidification transformation in Fe-Cr-Ni weld

In other regions, such as the weld centre and weld face there are equiaxed dendritic structure mainly (Fig. 4.12a), similar weld structure is reported in Roy et al. (2014) [5]. In the longitudinal samples it can be perceived the opposite effect than the showed with Cu in Fig. 4.11b and that is globules of steel embedded in a copper matrix in the intermixing zone generated by the penetration of steel into Cu matrix promoted by the turbulent-bursting behaviour of the keyhole that leads Maragani current to drag copper to the top of the weld bead. Since conductivity of copper is higher than the steel, solidification of the liquid metal in the weld pool will start from the fusion zone on the copper side, leading to the generation of this intermixing zone [4]. Regarding to interface microstructure, it can be seen a large amount of granular phases (within the red squares in Fig. 4.12b) due to interaction of stainless steel and copper in the liquid state in the interface region [25]. However, it can not be seen due to the low magnification, according to Chengwu et al. (2009) [4] they have diameters of 0.1-8.0  $\mu\text{m}$  and are composed mainly by Fe and Cu and Fe may be Fe-rich bcc solid solution ( $\alpha\text{-Fe}$ ) and Cu is the Cu-rich fcc solid solution (often called the  $\varepsilon$  phase). However, the performed EDX analysis of this structure such as *Bereich 2* - Area 2 of Sample No. 1 LS showed a high content in Fe (70.5%) than Cu (16.8%). These  $\varepsilon\text{-Cu}$  phase increases the strength of the welding, however in excess is harmful due to its intrinsic brittle character would overwhelm its beneficial effect on the toughness [16]. However the EDX measurements performed in those regions show that only a little amount of Cu is diffused into the intermixing zone that indicates again that the dilution ratio of the Cu is very limited despite the fact that according to lap configuration and nature of the welds the keyhole penetrated the copper plate, however absorption occurs in a depth  $\delta$  that according to the presented equation 2.2 and considering that  $k$  for metals typically is 1-10 and  $\gamma = 1070 \text{ nm}$ ,  $\delta \sim 10^{-6} \text{ cm}$ . Thus and the fact that Maragani stream of melt steel surround copper during the process explains that copper received only heat from the steel flow.

#### 4 Experimental results

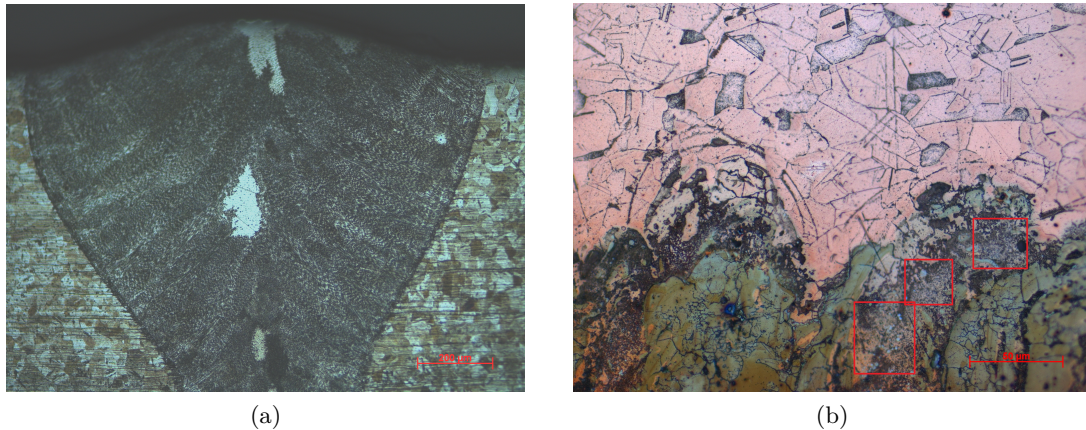


Figure 4.12: (a) Weld centre and weld face microstructure and (b) microstructure in the weld interface of Sample No. 1

Regarding to the HAZ of the copper side it can be observed from Fig. 4.11b and Fig. 4.10a how in the first one grains are much bigger in the first photo than to those of the metal base of the second photo considering that both were taken using the same magnification. Coarse grains close to the interface are integral, indicating that copper does not melt during welding and there is a rather rough morphology between copper and fusion zone, like liquid phase is frozen rapidly. However the raise in temperature leads to the recrystallization of copper in the solid state, causing significant grain growth. The fluid flow of the molten pool is very strong during laser welding, thus the liquid metal has a strong force acting on the interface of copper that becomes scraggly because copper became very soft at a high temperature. Subsequently, this scraggly morphology is frozen rapidly due to the rapid cooling induced by the high thermal conductivity of copper. Furthermore, this scraggly interface morphology is beneficial to improve the mechanical property of the joint. Actually, Fig. 4.11b show a really similar structure to the obtained results for butt joint though of Chen (2015) [24].

Going deeper into diffusion processes it has been detected that sample No. 1 depicts wider interface region than sample No. 7 as can be seen in Fig. 4.13. Also EDX measurements reported an overall higher diffusion in sample No. 1 that can be perceived not only in the wider interface region and highly mixed aspect of two metals but also in far points such as *Bereich 3* - Area 3 of Sample No. 1 QS (Fig. 4.16) located in the extreme of the interface zone in the side of the steel plate but still having a considerable content of Cu (24%) meanwhile analysed areas in sample No. 7 QS (Fig. 4.16) are much closer one each other and located around the well defined interface but clearly *Bereich 2* - Area 2 in the side of the steel has 63.8% Fe and *Bereich 3* - Area 3 in the side of copper has 93.3% of Cu. Broadly the results show a much less solubility and diffusion in sample No. 7. However this phenomenon is against expected since the welding parameters are the same but the welding speed is higher for Sample No. 1 (25 mm/s) than sample No. 7 (15 mm/s) higher heat transfer would increased the diffusion

#### 4 Experimental results

process and also decreased the viscosity of the melt favouring the mix of both metals. On the other hand, it is true that macrostructure defects does not contradict the theory since sample No. 7 shows slightly more pores. Two parameters that could play some role in this observed phenomenon are the efficiency and the gap dimension between plates. There are many researches that conclude that melting efficiency, that is the ratio energy required to create a molten pool from heat energy supplied to the energy absorbed by the work piece, through conduction and melting of the substrate is greater at higher welding speeds, thus the total power absorbed by the material increases with increase in welding speed [27], logically this possible influence must be taken into account carefully and only if the rest of parameters and conditions, as seem to be, are the same between the samples. Regarding to the gap existing between the two plates, naturally a wider gap leads to a worst heat transfer between the plates, as copper has a much higher thermal conductivity value the presence of air in between reduced drastically the heat transfer from steel which receives the impact of the laser beam and therefore the heat source, to the copper. The fact that sample No. 1 shows an appreciable narrower gap would have let a better energy transfer towards copper and therefore a higher temperature at the lower part of the weld bead, where are taken photos of Fig. 4.13 leading to a higher fluidity of steel and greater diffusion phenomena as well, and as a consequence a wider interface region than the one observed in sample No. 7. However, for analysing this fact Rosenthal Two-Dimensional is not valid any more being necessary to approach a Three-Dimensional model.

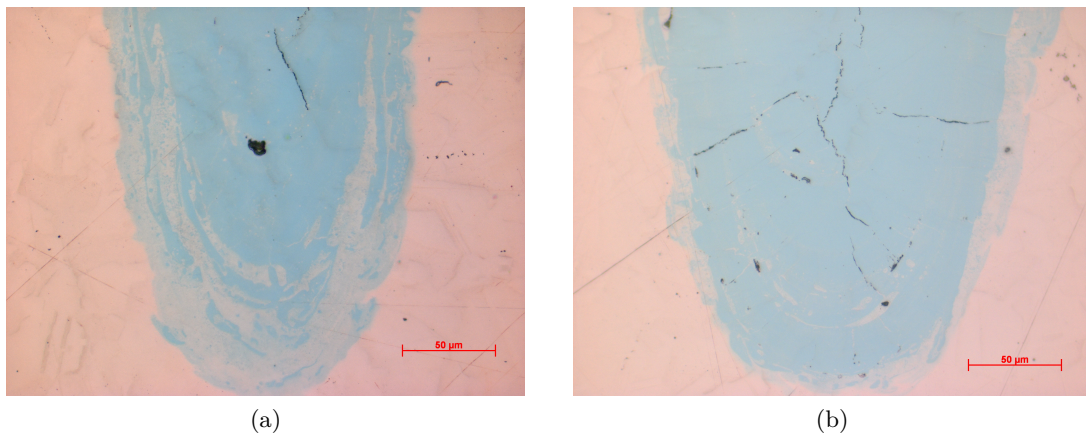


Figure 4.13: Interface region at the bottom of the weld seam within copper plate where it can be perceived the higher mixing rates in sample No. 1 (a) than sample No. 7 (b). They were taken before submitting them into the etching solution

It is important to consider the rest of the elements and its proportion detected. In general, values are the expected ones, the presence of gold and palladium is due to the generation of a conductive film using these elements as described in 3.2.5. Content of C and Si is much higher considering the expected chemical composition of the austenitic stainless steel used but it may be due to contamination through polishing process as grained

#### 4 Experimental results

papers are made with silicon carbides. Furthermore in some regions such as *Punkt 1* - Point 1 and *Punkt 2* - Point 2 of sample No. 1 LS (Fig. 4.14) there are rests ( $\sim 0.2\%$ ) of Vanadium, unexpectedly rests of Calcium ( $\sim 0.3\%$ ) are detected in *Bereich 1* - Area 1 in sample No. 7 QS and *Bereich 2* - Area 2 of sample No. 1 LS maybe due to contamination from rests of previous samples polished with the same naps. Also it is interesting to observe the different quantity of chromium and nickel in each sample. Sample No. 1 has about 10% Cr and 5.5% Ni and sample No. 7 has around 15% Cr and 7.5% Ni considering that are analysis performed in interface regions but nevertheless indicating higher content of Ni and Cr for sample No. 7 in all points and areas.

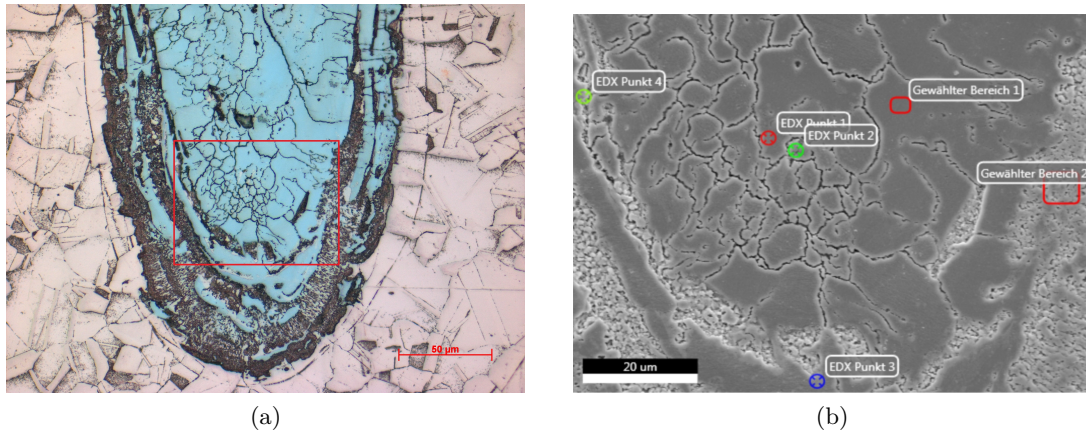


Figure 4.14: (a) view of the bottom of the weld and interface region of sample No. 1 and (b) location of the analysed points and areas with SEM method

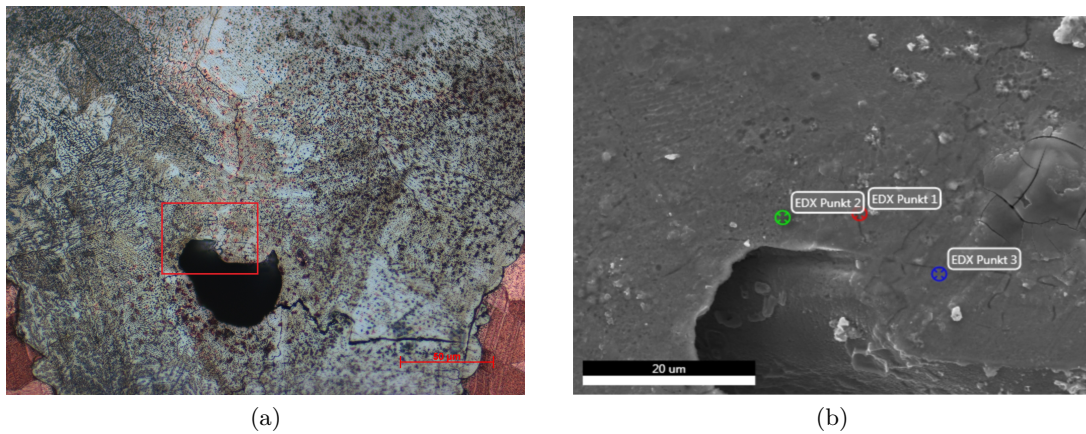


Figure 4.15: (a) view of the central part of the weld near the main pore and (b) location of the analysed points with SEM method

## 4 Experimental results

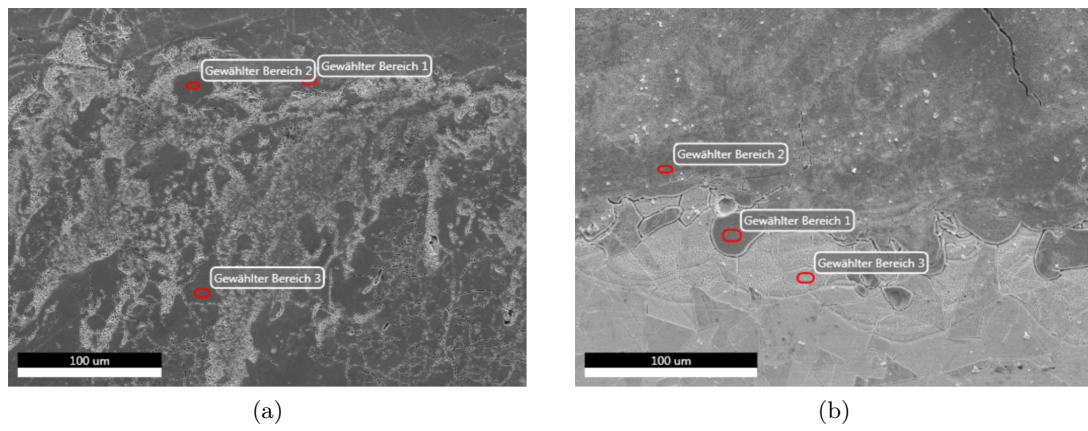


Figure 4.16: View of the points and areas analysed in the longitudinal samples (a) No. 1 and (b) No. 7. The clear areas corresponds to copper, the clear grained ones to the mentioned Cu- $\epsilon$  phases and the dark zones to the steel

## 5 Conclusions and Outlook

Based in the investigation conducted regarding to the laser welding of dissimilar metals such as copper and steel, the following are concluded for contributing to the optimization of the process and ensuring a general good quality of the weldment:

1. For these pair of dissimilar metals, in lap configuration, austenitic stainless steel must be the one which receives the laser beam impact in order to control dilution ratios between steel and copper, reduce the amount of copper dissolved in the molten steel in order to avoid many defects. Additional important reasons to support this assertion are related to intrinsic welding properties more favourable in steel than in copper such as higher absorptivity, less reflectivity and thermal conductivity that contribute to increase the quality and efficiency of the welding. The lack of researches using this configuration, being the most common the butt one, it has required implement and transfer improvements based on butt configuration experiments into lap configuration.
2. In view of the hot cracking present in samples No. 1 & 7, analysed extensively, a fixation system that does not constrain the thermal dilatation in the plane of the plates (bi-dimensionally) during the welding procedure it would be beneficial to avoid macrodefects such as thermal distortion and stresses that make more feasible hot-cracking phenomena. Therefore the installation of specific parts in the fixation system for ensure reproducibility would be highly recommended to replace them or remove at least partially and search for a solution that implement both requirements.
3. According to the results and welding parameters used, the best weld beam obtained correspond to sample No. 7. Therefore parameters used for welding this sample are the most convenient ones. It presents a notable uniformity, without superficial irregularities. Despite of having slightly more porosity than the second best obtained weldment (sample No. 1) it has really few macrodefects such as hot-cracking or inclusions. Microstructurally it also presents appropriate features such as a well defined and narrow interface between steel and copper with very few inclusions of one material into another result of a lack of turbulences in the melt pool and lack of melted copper but at the same time a scraggly morphology that benefits mechanical properties of the joint.
4. According to the selected parameters and conditions of the welding, sample No. 1 has a wider interface than sample No. 7 that can only be explained by the existing gap between samples, much wider for the second one. These gap can deteriorate the heat conduction from the steel plate to the copper plate leading a reduction of

## 5 Conclusions and Outlook

the temperature in the bottom part and its vicinity and can lead to a reduction of the fluidity of the melt pool near than for narrower gaps.

5. Further researches based in this investigation would be suggested by analysing extensively the mechanical properties of the samples. Tensile strength may be weakly dependent on the melting of the copper but the melting of the copper might induce a decrease in the toughness joint. Also, obtain additional samples with a fixation system that does not constrain the thermal dilation would be highly recommended. Increase slightly the shield gas flow rate considering that the fixation elements does not provoke disturbances to the flow and therefore turbulences would be another further point to examine.

### **Acknowledgements**

The author is grateful to the Technische Universität Wien and to Dr. Gerhard Liedl for the opportunity to conduct this experimental research as a Bachelor Thesis and provide all necessary means for make it possible. Also I appreciate the help of Robert Pospichal, Gerald Humenberger, Edith Ansiemo and Karin Whitmore. Parts of the work were carried out using facilities at the University Service Centre for Transmission Electron Microscopy, Vienna University of Technology, Austria

# Appendix

Equipment, Drawing Plans and EDX Measurements

## 5 Conclusions and Outlook



(1) Picture that shows how the Samples are placed in the fixation system



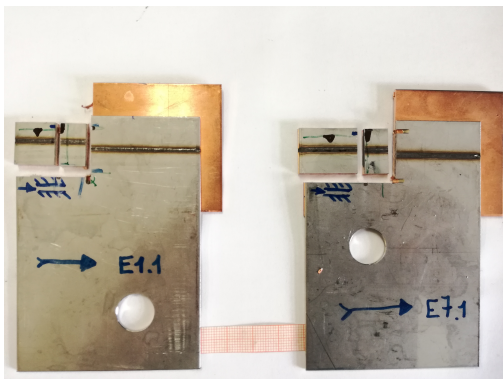
(2) Circular vertical axis saw



(3) In the background the mounting press for generation of the mounting samples and in the foreground two disc polishing machines with suitable supports for the mounted samples



(4) Disc cutting machine with horizontal axis used for obtain a sample from weld plates No.1 & 7



(5) Samples No.1 & 7 after being cut and ready for being mounted in transparent thermo-plastic. The black marks point the face from where are going to be polished and analysed

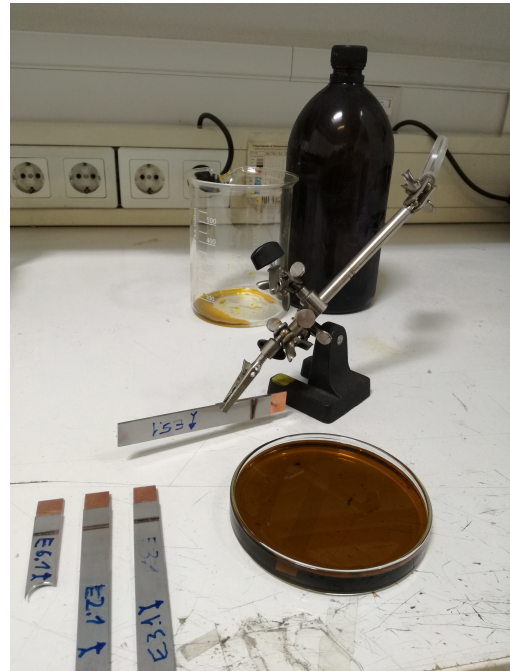


(6) Final aspect of the mounted samples No. 1 & 7 after EDX measurements. It can be appreciated the thin dark film on the upper surface of Au-Pd and the electric path towards the bottom part. They were mounted in order to be seen the seams from the lateral surface

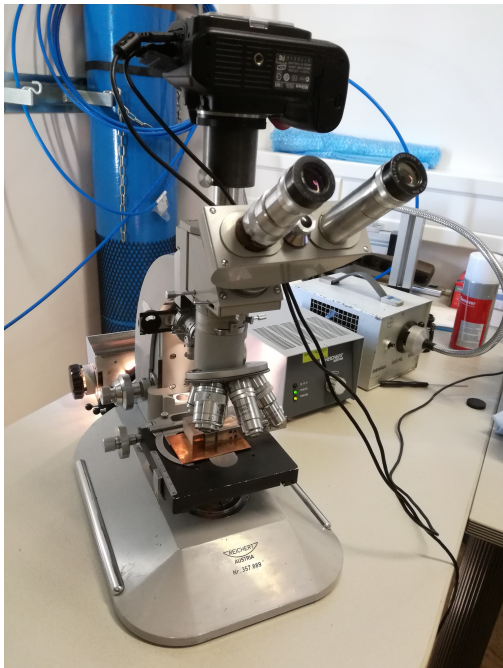
## 5 Conclusions and Outlook



(7) Disc cutting machine with horizontal axis cutting precisely along the weld line for obtaining an accurate longitudinal sample from one of the weld plates



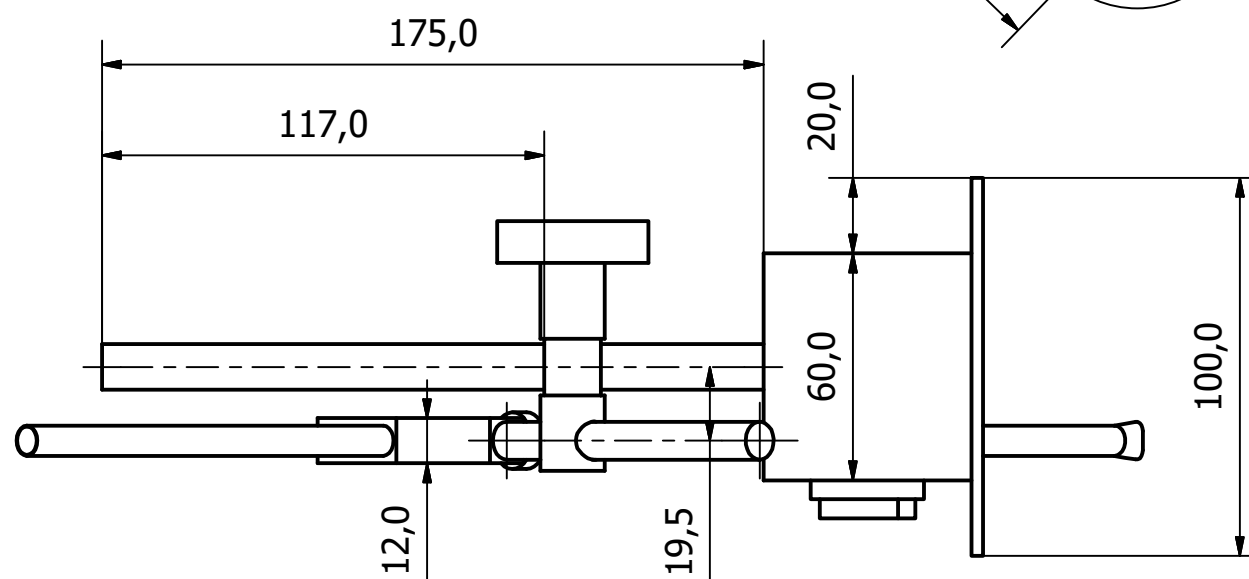
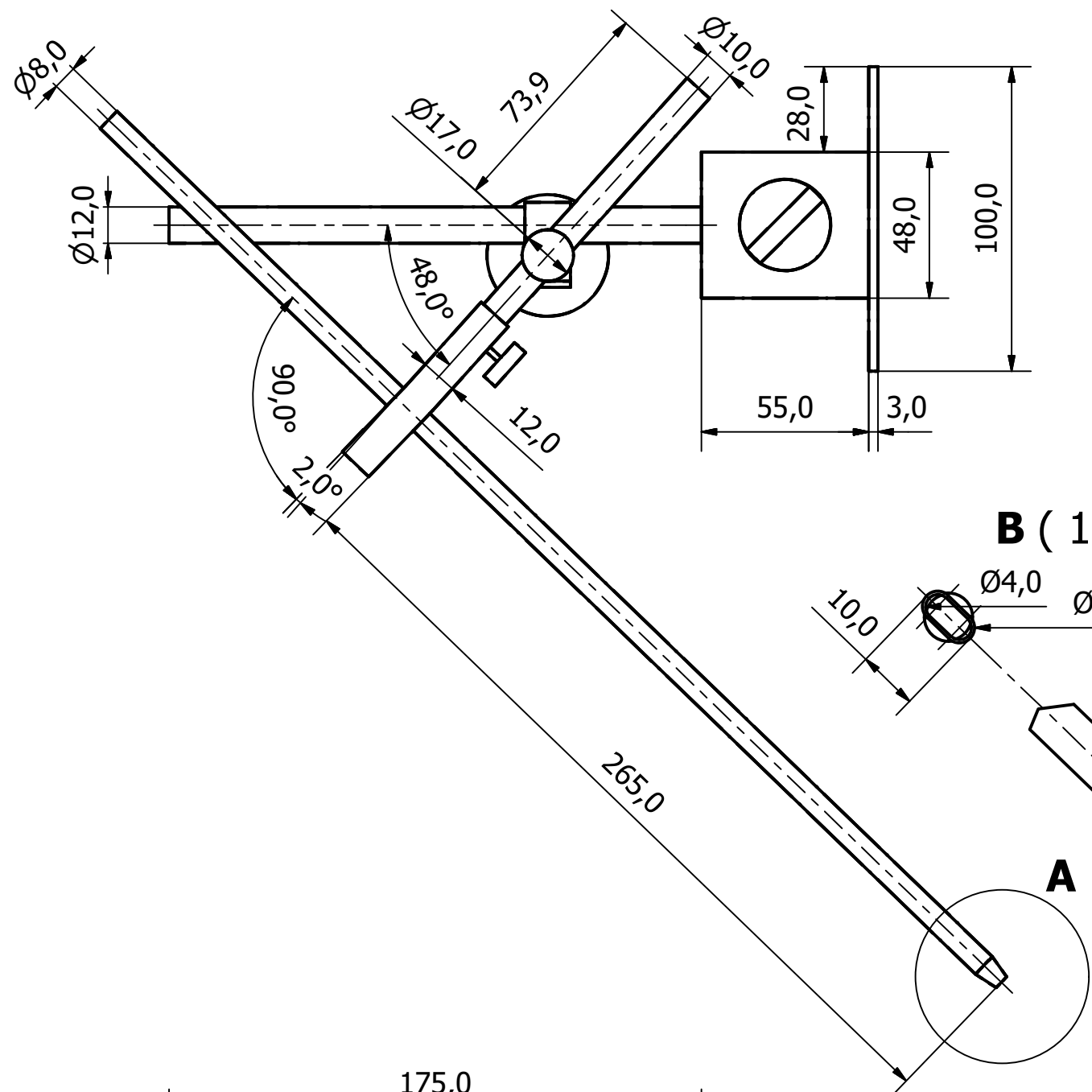
(8) Adler reagent used for samples No.2, 3, 5 & 6 and tweezers system for submerge them in the etching solution



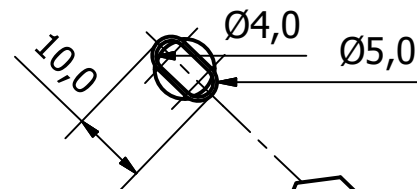
(9) Optical Microscope used for analysing Samples No. 2, 3, 5 & 6 in the laboratory of Laser Technology



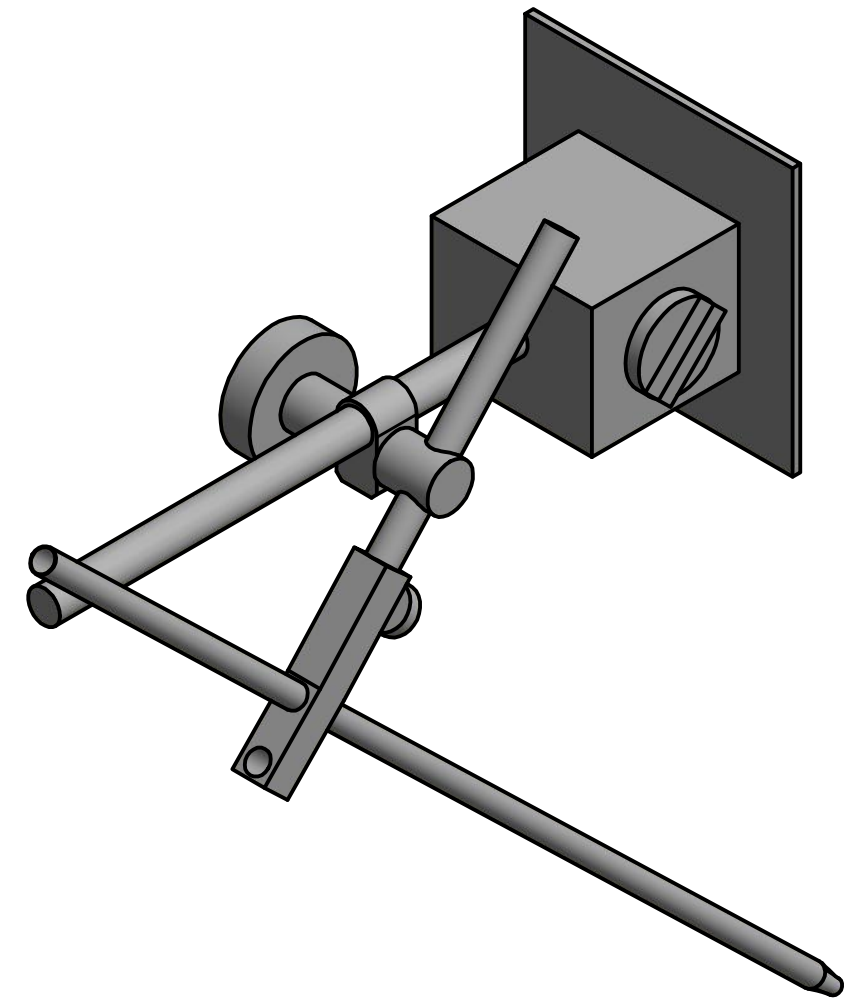
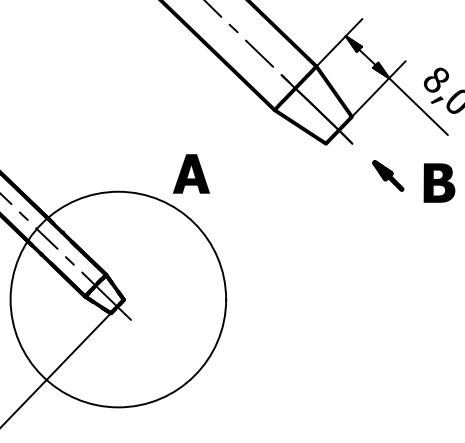
(10) Optical Microscope used for analysing Samples No. 1 & 7 in the Center of Transmission Electromicroscopie



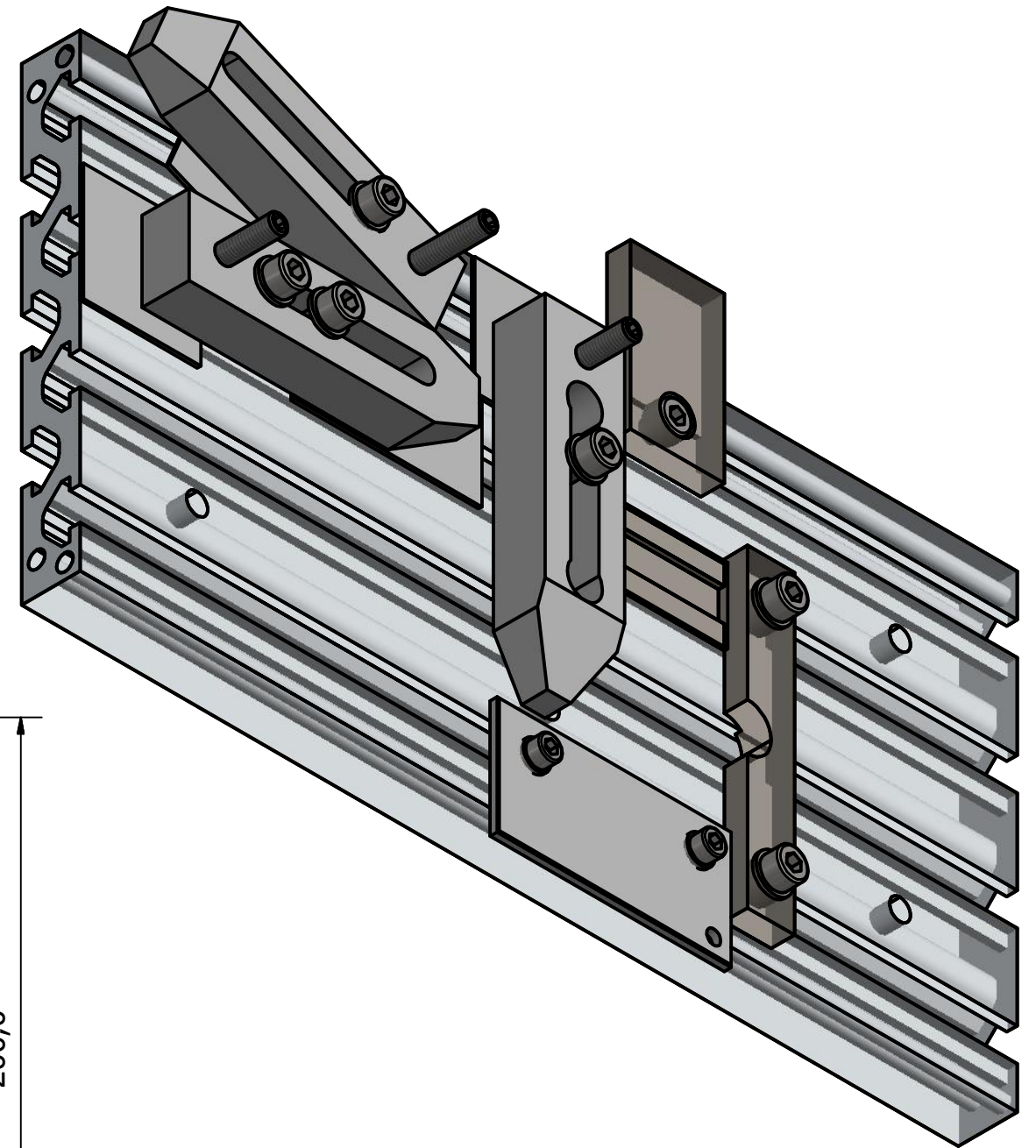
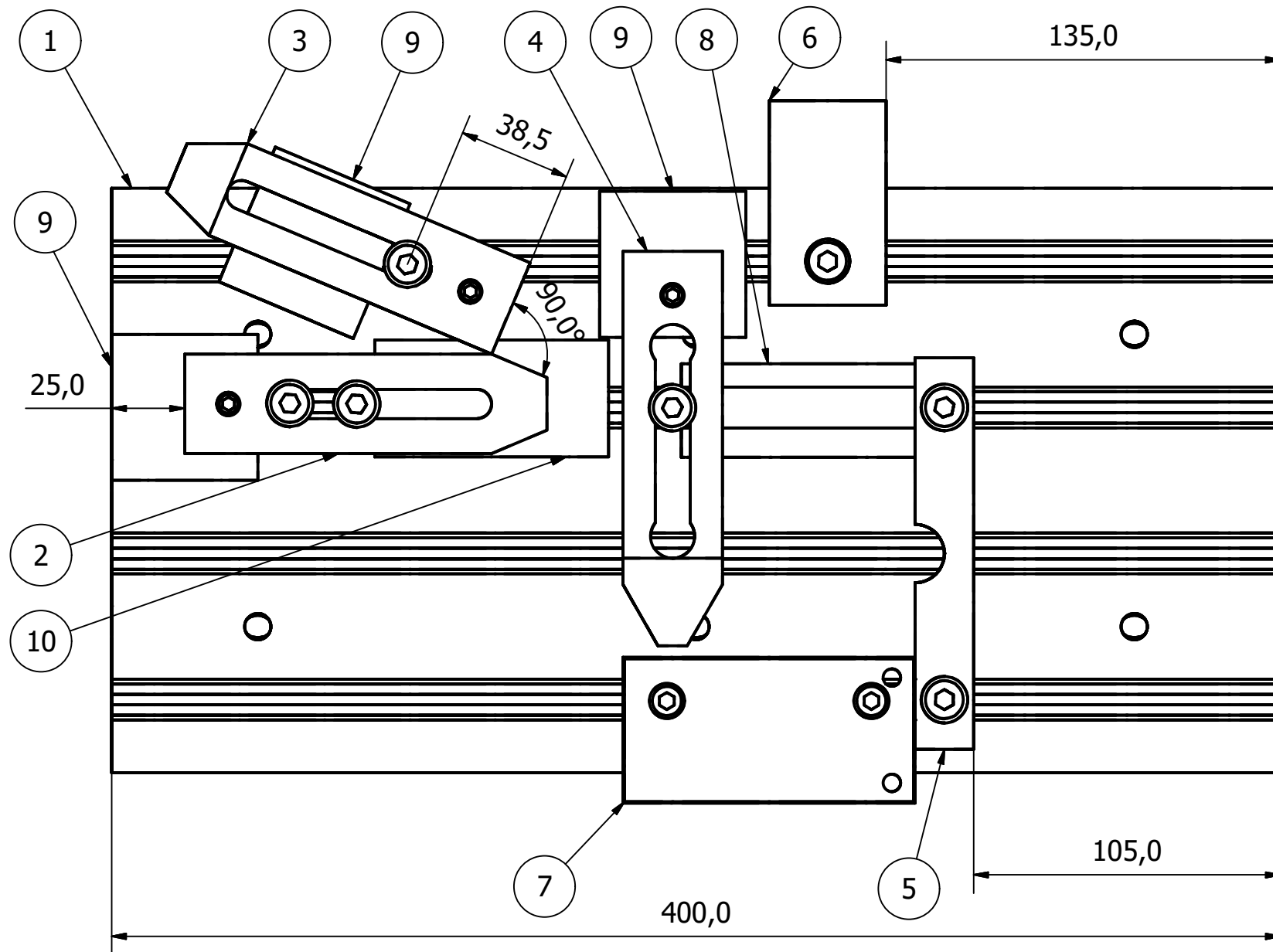
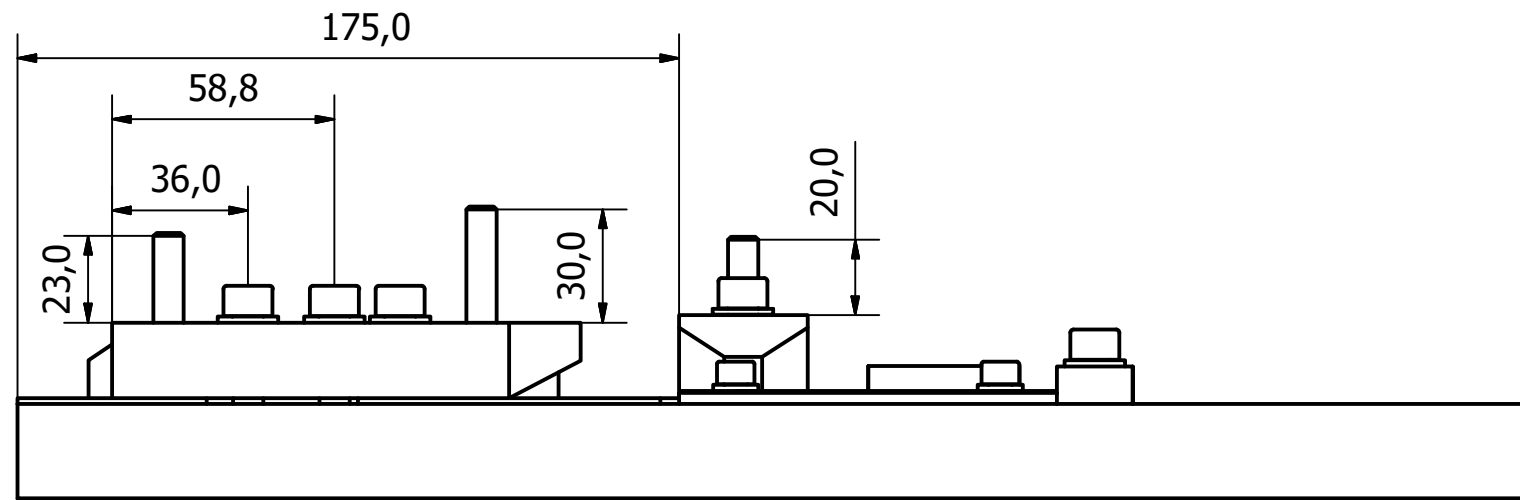
**B (1:1)**



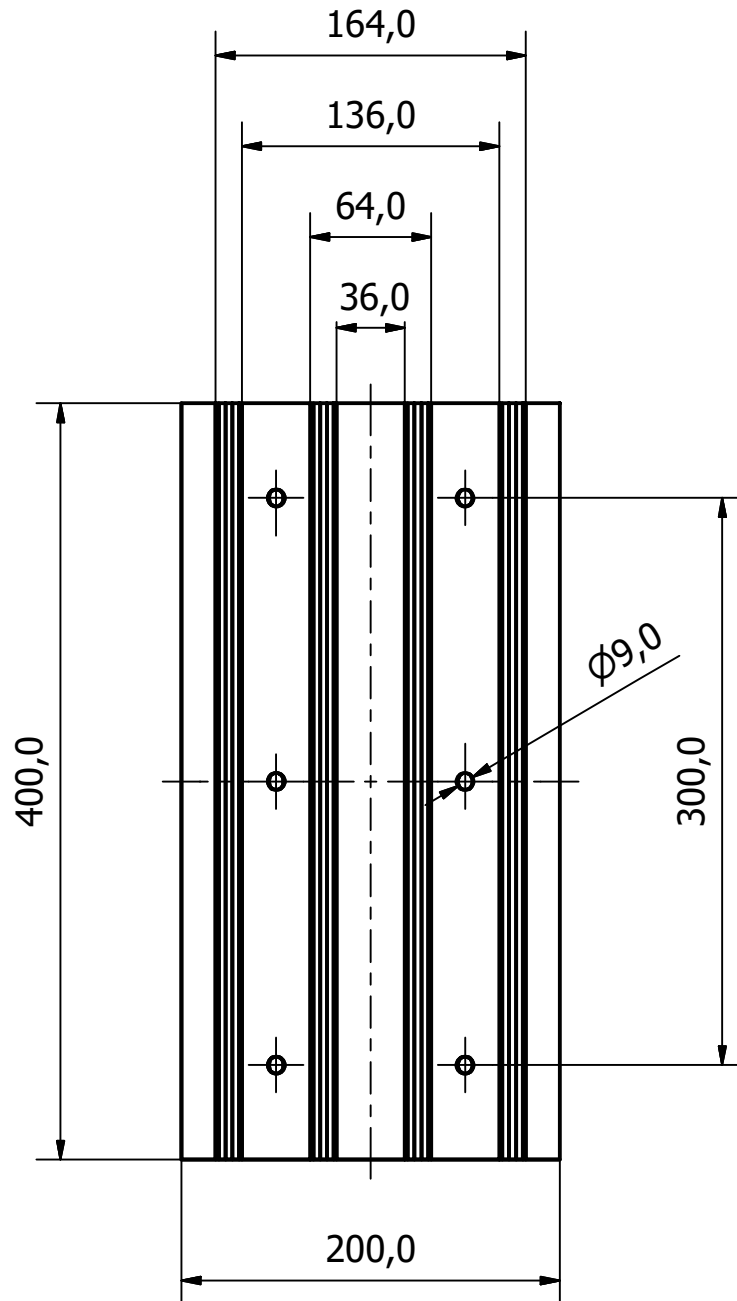
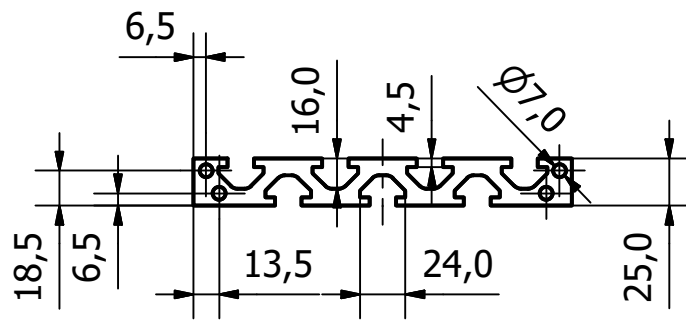
**A (1:1)**



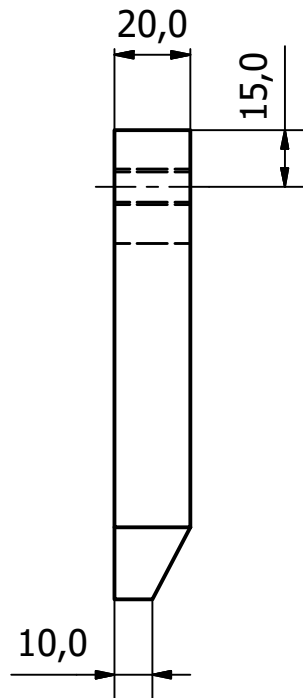
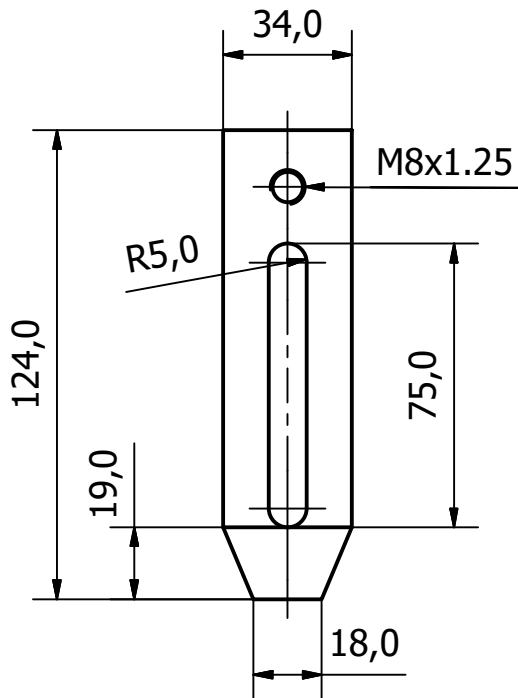
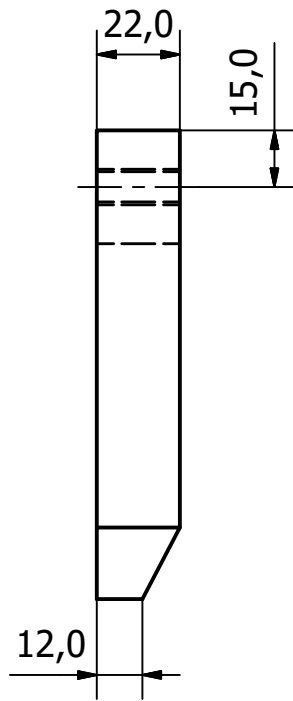
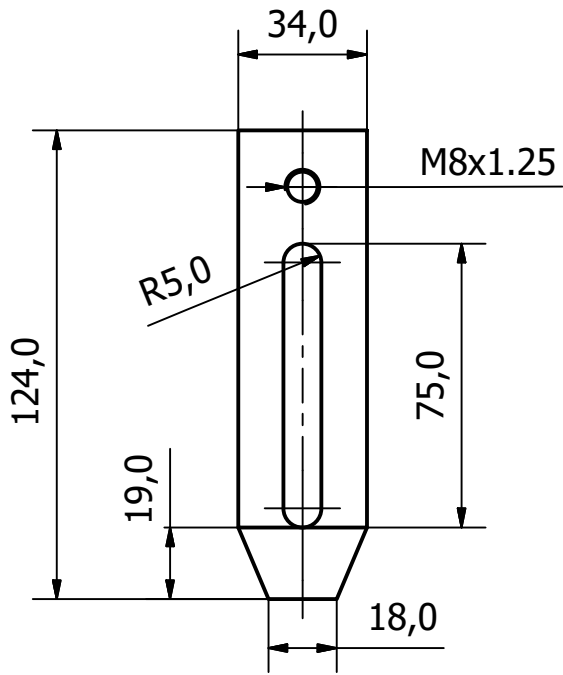
Designed by <b>JUAN SIMÓN MUZÁS</b>	Date 12/05/2017
Scale 1:2	 
Title <b>LASER WELDING OF DISSIMILAR MATERIALS</b>	
Title <b>SHIELD GAS NOZZLE</b>	
Edition	Sheet 1/7



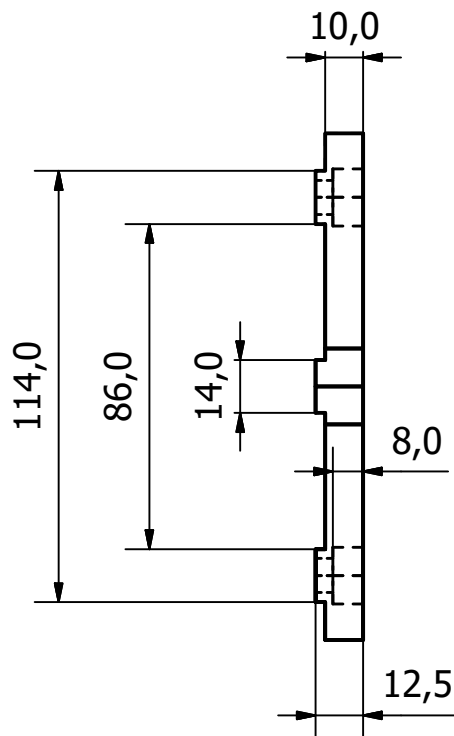
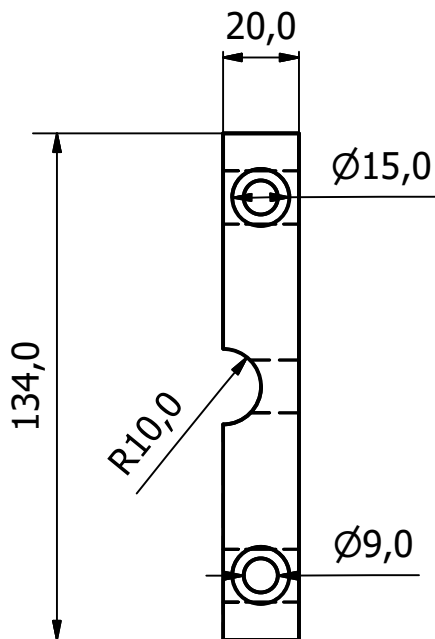
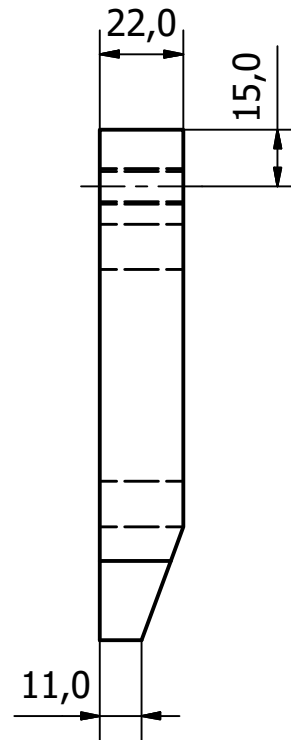
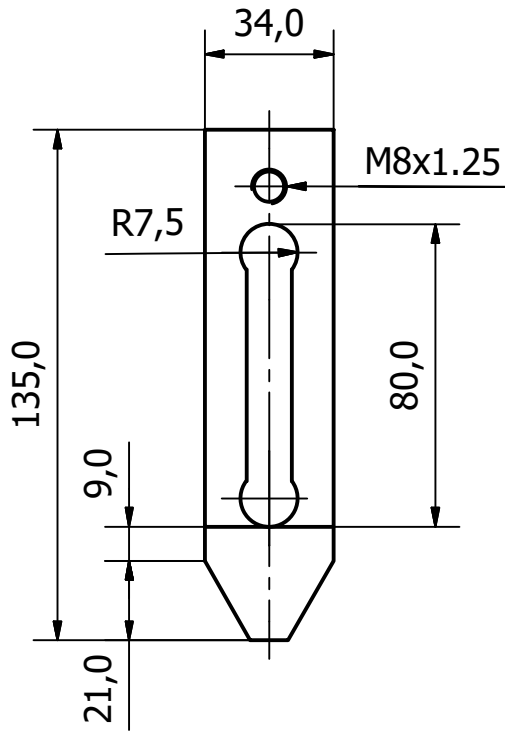
Designed by <b>JUAN SIMÓN MUZÁS</b>		Date <b>19/05/2017</b>	
Scale <b>1:2</b>	 	Title <b>LASER WELDING OF DISSIMILAR MATERIALS</b>	
		Edition <b>SAMPLE FIXATION SYSTEM</b>	Sheet <b>2/7</b>



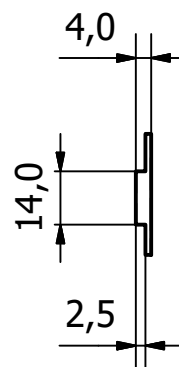
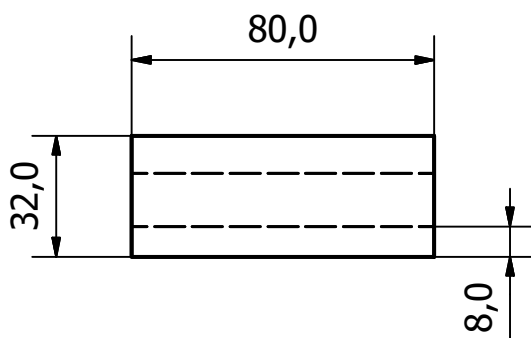
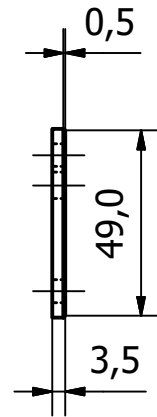
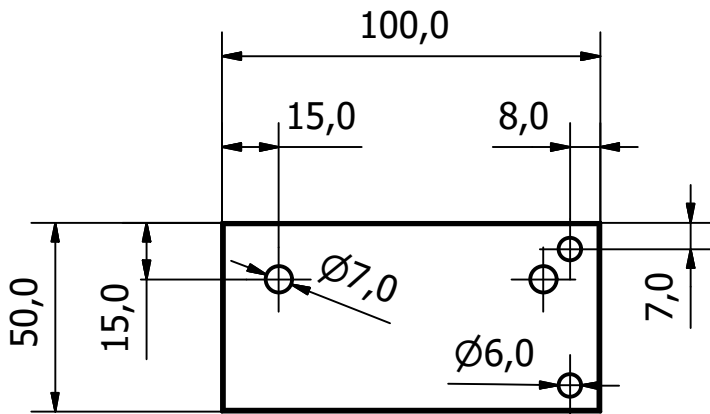
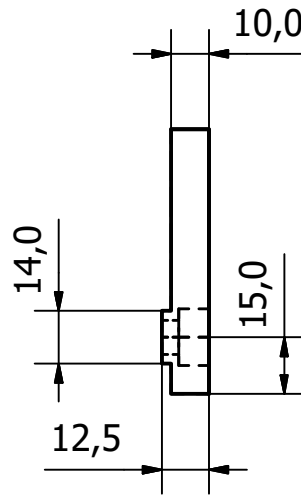
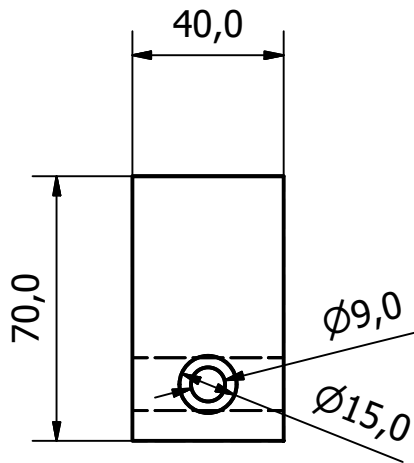
Designed by <b>JUAN SIMÓN MUZÁS</b>		Date <b>21/05/2017</b>	
Scale <b>1:4</b>	 	<b>LASER WELDING OF DISSIMILAR MATERIALS</b>	
	Title <b>PART 1</b>	Edition	Sheet <b>3/7</b>



Designed by <b>JUAN SIMÓN MUZÁS</b>		Date <b>21/05/2017</b>	
Scale <b>1:2</b>	  Lasergestützte Fertigung	<b>LASER WELDING OF DISSIMILAR MATERIALS</b>	
Title <b>PARTS 2 &amp; 3</b>		Edition	Sheet <b>4/7</b>

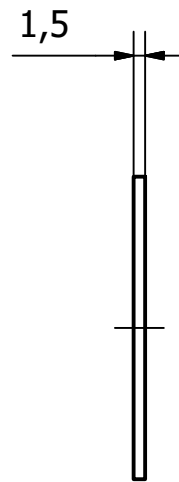
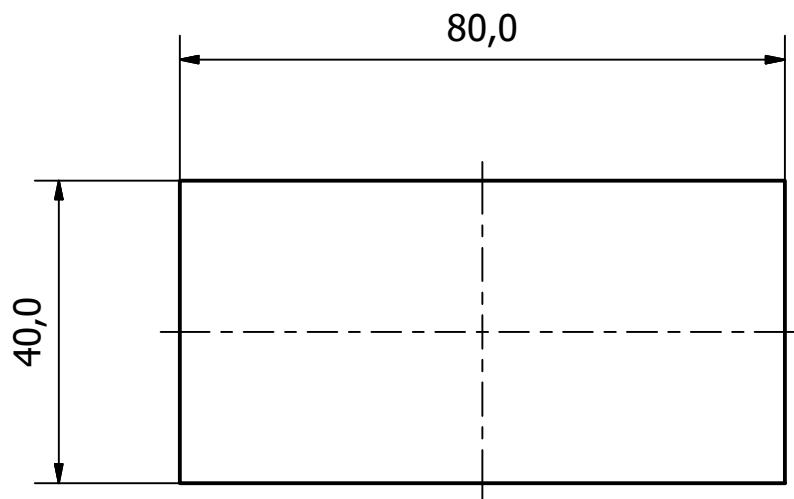
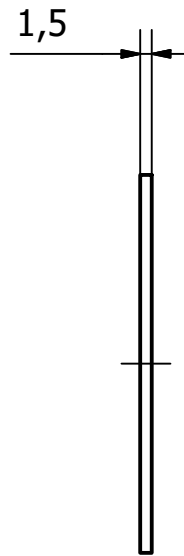
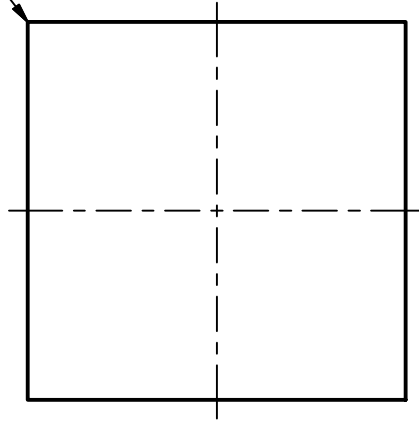


Designed by <b>JUAN SIMÓN MUZÁS</b>		Date <b>21/05/2017</b>	
Scale <b>1:2</b>	  <b>Lasergestützte Fertigung</b>	<b>LASER WELDING OF DISSIMILAR MATERIALS</b>	
Title <b>PARTS 4 &amp; 5</b>		Edition	Sheet <b>5/7</b>



Designed by <b>JUAN SIMÓN MUZÁS</b>		Date <b>21/05/2017</b>	
Scale <b>1:2</b>	  Lasergestützte Fertigung	<b>LASER WELDING OF DISSIMILAR MATERIALS</b>	
Title <b>PARTS 6, 7 &amp; 8</b>		Edition	Sheet <b>6/7</b>

□50,0

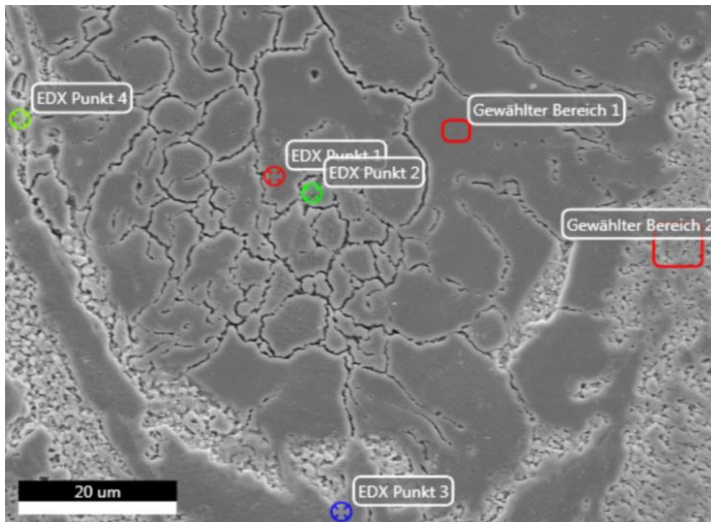


Designed by <b>JUAN SIMÓN MUZÁS</b>		Date <b>21/05/2017</b>	
Scale <b>1:1</b>	 	<b>LASER WELDING OF DISSIMILAR MATERIALS</b>	
	Title <b>PARTS 9 &amp; 10</b>	Edition	Sheet <b>7/7</b>

E165 465A

Autor: whitmore  
Erstellt: 05/23/2017 12:42:10 PM  
Probenbezeichnung: Dark 1.1 LS

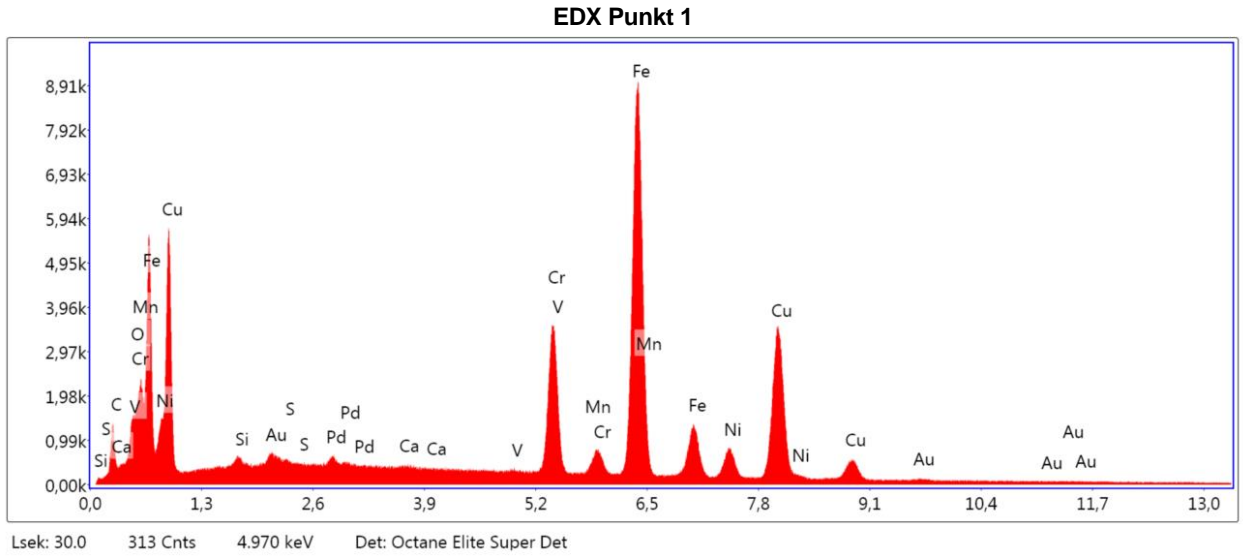
## Bereich 1



Notizen:

EDX Punkt 1

kV: 20    Vergr.: 3999    Abnahmewinkel: 36.8    Live Messdauer(s): 30    Filterzeit(µs): 3.84    Auflösung:(eV)



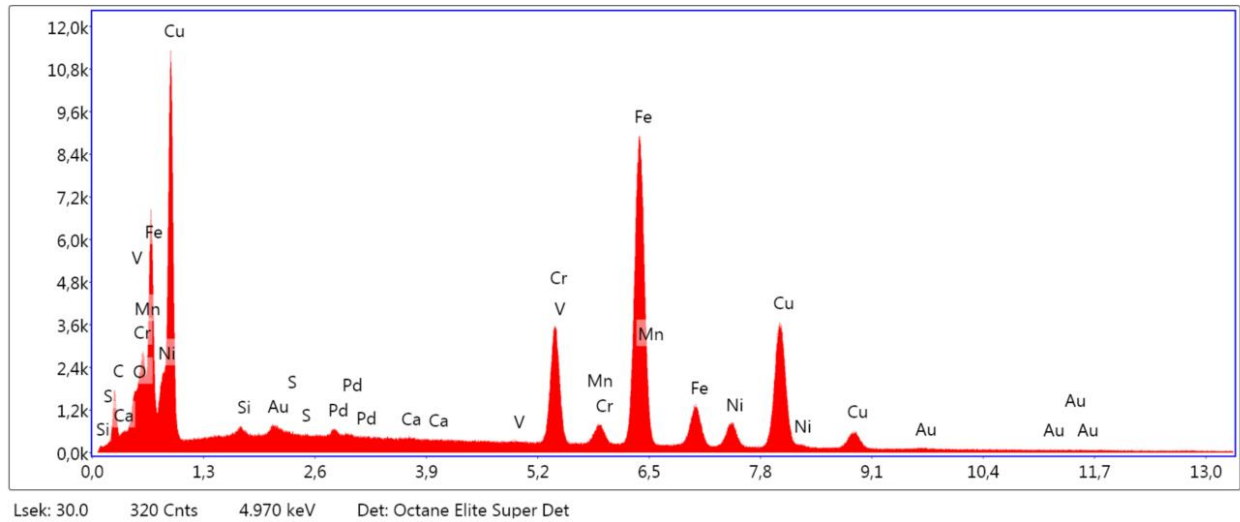
**eZAF Quant. Ergebnisse**

Element	Gewicht%	Atom%	Net. Int.	Error %	Kratio	Z	R	A	F
C K	4.2	17.1	265.0	11.1	0.0110	1.3095	0.8386	0.2022	1.0000
O K	0.9	2.7	227.5	10.1	0.0042	1.2600	0.8632	0.3856	1.0000
Si K	0.3	0.5	100.5	16.8	0.0015	1.1582	0.9214	0.4389	1.0060
S K	0.1	0.1	37.9	52.0	0.0007	1.1375	0.9377	0.6679	1.0153
Ca K	0.1	0.2	50.8	38.4	0.0014	1.1022	0.9670	0.9144	1.0768
V K	0.2	0.2	72.6	23.4	0.0027	0.9783	0.9862	0.9756	1.1899
Cr K	10.5	9.8	2885.9	3.1	0.1228	0.9943	0.9921	0.9854	1.2169
Mn K	1.0	0.9	210.1	11.8	0.0103	0.9747	0.9976	0.9898	1.1258
Fe K	44.2	38.6	8089.1	2.3	0.4580	0.9916	1.0028	0.9777	1.0873
Ni K	5.2	4.3	669.4	4.8	0.0505	1.0047	1.0119	0.9357	1.0572
Cu K	33.4	25.6	3461.8	2.8	0.3108	0.9555	1.0156	0.9490	1.0448

## EDX Punkt 2

kV: 20    Vergr.: 3999    Abnahmewinkel: 36.8    Live Messdauer(s): 30    Filterzeit(µs): 3.84    Auflösung:(eV)

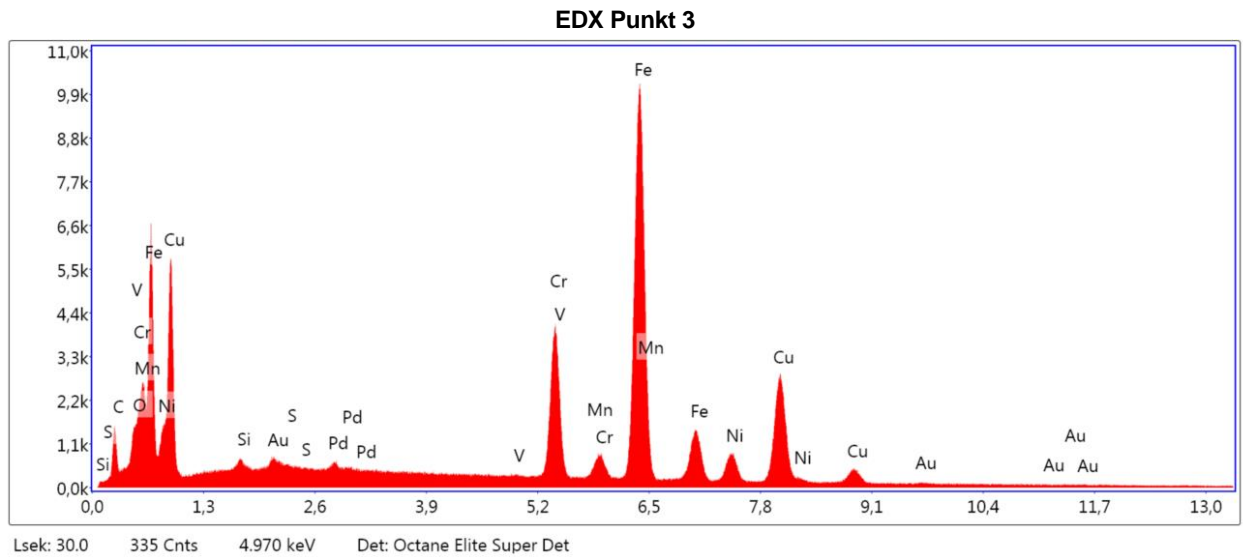
## EDX Punkt 2

**eZAF Quant. Ergebnisse**

Element	Gewicht%	Atom%	Net. Int.	Error %	Kratio	Z	R	A	F
C K	5.2	20.6	337.4	11.7	0.0134	1.3060	0.8399	0.2039	1.0000
O K	0.8	2.3	203.1	11.6	0.0036	1.2565	0.8644	0.3784	1.0000
Si K	0.2	0.3	67.7	23.8	0.0010	1.1550	0.9226	0.4397	1.0060
S K	0.0	0.0	6.4	62.7	0.0001	1.1344	0.9389	0.6691	1.0152
Ca K	0.1	0.1	37.1	55.0	0.0010	1.0992	0.9681	0.9152	1.0765
V K	0.2	0.2	71.1	23.4	0.0026	0.9756	0.9872	0.9760	1.1902
Cr K	10.1	9.2	2851.4	3.1	0.1168	0.9915	0.9931	0.9858	1.2171
Mn K	1.1	1.0	255.2	9.0	0.0120	0.9719	0.9986	0.9902	1.1278
Fe K	42.8	36.4	8055.2	2.3	0.4391	0.9887	1.0037	0.9787	1.0903
Ni K	5.5	4.4	729.4	4.6	0.0530	1.0018	1.0127	0.9377	1.0578
Cu K	33.9	25.4	3608.1	2.8	0.3119	0.9527	1.0164	0.9506	1.0447

## EDX Punkt 3

kV: 20    Vergr.: 3999    Abnahmewinkel: 36.8    Live Messdauer(s): 30    Filterzeit(µs): 3.84    Auflösung:(eV)

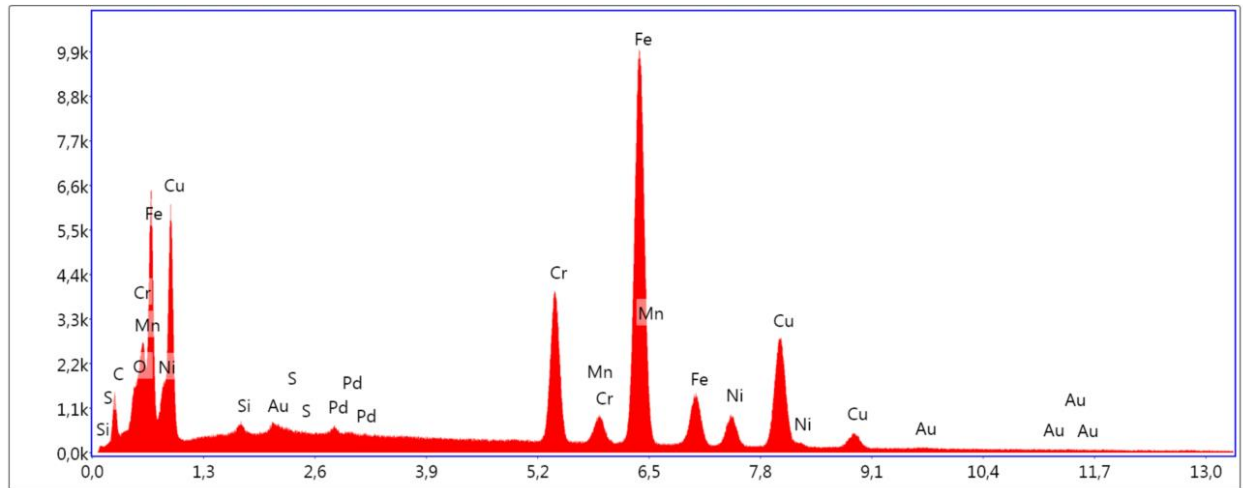
**eZAF Quant. Ergebnisse**

Element	Gewicht%	Atom%	Net. Int.	Error %	Kratio	Z	R	A	F
CK	4.6	18.5	302.0	11.2	0.0123	1.3053	0.8405	0.2065	1.0000
OK	0.8	2.3	200.7	11.5	0.0037	1.2559	0.8651	0.3922	1.0000
SiK	0.3	0.5	110.4	16.0	0.0016	1.1544	0.9233	0.4472	1.0063
SK	0.1	0.1	25.8	58.3	0.0004	1.1337	0.9395	0.6756	1.0159
VK	0.2	0.2	57.2	29.5	0.0021	0.9749	0.9878	0.9777	1.1980
CrK	11.5	10.6	3227.5	3.1	0.1354	0.9908	0.9936	0.9871	1.2235
MnK	1.0	0.9	220.1	11.3	0.0106	0.9712	0.9991	0.9910	1.1166
FeK	49.5	42.5	9054.4	2.2	0.5054	0.9880	1.0042	0.9770	1.0731
NiK	5.7	4.7	742.3	4.5	0.0552	1.0010	1.0132	0.9290	1.0519
CuK	26.3	19.8	2746.6	3.0	0.2431	0.9519	1.0168	0.9434	1.0456

## Gewählter Bereich 1

kV: 20    Vergr.: 3999    Abnahmewinkel: 36.8    Live Messdauer(s): 30    Filterzeit(µs): 3.84    Auflösung:(eV)

## Gewählter Bereich 1



Lsek: 30.0    328 Cnts    4.970 keV    Det: Octane Elite Super Det

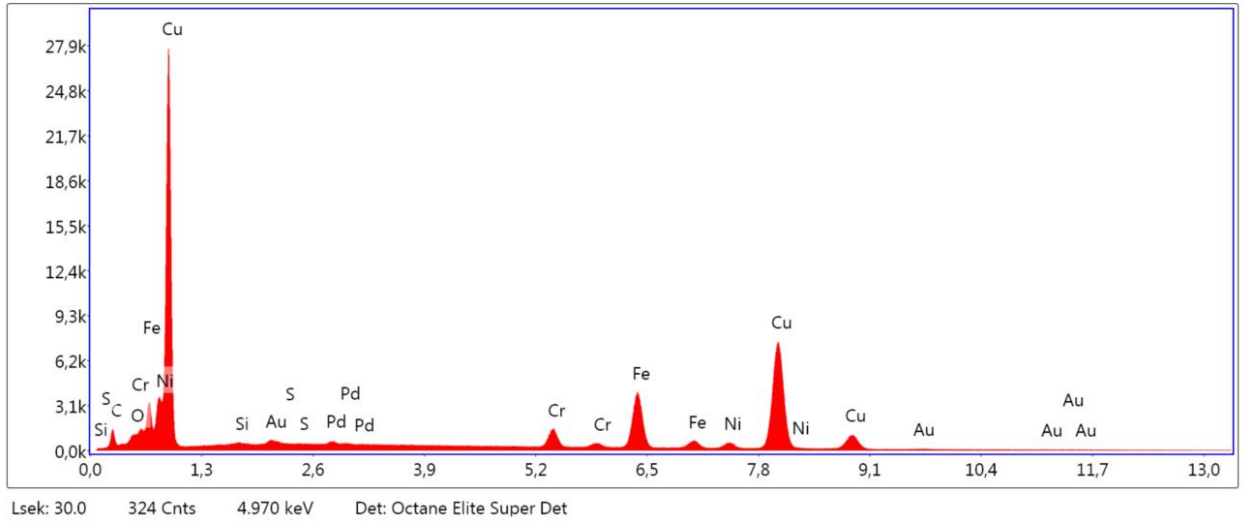
**eZAF Quant. Ergebnisse**

Element	Gewicht%	Atom%	Net. Int.	Error %	Kratio	Z	R	A	F
C K	4.4	17.5	279.1	11.7	0.0116	1.3065	0.8400	0.2058	1.0000
O K	0.8	2.5	217.0	11.3	0.0040	1.2570	0.8646	0.3967	1.0000
Si K	0.3	0.5	105.3	15.0	0.0015	1.1554	0.9228	0.4460	1.0063
S K	0.1	0.1	27.8	58.2	0.0005	1.1347	0.9391	0.6746	1.0159
Cr K	11.5	10.6	3179.5	3.1	0.1360	0.9917	0.9932	0.9870	1.2245
Mn K	1.2	1.0	250.7	10.5	0.0123	0.9721	0.9987	0.9912	1.1171
Fe K	49.4	42.7	8925.1	2.2	0.5077	0.9890	1.0038	0.9772	1.0738
Ni K	5.8	4.8	744.5	4.7	0.0564	1.0020	1.0128	0.9291	1.0520
Cu K	26.6	20.2	2743.9	3.0	0.2475	0.9528	1.0165	0.9435	1.0455

Gewählter Bereich 2

kV: 20      Vergr.: 3999      Abnahmewinkel: 36.8      Live Messdauer(s): 30      Filterzeit(µs): 3.84      Auflösung:(eV)

Gewählter Bereich 2



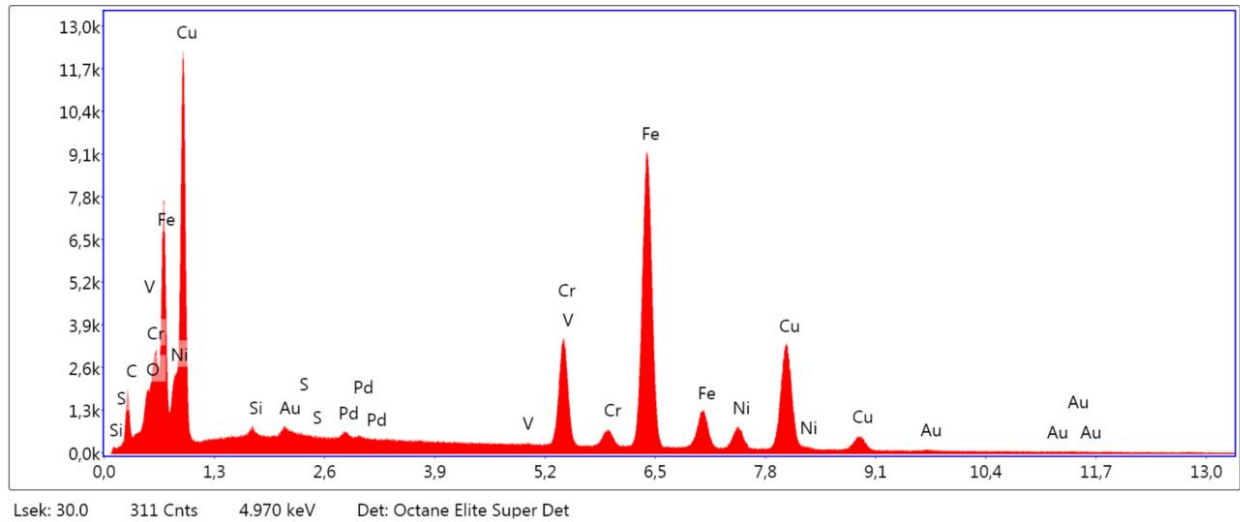
**eZAF Quant. Ergebnisse**

Element	Gewicht%	Atom%	Net. Int.	Error %	Kratio	Z	R	A	F
C K	5.2	21.5	297.8	12.1	0.0125	1.3212	0.8321	0.1850	1.0000
O K	0.7	2.1	159.5	11.9	0.0030	1.2713	0.8566	0.3479	1.0000
Si K	0.2	0.3	61.2	26.2	0.0009	1.1691	0.9151	0.4016	1.0051
S K	0.0	0.0	1.0	78.1	0.0000	1.1484	0.9315	0.6315	1.0127
Cr K	3.9	3.8	1076.0	4.0	0.0465	1.0046	0.9867	0.9789	1.2193
Fe K	16.8	14.9	3530.1	3.2	0.2032	1.0021	0.9977	0.9862	1.2410
Ni K	2.7	2.3	386.4	7.0	0.0296	1.0158	1.0072	0.9747	1.1131
Cu K	70.5	55.1	7534.8	2.2	0.6875	0.9662	1.0112	0.9812	1.0409

## EDX Punkt 4

kV: 20    Vergr.: 3999    Abnahmewinkel: 36.8    Live Messdauer(s): 30    Filterzeit(μs): 3.84    Auflösung:(eV)

## EDX Punkt 4

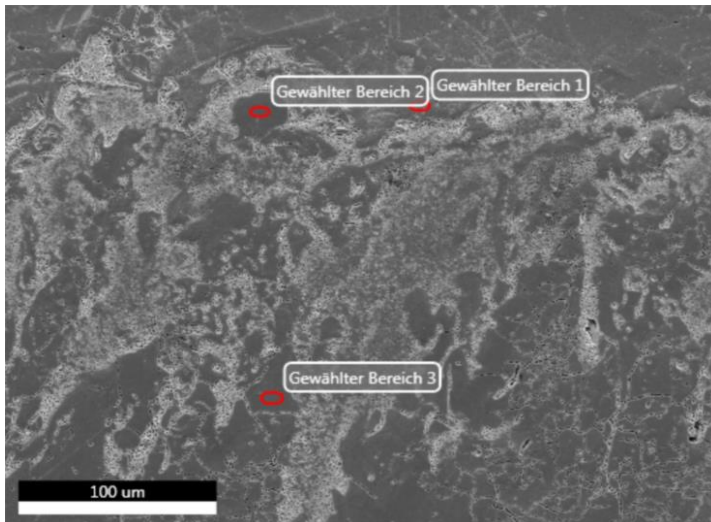
**eZAF Quant. Ergebnisse**

Element	Gewicht%	Atom%	Net. Int.	Error %	Kratio	Z	R	A	F
CK	5.7	22.0	360.6	10.5	0.0150	1.3019	0.8414	0.2053	1.0000
OK	1.0	3.0	263.2	10.0	0.0049	1.2526	0.8660	0.3790	1.0000
SiK	0.2	0.4	78.7	20.0	0.0012	1.1513	0.9241	0.4430	1.0060
SK	0.0	0.0	6.2	62.7	0.0001	1.1307	0.9403	0.6721	1.0153
VK	0.1	0.1	44.3	43.4	0.0017	0.9724	0.9885	0.9770	1.1926
CrK	10.0	9.0	2771.9	3.1	0.1182	0.9882	0.9943	0.9866	1.2254
FeK	45.6	38.0	8302.1	2.2	0.4711	0.9854	1.0049	0.9796	1.0854
NiK	5.3	4.2	676.8	4.8	0.0512	0.9984	1.0138	0.9361	1.0564
CuK	31.9	23.4	3294.3	2.8	0.2964	0.9493	1.0174	0.9493	1.0449

E165 465A

Autor: whitmore  
Erstellt: 05/23/2017 12:56:48 PM  
Probenbezeichnung: Dark 1.1 QS

## Bereich 2

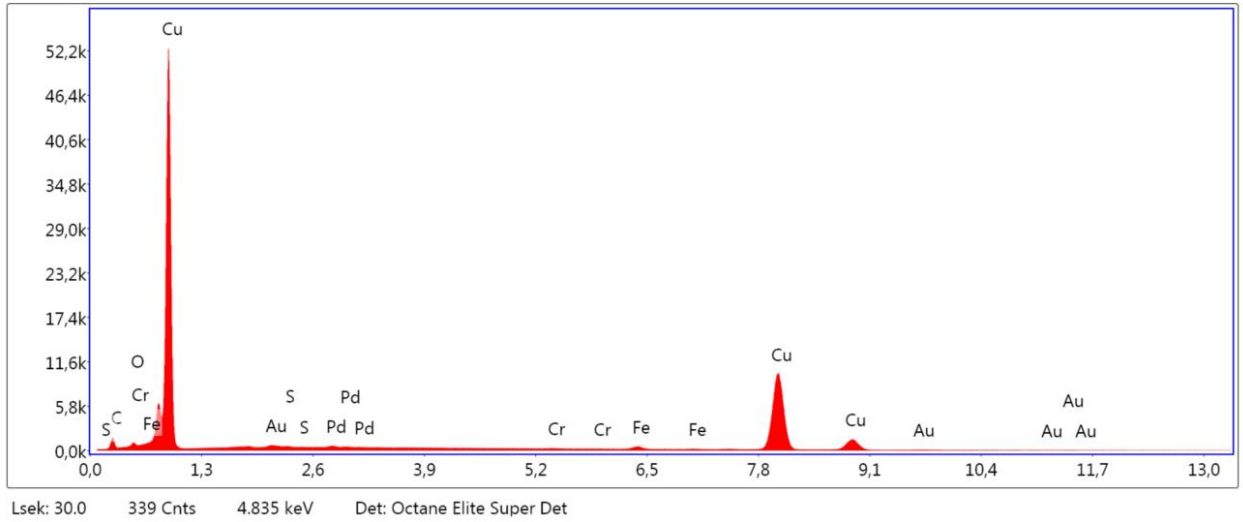


Notizen:

Gewählter Bereich 1

kV: 20      Vergr.: 1000      Abnahmewinkel: 36.7      Live Messdauer(s): 30      Filterzeit(µs): 3.84      Auflösung:(eV)

Gewählter Bereich 1



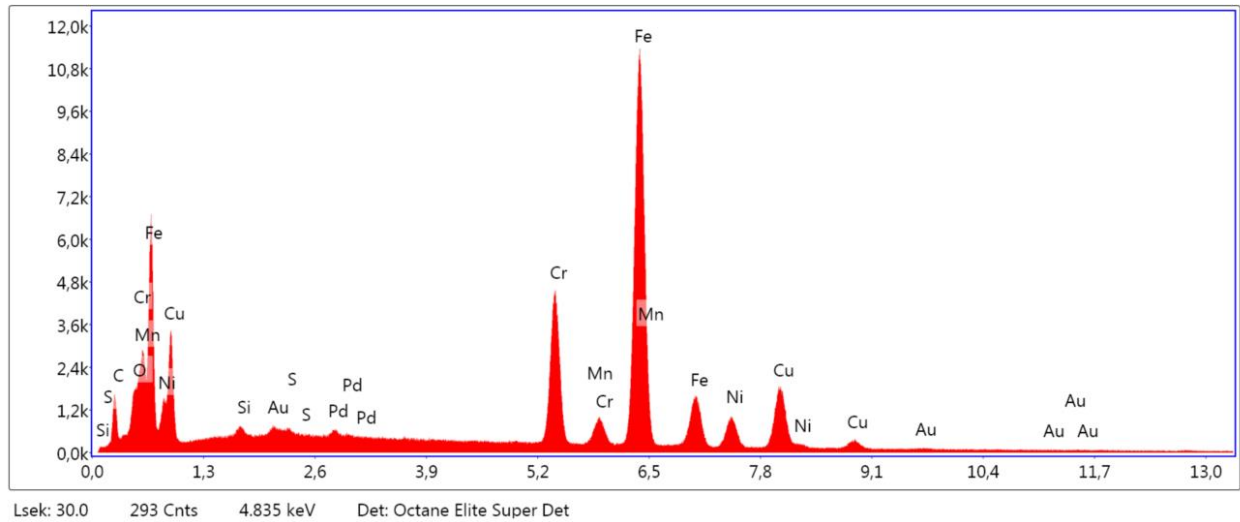
**eZAF Quant. Ergebnisse**

Element	Gewicht%	Atom%	Net. Int.	Error %	Kratio	Z	R	A	F
CK	6.2	25.5	350.0	11.3	0.0143	1.3256	0.8297	0.1775	1.0000
OK	0.8	2.4	172.0	11.8	0.0031	1.2756	0.8542	0.3244	1.0000
SK	0.1	0.1	25.0	59.0	0.0004	1.1525	0.9292	0.6142	1.0135
CrK	0.1	0.1	26.0	56.4	0.0011	1.0086	0.9847	0.9754	1.2891
FeK	0.9	0.8	249.7	11.1	0.0140	1.0062	0.9958	0.9912	1.5455
CuK	91.9	71.1	10240.2	2.0	0.9080	0.9704	1.0096	1.0005	1.0392

## Gewählter Bereich 2

kV: 20    Vergr.: 1000    Abnahmewinkel: 36.7    Live Messdauer(s): 30    Filterzeit(μs): 3.84    Auflösung:(eV)

## Gewählter Bereich 2

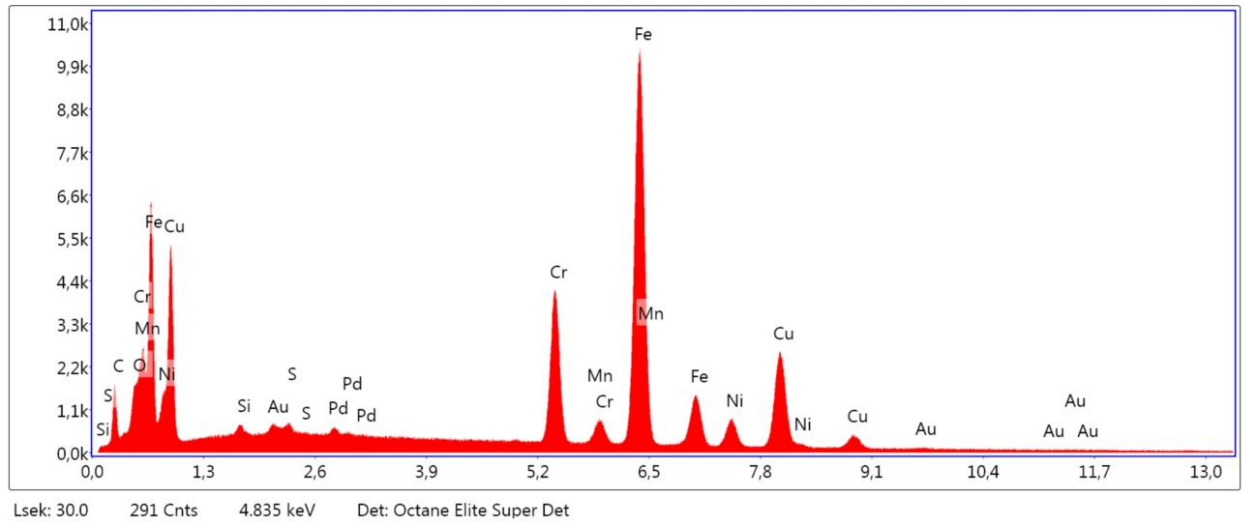
**eZAF Quant. Ergebnisse**

Element	Gewicht%	Atom%	Net. Int.	Error %	Kratio	Z	R	A	F
CK	5.0	19.5	333.1	10.6	0.0136	1.2987	0.8435	0.2113	1.0000
OK	1.0	2.8	259.9	9.9	0.0047	1.2495	0.8681	0.4004	1.0000
SiK	0.3	0.6	122.2	14.8	0.0018	1.1483	0.9261	0.4590	1.0066
SK	0.2	0.3	91.1	17.4	0.0016	1.1276	0.9423	0.6867	1.0168
CrK	12.8	11.5	3619.8	3.0	0.1517	0.9852	0.9960	0.9890	1.2313
MnK	1.2	1.0	251.6	9.9	0.0121	0.9657	1.0014	0.9925	1.1056
FeK	56.1	46.8	10042.7	2.1	0.5598	0.9823	1.0065	0.9760	1.0577
NiK	6.6	5.2	834.3	4.4	0.0620	0.9951	1.0152	0.9208	1.0461
CuK	16.8	12.3	1736.5	3.4	0.1535	0.9462	1.0188	0.9366	1.0468

## Gewählter Bereich 3

kV: 20    Vergr.: 1000    Abnahmewinkel: 36.7    Live Messdauer(s): 30    Filterzeit(μs): 3.84    Auflösung:(eV)

## Gewählter Bereich 3

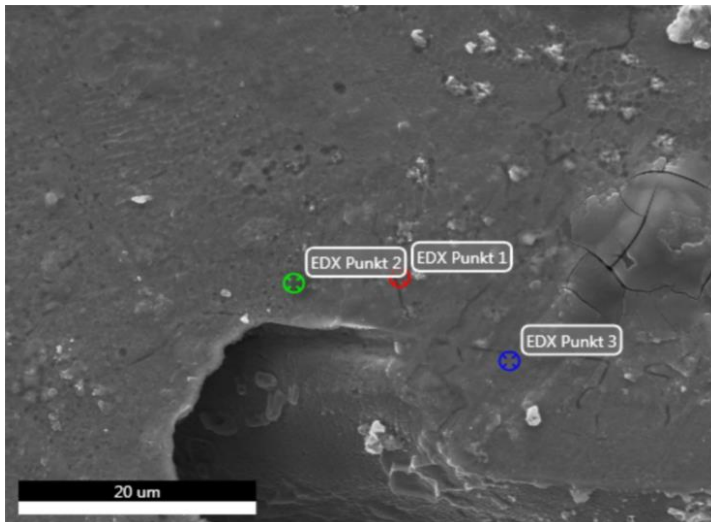
**eZAF Quant. Ergebnisse**

Element	Gewicht%	Atom%	Net. Int.	Error %	Kratio	Z	R	A	F
CK	5.3	20.6	347.3	10.6	0.0141	1.3001	0.8427	0.2077	1.0000
OK	1.0	2.9	267.1	9.9	0.0048	1.2509	0.8673	0.3906	1.0000
SiK	0.3	0.5	99.3	17.2	0.0014	1.1497	0.9254	0.4521	1.0064
SK	0.3	0.4	129.3	12.5	0.0022	1.1290	0.9416	0.6805	1.0161
CrK	11.9	10.6	3344.5	3.1	0.1396	0.9866	0.9953	0.9878	1.2250
MnK	0.9	0.8	203.2	12.0	0.0098	0.9670	1.0008	0.9918	1.1138
FeK	50.8	42.3	9252.8	2.2	0.5137	0.9837	1.0059	0.9770	1.0688
NiK	5.5	4.3	708.2	4.7	0.0524	0.9966	1.0147	0.9276	1.0507
CuK	24.0	17.6	2503.8	3.1	0.2204	0.9476	1.0183	0.9423	1.0460

E165 465A

Autor: whitmore  
Erstellt: 05/23/2017 1:21:10 PM  
Probenbezeichnung: bright 7.1 LS

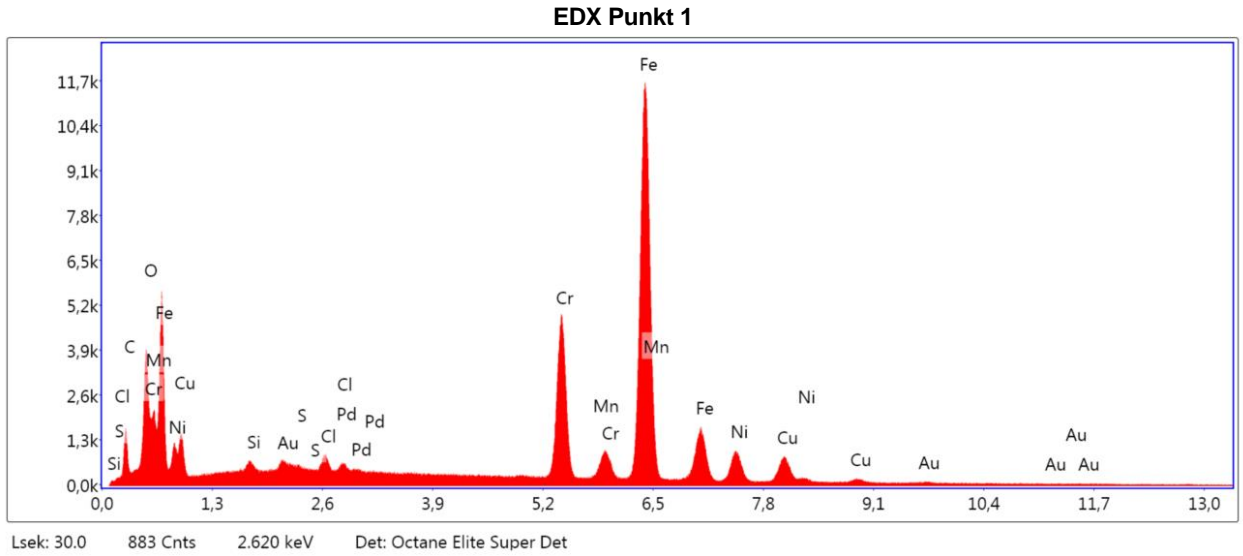
## Bereich 2



Notizen:

EDX Punkt 1

kV: 20    Vergr.: 5999    Abnahmewinkel: 37.1    Live Messdauer(s): 30    Filterzeit(µs): 3.84    Auflösung:(eV)



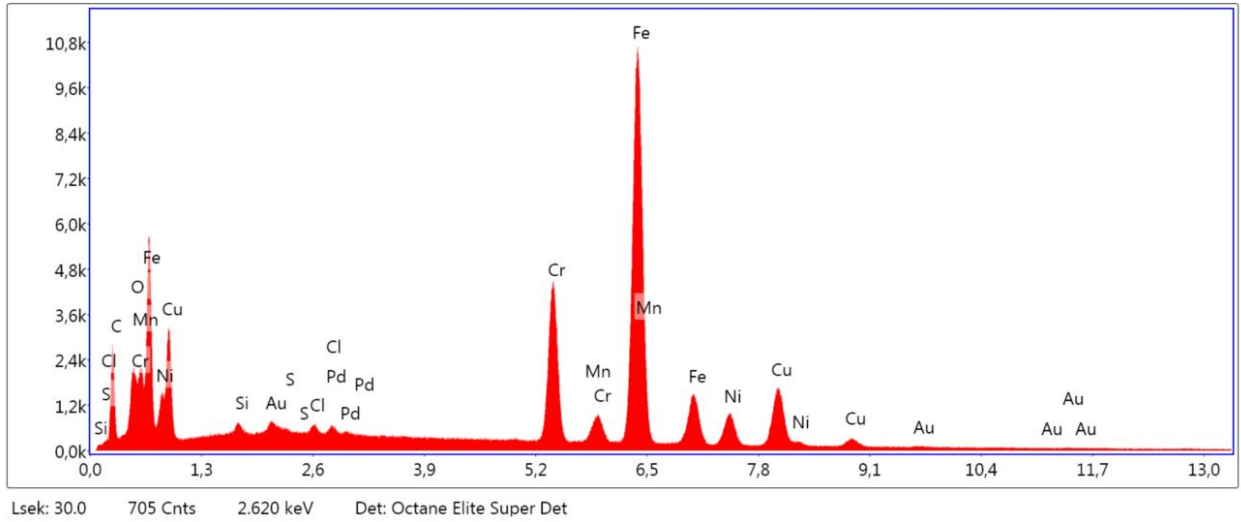
**eZAF Quant. Ergebnisse**

Element	Gewicht%	Atom%	Net. Int.	Error %	Kratio	Z	R	A	F
CK	5.1	18.5	349.3	10.6	0.0140	1.2841	0.8502	0.2160	1.0000
OK	3.7	10.1	1043.3	7.7	0.0187	1.2354	0.8748	0.4119	1.0000
SiK	0.4	0.6	140.3	12.9	0.0020	1.1350	0.9326	0.4796	1.0071
SK	0.2	0.2	75.3	20.4	0.0013	1.1144	0.9486	0.7052	1.0180
ClK	0.6	0.7	262.4	10.5	0.0049	1.0615	0.9562	0.7867	1.0277
CrK	14.2	11.9	4008.2	3.0	0.1658	0.9731	1.0013	0.9915	1.2320
MnK	1.5	1.2	315.6	7.5	0.0150	0.9537	1.0066	0.9941	1.0941
FeK	60.1	46.7	10592.9	2.0	0.5829	0.9700	1.0115	0.9751	1.0449
NiK	7.0	5.2	879.2	4.3	0.0645	0.9824	1.0198	0.9163	1.0419
CuK	7.3	5.0	747.2	4.6	0.0652	0.9339	1.0231	0.9328	1.0487

EDX Punkt 2

kV: 20    Vergr.: 5999    Abnahmewinkel: 37.1    Live Messdauer(s): 30    Filterzeit(µs): 3.84    Auflösung:(eV)

EDX Punkt 2

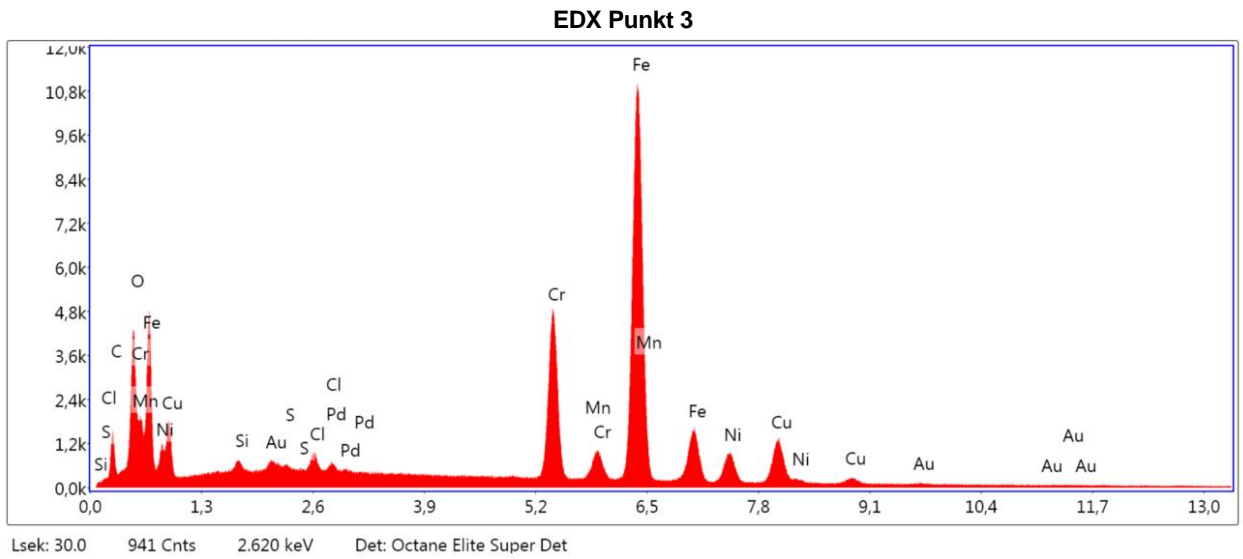


**eZAF Quant. Ergebnisse**

Element	Gewicht%	Atom%	Net. Int.	Error %	Kratio	Z	R	A	F
CK	10.2	33.4	719.2	9.7	0.0280	1.2715	0.8546	0.2193	1.0000
OK	1.9	4.7	479.4	9.0	0.0083	1.2232	0.8792	0.3616	1.0000
SiK	0.5	0.7	201.1	13.8	0.0028	1.1236	0.9367	0.4805	1.0067
SK	0.2	0.2	78.0	22.4	0.0013	1.1033	0.9527	0.7050	1.0170
ClK	0.4	0.4	168.4	12.4	0.0031	1.0508	0.9601	0.7865	1.0264
CrK	12.5	9.4	3576.1	3.0	0.1439	0.9632	1.0048	0.9917	1.2263
MnK	1.3	0.9	278.0	8.6	0.0129	0.9440	1.0099	0.9948	1.1039
FeK	52.1	36.8	9524.7	2.1	0.5100	0.9601	1.0147	0.9786	1.0572
NiK	6.3	4.3	825.9	4.4	0.0589	0.9721	1.0227	0.9277	1.0465
CuK	14.8	9.2	1564.1	3.4	0.1328	0.9241	1.0258	0.9424	1.0479

EDX Punkt 3

kV: 20      Vergr.: 5999      Abnahmewinkel: 37.1      Live Messdauer(s): 30      Filterzeit(µs): 3.84      Auflösung:(eV)



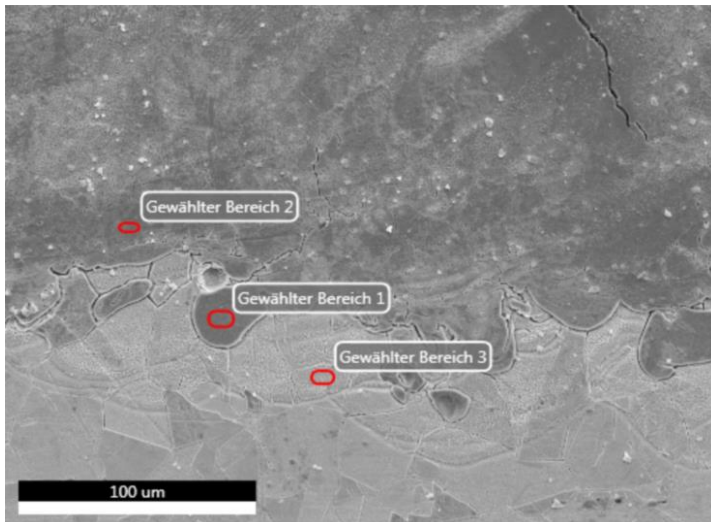
**eZAF Quant. Ergebnisse**

Element	Gewicht%	Atom%	Net. Int.	Error %	Kratio	Z	R	A	F
CK	4.8	17.5	324.3	11.1	0.0129	1.2855	0.8496	0.2131	1.0000
OK	4.2	11.4	1173.7	7.7	0.0209	1.2368	0.8742	0.4104	1.0000
SiK	0.4	0.6	140.8	13.1	0.0020	1.1363	0.9320	0.4746	1.0069
SK	0.2	0.2	68.5	22.5	0.0012	1.1157	0.9480	0.7007	1.0175
ClK	0.6	0.8	292.3	10.1	0.0054	1.0627	0.9556	0.7830	1.0269
CrK	14.0	11.7	3930.1	3.0	0.1616	0.9743	1.0008	0.9906	1.2231
MnK	1.4	1.1	306.3	7.6	0.0145	0.9549	1.0061	0.9935	1.0974
FeK	56.0	43.7	9964.8	2.1	0.5451	0.9713	1.0110	0.9750	1.0513
NiK	6.6	4.9	838.8	4.4	0.0612	0.9837	1.0194	0.9208	1.0443
CuK	11.8	8.1	1216.0	3.6	0.1055	0.9351	1.0227	0.9367	1.0481

E165 465A

Autor: whitmore  
Erstellt: 05/23/2017 1:32:33 PM  
Probenbezeichnung: bright 7.1 QS

## Bereich 1



Notizen:

## Gewählter Bereich 1

kV: 20

Vergr.: 1200

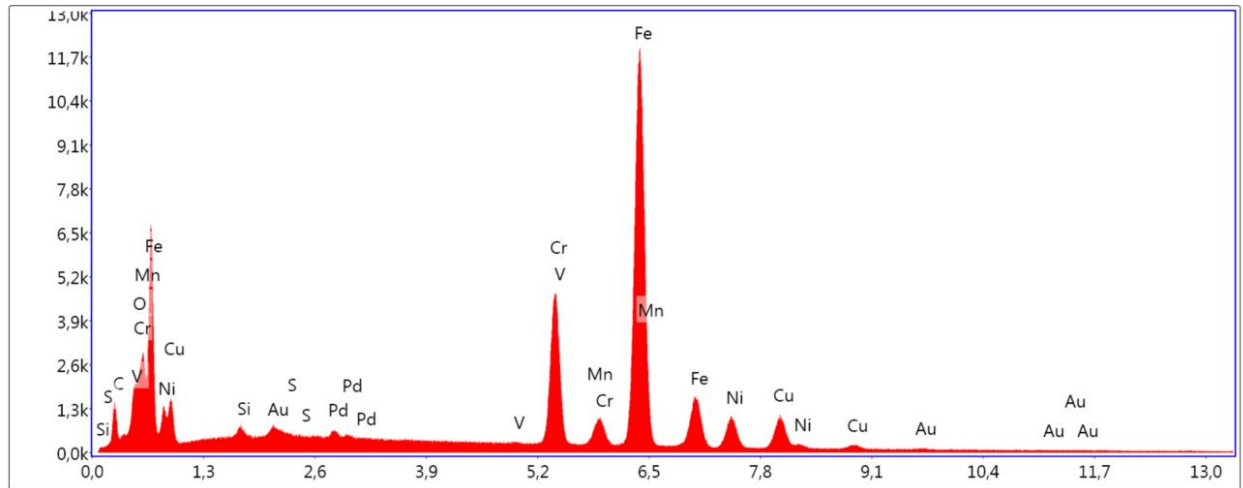
Abnahmwinkel: 37.2

Live Messdauer(s): 30

Filterzeit(µs): 3.84

Auflösung:(eV)

## Gewählter Bereich 1



Lsek: 30.0 337 Cnts 4.945 keV Det: Octane Elite Super Det

**eZAF Quant. Ergebnisse**

Element	Gewicht%	Atom%	Net. Int.	Error %	Kratio	Z	R	A	F
CK	4.3	16.8	288.3	11.1	0.0119	1.2983	0.8441	0.2162	1.0000
OK	1.2	3.6	338.2	9.6	0.0063	1.2491	0.8687	0.4161	1.0000
SiK	0.4	0.6	138.4	13.4	0.0020	1.1478	0.9267	0.4694	1.0069
SK	0.1	0.1	34.5	57.5	0.0006	1.1272	0.9429	0.6958	1.0176
VK	0.2	0.2	55.7	29.6	0.0021	0.9690	0.9907	0.9819	1.2162
CrK	14.0	12.6	3880.7	3.0	0.1665	0.9847	0.9965	0.9904	1.2365
MnK	1.5	1.3	318.6	7.4	0.0157	0.9652	1.0019	0.9930	1.0967
FeK	61.8	52.0	10713.9	2.1	0.6117	0.9818	1.0069	0.9746	1.0469
NiK	7.2	5.8	889.4	4.3	0.0677	0.9945	1.0156	0.9140	1.0421
CuK	9.3	6.9	936.8	4.2	0.0848	0.9456	1.0192	0.9308	1.0478

## Gewählter Bereich 2

kV: 20

Vergr.: 1200

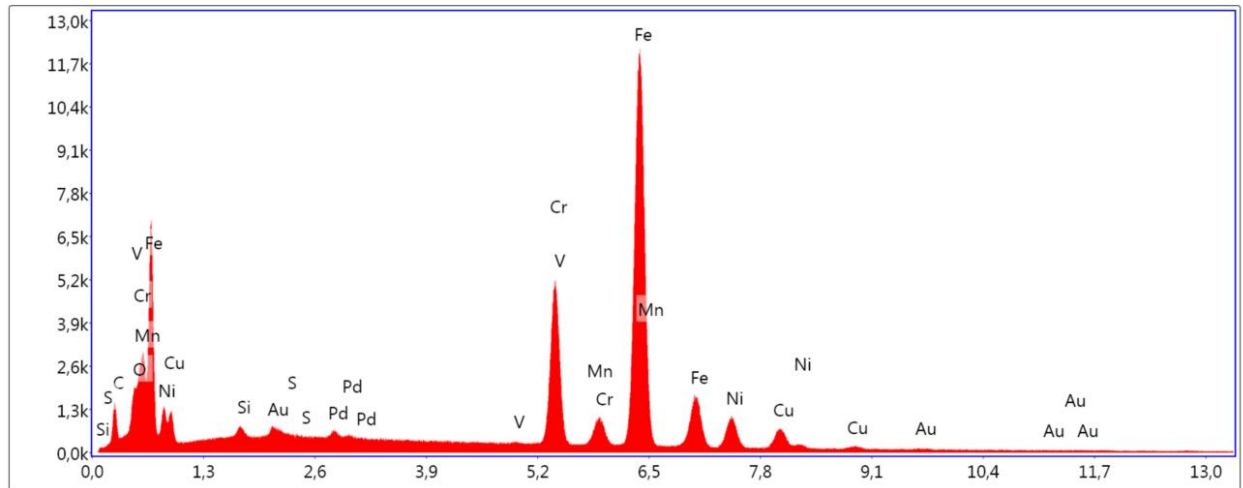
Abnahmwinkel: 37.2

Live Messdauer(s): 30

Filterzeit(µs): 3.84

Auflösung:(eV)

## Gewählter Bereich 2



Lsek: 30.0 332 Cnts 4.945 keV Det: Octane Elite Super Det

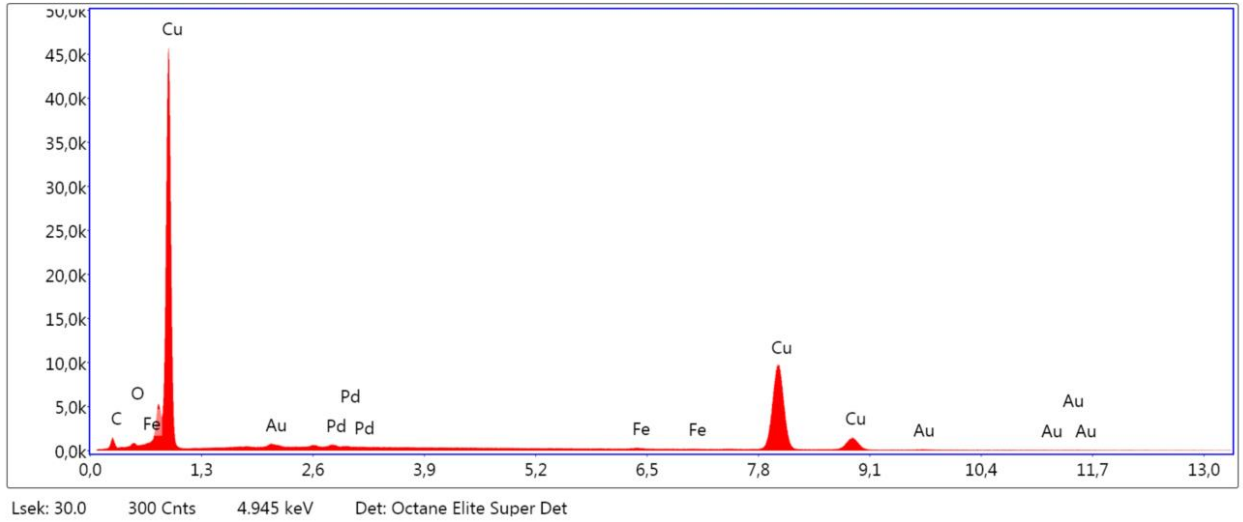
**eZAF Quant. Ergebnisse**

Element	Gewicht%	Atom%	Net. Int.	Error %	Kratio	Z	R	A	F
CK	4.3	17.0	292.3	11.9	0.0121	1.2974	0.8446	0.2181	1.0000
OK	1.0	3.0	287.5	9.6	0.0053	1.2482	0.8692	0.4196	1.0000
SiK	0.4	0.7	155.4	12.8	0.0023	1.1470	0.9272	0.4734	1.0070
SK	0.1	0.1	32.6	57.6	0.0006	1.1264	0.9434	0.6992	1.0179
VK	0.2	0.1	48.9	35.3	0.0019	0.9682	0.9912	0.9827	1.2169
CrK	15.0	13.6	4151.6	3.0	0.1786	0.9839	0.9969	0.9910	1.2340
MnK	1.5	1.3	311.9	7.7	0.0155	0.9644	1.0023	0.9933	1.0924
FeK	63.8	53.6	10943.3	2.0	0.6265	0.9810	1.0073	0.9731	1.0429
NiK	7.5	6.0	914.5	4.3	0.0698	0.9937	1.0160	0.9110	1.0407
CuK	6.2	4.6	617.1	5.1	0.0560	0.9448	1.0195	0.9284	1.0483

Gewählter Bereich 3

kV: 20    Vergr.: 1200    Abnahmewinkel: 37.2    Live Messdauer(s): 30    Filterzeit(µs): 3.84    Auflösung:(eV)

Gewählter Bereich 3



**eZAF Quant. Ergebnisse**

Element	Gewicht%	Atom%	Net. Int.	Error %	Kratio	Z	R	A	F
C K	5.7	23.7	307.1	12.1	0.0131	1.3289	0.8284	0.1770	1.0000
O K	0.8	2.4	168.4	11.8	0.0032	1.2787	0.8529	0.3290	1.0000
Fe K	0.3	0.2	72.2	24.0	0.0042	1.0089	0.9948	0.9911	1.5695
Cu K	93.3	73.6	9935.7	2.0	0.9263	0.9730	1.0087	1.0011	1.0391

## List of Figures

2.1	The structure of a fiber laser includes a doped inner core, which is the laser itself; an undoped outer core, called inner cladding through which the pump light is channelled and an outer cladding [9] . . . . .	9
2.2	Absorption of light in % at a different wavelengths on metallic materials at room temperature [17] . . . . .	10
2.3	Simulation taken as an example of application of Rosenthal's 2D equation that shows the gradients of temperature in a random welding of a sheet [1]- <i>modified</i> . . . . .	11
2.4	Relation between Depth, Power Density and Power with the range of each welding category [20] . . . . .	12
2.5	Process of keyhole laser welding (a) high speed image of the top surface, slightly tilted from the side as points the arrow in the draw, (b) sketch of a vertical x-z-section of the melt pool and the keyhole and (c) high speed image of the upper part of the keyhole front surface waves also slightly tilted from the rear side [14] . . . . .	14
2.6	Heiple's model for Maragoni convection in a weld pool: (a, b, c) low sulphur-steel; (d, e, f) high-sulphur steel [3] . . . . .	15
2.7	Zones in a laser weld and thermal cycle that represents the different cooling rates depending on the distance from the fusion zone . . . . .	16
2.8	Melt pool formation where $v_s(max) = v_b$ being $v_b$ the welding speed [21] .	17
2.9	Dendrite regions growth of the fusion zone of Sample No. 1 . . . . .	17
3.1	Binary diagram Fe-Cu [25] . . . . .	20
3.2	In first term the held device, in the background the robot actuator and laser head . . . . .	22
3.3	Schema of the offset . . . . .	24
3.4	Regression equation 2.1, penetration as a function of welding speed . . . .	27
3.5	Graphs that match power output, welding speed and thickness [29] . . . .	27
3.6	Graph obtained from the documentation of the Fiber Laser used . . . . .	28
3.7	Weld bead of each of the 7 samples obtained. From now forwards, in all photos showing a welding bead, direction of welding goes from left to right side of the picture . . . . .	31
4.1	On the left of the photo melt flow currents of steel going up can be clearly seen as in the right not due to the misalignment of the surface cut plane and the central weld line . . . . .	32
4.2	Transversal view of the weld seams of each sample obtained with a magnification of x12.5 using Bertrand lens for better contrast (a, b, c, d) and with a magnification of x50 (e, f) . . . . .	33

*List of Figures*

4.3	Spatters detected in both sides of the seam in sample No. 6 . . . . .	35
4.4	Burn-through effects in sample No. 5 . . . . .	35
4.5	Image of one hump, it can be appreciated the drastic change of the seam appearance. These periodical humps were distanced approximately 5 mm one each other in sample No. 3 . . . . .	36
4.6	High temperature cracking and solidification cracking detected in both samples No. 1 & 7 . . . . .	37
4.7	Some liquation cracks detected on the bottom of the photo and in the HAZ of sample No. 1. . . . .	37
4.8	Different kind of defects in laser weld beads . . . . .	38
4.9	Number of pores detected for a same arbitrary area located far from the edges with two photos taken with 25x magnification. There are much more hot cracking in sample No. 1, though . . . . .	38
4.10	Base materials, commercially pure copper and austenitic stainless steel with a magnification of 500x . . . . .	40
4.11	Primary austenite solidification and postsolidification transformation in Fe-Cr-Ni weld . . . . .	41
4.12	(a) Weld centre and weld face microstructure and (b) microstructure in the weld interface of Sample No. 1 . . . . .	42
4.13	Interface region at the bottom of the weld seam within copper plate where it can be perceived the higher mixing rates in sample No. 1 (a) than sample No. 7 (b). They were taken before submitting them into the etching solution . . . . .	43
4.14	(a) view of the bottom of the weld and interface region of sample No. 1 and (b) location of the analysed points and areas with SEM method . . .	44
4.15	(a) view of the central part of the weld near the main pore and (b) location of the analysed points with SEM method . . . . .	44
4.16	View of the points and areas analysed in the longitudinal samples (a) No. 1 and (b) No. 7. The clear areas corresponds to copper, the clear grained ones to the mentioned Cu- $\epsilon$ phases and the dark zones to the steel . . . .	45

## List of Tables

2.1	Thermal Properties of stainless steel and copper . . . . .	11
3.1	Chemical composition of each specimen, wt% . . . . .	20
3.2	Initial offsets . . . . .	24
3.3	Number of grain of the papers used and time in the disc polishing machine	24
3.4	Fit Parameters a and b (see eq. 3.2) and Regression Coefficient, r, for Laser Welding Data . . . . .	26
3.5	Selected welding parameters for each sample and predicted penetration depth in each case . . . . .	29

## Nomenclature

- $A$  Absorptivity, see equation (2.1)
- $g$  Workpiece thickness, see equation (2.3)
- $Q'$  Heat transferred from heat source to workpiece, see equation (2.3)
- $v$  Welding speed, see equation (2.3)
- Welding speed, see equation (2.6)
- Welding speed, see equation (3.2)
- $\alpha$  Workpiece thermal diffusivity, namely  $\kappa/\rho C$ , where  $\rho$  and  $C$  are density and specific heat of the workpiece respectively, see equation (2.3)
- $K_o$  Modified Bessel function of second kind zero order, see equation (2.3)
- $r$  Radial distance from origin, namely,  $(x^2 + y^2)^{1/2}$ , see equation (2.3)
- $p_v$  Pyhydrostatic pressure, see equation (2.4)
- Pyhydrostatic pressure, see equation (2.5)
- $n$  Rear refractive index, see equation (2.1)
- $p_l$  Surface tension, see equation (2.4)
- $p_\sigma$  Vaporization pressure, see equation (2.4)
- Vaporization pressure, see equation (2.5)
- $p_g$  Hydrodynamic pressure, see equation (2.4)
- $p_h$  radiation pressure, see equation (2.4)
- $v_s$  Solidification rate, see equation (2.6)
- $\theta$  Angle between welding speed and normal to the molten trace at one point, see equation (2.6)
- CEV Carbon Equivalent Value, see equation (3.1)
- $P$  Output power, see equation (3.2)
- Output power, see equation (3.3)

*List of Tables*

$k$	Imaginary part of the refractive index, see equation (2.1)
$d$	Penetration depth, see equation (3.2)
$a, b$	Fit parameters, see equation (3.2)
$q_p$	Average power density, see equation (3.3)
$D$	Focal point diameter, see equation (3.3)
	Imaginary part of the refractive index, see equation (2.2)
$\delta$	Depth where absorption occurs, see equation (2.2)
$\lambda$	Laser wavelength, see equation (2.2)
$T$	Temperature, see equation (2.3)
$T_o$	Workpiece temperature before welding, see equation (2.3)
$\kappa$	Workpiece thermal conductivity, see equation (2.3)

## References

- [1] H. Henein A. Lecoanet D. G. Ivey. *Simulation of the Temperature Profile During Welding with COMSOL Multiphysics Software Using Rosenthal's Approach*. Tech. rep. Department of Chemical Materials Engineering, University of Alberta, Canada, 2014. URL: [https://www.comsol.com/paper/download/194353/lecoanet\\_paper.pdf](https://www.comsol.com/paper/download/194353/lecoanet_paper.pdf). accessed: 29.5.2017.
- [2] Inc. Amada Miyachi America. *Laser Welding Fundamentals*. Tech. rep. Amada Miyachi America, Inc., 2016. URL: [http://www.amadamiyachi.com/servlet/servlet.FileDownload?retURL=%2Fapex%2Feducationalresources\\_articles&file=0158000001Jz8A](http://www.amadamiyachi.com/servlet/servlet.FileDownload?retURL=%2Fapex%2Feducationalresources_articles&file=0158000001Jz8A). accessed: 27.3.2017.
- [3] Lee Aucott. *Mechanism of solidification cracking during welding of high strength steels for subsea linepipe*. Tech. rep. University of Leicester, 2015. URL: [reasearchGate](https://www.researchgate.net/publication/3158000001Jz8A). accessed: 30.5.2017.
- [4] Xiancheng Zhang Jian Huang Jun Fu Yixiong Wu Chengwu Yao Binshi Xu. *Interface microstructure and mechanical properties of laser welding copper-steel dissimilar joint*. Tech. rep. School of materials Science, Engineering Shanghai Jiaotong University, Shanghai Key Laboratory of Materials Laser Processing and Modification, National Key Laboratory for Remanufacturing, Beijing. China, 2009. URL: [Compendex](https://www.compendex.com/record/10.1002/9781118444444.ch10). accessed: 27.3.2017.
- [5] et al. Chethan Roy Vipin V Pavanan. *Characterization of Metallurgical and Mechanical Properties of Commercially Pure Copper and AISI 304 Dissimilar Weldments*. Tech. rep. School of mechanical and Building Sciences, VIT University, Vellore, India, 2014. accessed: 10.5.2017.
- [6] Liang Dong and Bryce Samson. *Fiber Lasers: Basics, Technology and Applications*. 1st ed. CRC Press, 2017.
- [7] John Dyson. *Austenitic Stainless Steels*. Version 3.4.2. 2014. URL: <http://www.gowelding.com/met/austenitic.html>. accessed: 5.6.2017.
- [8] Rodovan Kovacevic Fanrong Kong. *Development of a Comprehensive Process Model for Hybrid Laser-Arc Welding*. Tech. rep. Southern Methodist University, Dallas, Texas, USA, 2012. URL: <https://www.intechopen.com/books/welding-processes/development-of-a-comprehensive-process-model-for-hybrid-laser-arc-welding>. accessed: 31.5.2017.
- [9] Jeff Hecht. *Fiber Lasers: The State of Art*. Version 3.4.2. 2012. URL: <http://www.laserfocusworld.com/articles/print/volume-48/issue-04/features/the-state-of-the-art.html>. accessed: 28.5.2017.
- [10] D.K.Y. Low J. Lawrence J. Pou and E. Toyserkani. *Advances in laser materials processing*. 1st ed. Woodhead Publishing Limited, 2010.

## References

- [11] Reijonen Joni. *The effect of focal point parameters in fiber laser welding of structural steel*. Tech. rep. Lappeenranta University of Technology, 2015. URL: <http://www.doria.fi/handle/10024/109212>. accessed: 25.4.2017.
- [12] Alexander H.F. Kaplan Josefine Svenungsson Isabelle Choquet. *Laser welding process - a review of keyhole welding modelling*. Tech. rep. Department of Engineering Sciences and Mathematics, Luleå University of Technology, Sweden, 2015. URL: [Compendex](#). accessed: 30.5.2017.
- [13] et al. Kaibin Li Dong Li. *Microstructure evolution and mechanical properties of multiple layer laser cladding coating of 308L stainless steel*. Tech. rep. Department of Materials Engineering, Shanghai University of Engineering Science, Shanghai, China, 2015. URL: <http://www.sciencedirect.com/science/article/pii/S0169433215004985>. accessed: 3.6.2017.
- [14] Alexander F. H. Kaplan. *Fresnel absorption of 1  $\mu\text{m}$ - and 10  $\mu\text{m}$ -laser beams at the keyhole wall during laser beam welding: Comparison between smooth and wavy surfaces*. Tech. rep. Department of Engineering Sciences and Mathematics, Luleå University of Technology, Sweden, 2012. URL: [Compendex](#). accessed: 30.5.2017.
- [15] Sindo Kou. *Welding Metallurgy*. 2nd ed. Wiley, 2003.
- [16] et al. Kun Li Jiguo Shan. *The role of copper in microstructures and mechanical properties of laser-welded Fe-19Ni-3Mo-1.5Ti maraging steel joint*. Tech. rep. Tsinghua University Institute for Special Steel, Central Iron and Steel Research Institute, Beijing, 2017. URL: [Compendex](#). accessed: 27.3.2017.
- [17] Cleemann L. *Schweissen mit CO<sub>2</sub>-Hochleistungslasern*. 1st ed. Technologie Aktuell, 1987.
- [18] M. Schmidt M. Weigl. *Influence of the feed rate and the lateral beam displacement on the joining quality of laser-welded copper-stainless steel connections*. Tech. rep. Bayerisches Laserzentrum University of Erlangen-Nueremberg, Erlangen, Germany, 2010. URL: [Compendex](#). accessed: 26.3.2017.
- [19] Gene Mathers. *Welding of austenitic stainless steel*. Version 3.4.2. 2017. URL: <http://www.twi-global.com/technical-knowledge/job-knowledge/welding-of-austenitic-stainless-steel-103/>. accessed: 2.6.2017.
- [20] Michael Müller. *Fine Welding with Lasers*. Version 3.4.2. 2013. URL: [http://engineers.org.il/\\_Uploads/10355RofinFineWeldingwithLaser.pdf](http://engineers.org.il/_Uploads/10355RofinFineWeldingwithLaser.pdf). accessed: 28.3.2017.
- [21] Kamran Mumatz Neil J. Harrison I. Todd. *Reduction of micro-cracking in nickel superalloys processed by Selective Laser Melting: A fundamental alloy design approach*. Tech. rep. Department of Mechanical Engineering, department of material Science and Engineering, University of Sheffield, UK, 2015. URL: [https://www.researchgate.net/publication/276414114\\_Reduction\\_of\\_micro-cracking\\_in\\_nickel\\_superalloys\\_processed\\_by\\_Selective\\_Laser\\_Melting\\_A\\_fundamental\\_alloy\\_design\\_approach](https://www.researchgate.net/publication/276414114_Reduction_of_micro-cracking_in_nickel_superalloys_processed_by_Selective_Laser_Melting_A_fundamental_alloy_design_approach). accessed: 31.5.2017.

## References

- [22] G. Petzow. *Metallographic Etching*. 2nd ed. ASM International, 1999.
- [23] J.M. Vitek S. A. David S. S. Babu. *Welding: Solidification and Microstructure*. Tech. rep. Oaf Ridge National Laboratory, Metals Ceramics Division Building, Tennessee, USA, 2003. URL: <http://www.tms.org/pubs/journals/JOM/0306/David-0306.html>. accessed: 31.5.2017.
- [24] et al. Shuhai Chen Jihua Huang. *Influence of processing parameters on the characteristics of stainless steel/copper laser welding*. Tech. rep. University of Science, Technology, Beijing State Key Laboratory of Advanced Welding and Joining, Harbin Institute of Technology, Harbin, China, 2015. URL: [Compendex](#). accessed: 19.3.2017.
- [25] A. Kh. Gilmutdinov S.V. Kuryntsev A.E. Morushkin. *Fiber laser welding of austenitic steel and commercially pure copper butt joint*. Tech. rep. Kazan National research Technical University Named After A.N. Tupolev - KAI, Russia, 2017. URL: [Compendex](#). accessed: 19.3.2017.
- [26] A.C. Spowage T.A. Mai. *Characterisation of dissimilar joints in laser welding of steel-kovar, copper-steel and copper-aluminium*. Tech. rep. Singapore Institute of Manufacturing Technology, Singapore, 2004. URL: [Compendex](#). accessed: 28.3.2017.
- [27] Reddy Y. P. et al. Tadamalle A.P. *Influence of welding speed on the melting efficiency of Nd:YAG laser welding*. Tech. rep. Department of Mechanical Engineering, Shinhad College of Engineering, Pune, India, 2014. URL: [file:///C:/Users/user/Downloads/Influence\\_URN-NBN-SI-DOC-PF7SORXP%20\(1\).pdf](file:///C:/Users/user/Downloads/Influence_URN-NBN-SI-DOC-PF7SORXP%20(1).pdf). accessed: 3.6.2017.
- [28] William Krupke Valentin Gapontsev. *Fiber lasers grow in power*. Version 3.4.2. 2002. URL: <http://www.laserfocusworld.com/articles/print/volume-38/issue-8/features/fiber-lasers/fiber-lasers-grow-in-power.html>. accessed: 28.3.2017.
- [29] Walter W. Duley. *Laser Welding*. 1st ed. John Wiley Sons, Inc., 1999.